Functional genetic screens to uncover the roles of chromatin modifiers in IDH-mutant glioma

by

Fulya Mina KÜÇÜKTAŞ

A Dissertation Submitted to the
Graduate School of Health Sciences
in Partial Fulfillment of the Requirements for
the Degree of

Master of Science

in

Cellular and Molecular Medicine

August 9, 2023

Functional genetic screens to uncover the roles of chromatin modifiers in IDH mutant glioma

Koç University

Graduate School of Health Sciences

This is to certify that I have examined this copy of a master's thesis by

Fulya Mina KÜÇÜKTAŞ

and have found that it is complete and satisfactory in all respects,
and that any and all revisions required by the final
examining committee have been made.

Committee Members:

Prof. Tuğba Bağcı Önder (Advisor)

Assoc. Prof. Adam Cribbs

Assist. Prof. Ece Öztürk

Date: 09.08.2023

To my loving family,

who have been my unwavering source of support

and encouragement throughout this journey

ABSTRACT

Functional genetic screens to uncover the roles of chromatin modifiers in IDH-mutant glioma

Fulya Mina KÜÇÜKTAŞ

Master of Science in Cellular and Molecular Medicine

August 9, 2023

Gliomas, a malignant group of central nervous system tumors, pose a significant health threat, particularly grade IV glioblastoma, which is the most aggressive type. Among gliomas, IDH-mutant gliomas exhibit a more favorable response to therapies, making them an intriguing target for precision treatments. This thesis delves into the investigation of essential epigenetic modifiers that may underlie vulnerabilities in IDH-mutant gliomas using a custom designed CRISPR-Cas9 epigenetic library called EPIKOL.

In the first part of the thesis, IDH-wildtype and IDH-mutant cells were generated from the A172 glioma cell line. Subsequently, CRISPR-Cas9 mediated screening with the EPIKOL library was performed on these cell lines to identify epigenetic modifiers that are essential for IDH-wildtype and/or IDH-mutant glioma cells. The candidates were then validated through functional *in vitro* assays, focusing on cell viability and colony formation ability. Among the validated genes, RBBP7, which plays a role in complexes involved in histone modification and gene expression regulation, emerged as a potential essential regulator of IDH-mutant glioma cells.

Overall, the findings from this study lay the foundation for identifying novel therapeutic targets for IDH-mutant glioma through further experiments and analyses. Future work will dissect out the gene regulatory function of RBBP7 in IDH-mutant cells using RNA sequencing. The investigation of essential epigenetic modifiers offers promising avenues for precision treatments in combating this challenging form of brain tumor.

ÖZETÇE

IDH-mutant gliomada kromatin değiştiricilerin rollerini ortaya çıkarmak için fonksiyonel genetik taramalar

Fulya Mina KÜÇÜKTAŞ

Hücresel ve Moleküler Tıp, Yüksek Lisans

9 Ağustos 2023

Gliomalar, merkezi sinir sistemi tümörleri arasında yer alan ve dört farklı sınıfa ayrılan bir grup tümördür. Özellikle en agresif tür olan dördüncü sınıf glioblastoma, önemli bir sağlık tehdidi oluşturur. Gliomalar içinde yer alan IDH-mutant gliomalar, tedavilere daha olumlu ve hassas bir yanıt gösterme eğilimindedir, bu da onları hedefe yönelik tedaviler için ilgi çekici kılar. Bu tez, özel olarak tasarlanmış bir CRISPR-Cas9 epigenetik kütüphane olan EPIKOL kullanarak IDH-mutant gliomaların hassasiyetine yol açan temel epigenetik düzenleyicilerin araştırılmasına odaklanmaktadır.

Tezin ilk bölümünde, A172 glioma hücre hattından IDH-wildtype ve IDH-mutant hücreler üretilmiştir. Ardından, bu hücre hatları üzerinde EPIKOL kütüphanesi ile CRISPR-Cas9 aracılı tarama yapılarak IDH-wildtype ve IDH-mutant glioma hücrelerinin hayati öneme sahip temel epigenetik düzenleyicileri belirlenmiştir. Aday genler daha sonra hücre canlılığı ve koloni oluşturma kabiliyeti gibi işlevsel in vitro deneylerle doğrulanmıştır. Doğrulanan genler arasında, histon modifikasyonu ve gen ekspresyon düzenlemesi ile ilişkili komplekslerde rol alan RBBP7, IDH-mutant glioma hücreleri için potansiyel bir temel hedef olarak ortaya çıkmıştır.

Bu çalışmadan elde edilen bulgular, ileri deneyler ve analizlerle IDH-mutant gliomalar için yeni terapötik hedeflerin belirlenmesine temel oluşturacaktır. Moleküler mekanizmalar hakkında daha derinlemesine bilgi edinmek için RBBP7'nin transkriptomik etkileşimleri RNA-seq analizi ile incelenecektir. Temel epigenetik düzenleyicilerin araştırılması, bu zorlu beyin tümörüyle mücadelede hedefe yönelik tedavilere yönelik umut vaat eden yollar sunmaktadır.

AKNOWLEDGEMENTS

I would like to express my deepest gratitude to my advisor, Prof. Tuğba Bağcı Önder for her unwavering support and guidance during my master's journey. I feel sincerely fortunate and thankful to have her as my advisor. Her encouragement persisted through every setback, and in every challenge, she directed me to view problems from different angles, find alternative solutions, and continue moving forward. I am truly grateful for her as a supportive and constructive advisor.

I also feel lucky to have Dr. Adam Cribbs and Dr. Ece Öztürk in my thesis jury, I would like to thank for their guidance and support throughout my thesis process. I would like to thank Koç University Research Centre for Translational Medicine (KUTTAM) and Scientific and Technological Research Council of Turkey (TUBITAK) for providing the financial support.

I am grateful for having Dr. Göktuğ Karabıyık and Ezgi Yağmur Kala Kalkan throughout my journey. I feel very lucky to have Nareg Değirmenci as an exceptional lab and road friend. Our discussions and their help were very precious both in every step and confusion in my project and personally. Thank you for giving me the space to ask any small question without hesitation and for always being there for me.

Within the TBO Lab, I am very grateful for Beril Esin for her invaluable friendship. Thank you for being on my "team" and being here supporting and motivating each other in every happiness and difficulty.

I would like to thank former members of the TBO Lab, Dr. Alişan Kayabölen, Dr. Ali Cenk Aksu. Even from the miles apart, they were always helping me. I would like to express my thanks to current TBO Lab members Dr. Ahmet Cingöz and Dr. Özlem Yedier Bayram, Ebru Yılmaz, Canan Bayraktar, Gizem Doğan Yılmaz, Beyza Nur Köseoğlu, Aksel Çelikkol, Sedef Saraç-Yalçınkaya, and İpek Kök for their valuable friendship and creating a warm laboratory environment.

I would like to express my thanks to Batuhan Altay for his endless support throughout the whole journey and to my goals and aspirations. His exceptional perspective and his passion to science have always been a true inspiration for me. Discussions with him always led me to think in different point of views. I am grateful to have him in my life.

I would like to thank to Enes Çiçek and Ayça Açar, who have always been supporting friends. Their valuable friendship opened a safe discussion space to me even we worked in different labs and on different topics, it was always very exciting to talk about projects and studies with different perspectives during our coffee breaks together.

I cannot express my gratitude enough with words to my parents Ayhan and Hatice, to my sister Bensu, and to my brother Umut. I am truly grateful for them being my biggest support and believing in my goals and dreams of pursuing a career in science. They always encourage me and provide help to move on in each step. Their unconditional love, guidance, cherish, and patience have been my endless source of motivation throughout my journey.

TABLE OF CONTENTS

LIST OF TABLES

LIST OF FIGURES

ABBREVIATIONS

2-HG	2-hydroxyglutarate
2-OG	2-oxoglutarate
5-hmC	5-hydroxymethylcytosine
5-mC	5-Methylcytosine
a-KG	a-ketoglutarate
AP	After puromycin selection
CNS	Central nervous system
CoA	Coenzyme A
CpG	Cystosine-guanine Dinucleotides
CRISPR	Clustered Regularly Interspaced Palindromic Repeats
DNMT	DNA methyltransferase
EGFR	Epidermal growth factor receptor
EMT	Epithelial mesenchymal transition
EPIKOL	Epigenetic Knockout Library
EP	Endpoint
GBM	Glioblastoma
gRNA	guide RNA
HAT	Histone Acetyltransferase
HDAC	Histone Deacetylase
HMT	Histone methyl transferase
IDH	Isocitrate dehydrogenase
IR	Ionized radiation
JmjC	Jumonji C domain containing
KMT	Lysine methyltransferase
LGG	Low-grade gliomas
mIDH	Mutant IDH
MOI	Multiplicity of infection
NADPH	Nicotinamide adenine dinucleotide phosphate
NGS	Next-Generation Sequencing

NuRD	Nucleosome remodeling and histone deacetylase
OS	Overall survival
P53	Tumor protein 53
PARP	Poly (ADP-ribose) polymerase
PCA	Principal component analysis
PCR	Polymerase chain reaction
PDGFRA	Platelet-derived growth factor receptor type A
PE	Phosphoenolpyruvate
PI3K	Phosphoinositide 3-kinase
PRC2	Polycomb repressive complex 2
PRMT	Protein arginine methyltransferase
PTEN	Phosphatase and tensin homolog
PTM	Post-translational modifications
PsPD	Pseudo-progression
RNA-Seq	RNA sequencing
RT	Radiation therapy
RT-PCR	Real-time PCR
sgRNA	Single guide RNA
TCA	Tricarboxylic acid
TET	Ten-eleven translocation
TMZ	Temozolomide
WHO	World Health Organization
WT	Wild type
µl	Microliter
µM	Micromolar

Chapter 1: **INTRODUCTION**

1.1 Glioma

Gliomas are the central nervous system (CNS) tumors that originate from glial cells. These diffusely infiltrative tumors have an impact on the surrounding brain tissues. The incidence rate of gliomas in the United States is 6 per 100,000 people in a year (Mesfin & Al-Dhahir, 2023; Neumaier et al., 2023), and the 30% of primary brain tumors and about 80% of all the malignant tumors are diffusely infiltrating lower-grade gliomas with a high resistance to therapy and ultimately, incurability (Neumaier et al., 2023; Rong et al., 2022; Schaff & Mellinghoff, 2023).

In 2021, the World Health Organization (WHO) introduced a classification system for gliomas consisting of four grades, ranging from grade I to grade IV, which are determined based on the proliferation degree and the presence of molecular and genetic markers. The mitotic index and the presence of necrosis serve as indicators of the proliferation degree (Mesfin & Al-Dhahir, 2023). As the glioblastoma (GBM) term is conserved for isocitrate dehydrogenase (IDH)-wildtype gliomas, which is the most common and aggressive type of central nervous system tumors and comprises about 50% of all gliomas, IDH-mutant tumors are characterized with the GBM histology as grade IV IDH-mutant astrocytoma (Grochans et al., 2022; Rong et al., 2022; N. Sharma et al., 2023).

1.1.1 Treatment options in glioma

For the most aggressive form of brain cancer, glioblastoma, there are existing treatment choices like surgery, radiotherapy, and pharmacotherapy, specifically chemotherapy with temozolomide (TMZ) used together with other treatments. Despite progress and available options in therapy, the typical survival period ranges from 14.6 to 20.5 months. In elderly patients, this median overall survival drops to 8.5 months from the time of diagnosis. Unfortunately, the treatment options for GBM remain limited, highlighting the need for new therapeutic approaches. The current approach for treating GBM involves surgically removing the primary tumor, followed by targeting any remaining tumor cells through a combination of radiation and TMZ chemotherapy. If the

complete removal of the tumor is not achieved, there is a risk of tumor recurrence facilitated by glioma stem cells (Rong et al., 2022).

This process leads to the formation of double strand breaks (DSB) in the DNA, eventually leading to cell death by inducing O^6-methylguanine (O^6MeG) by the cytotoxic effects of TMZ. DNA repair enzyme MGMT repairs the O^6MeG. The success of TMZ treatment is influenced by the presence of MGMT methylation. MGMT promoter methylation is associated with a higher efficacy in treatment compared to patients with an unmethylated MGMT promoter. The absence of MGMT, responsible for repairing O6MeG, results in GC -> AT transition mutations due to thymine mispairing. Moreover, TMZ demonstrates a higher success rate in elderly patients, similar to the general patient population. Typically, TMZ is combined with radiation therapy to achieve improved survival outcomes (Aasland et al., 2019; Rong et al., 2022).

1.2 Isocitrate dehydrogenase

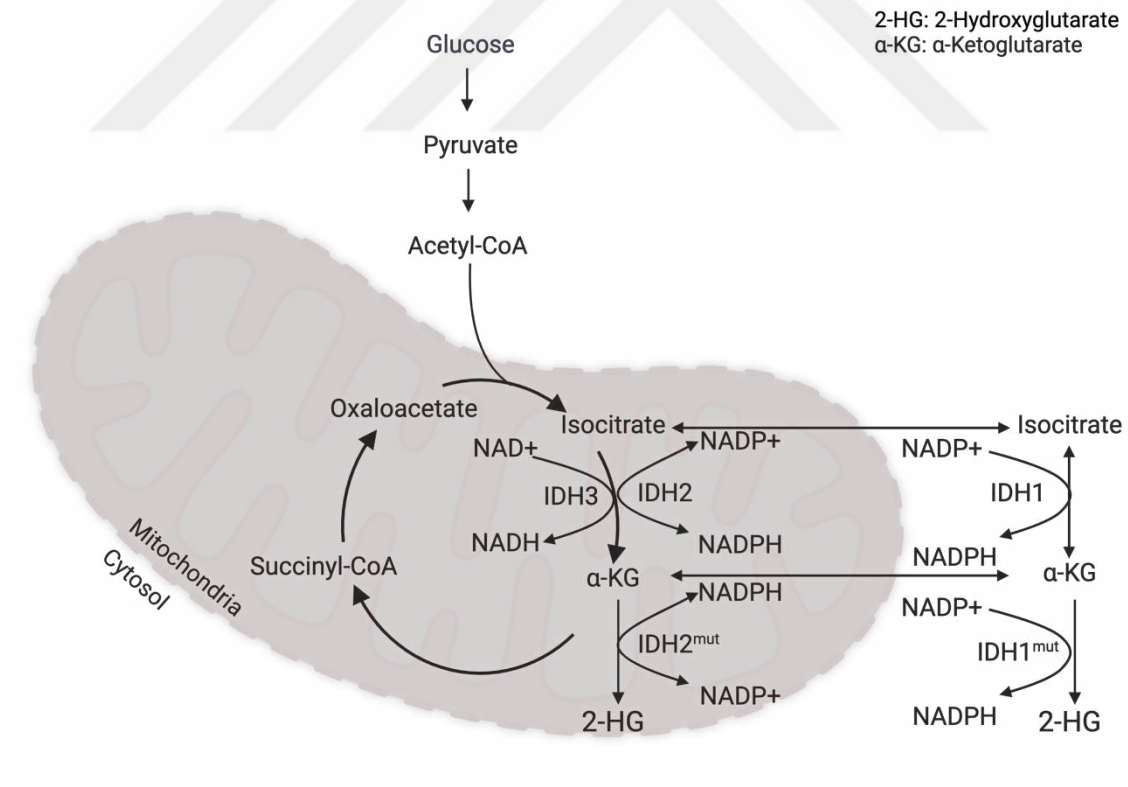

Figure 1.1: Isocitrate dehydrogenase metabolism in TCA cycle and IDH mutations

Isocitrate dehydrogenase (IDH) enzymes have critical roles in cellular metabolism such as Krebs cycle (also known as TCA or citric acid cycle). IDH enzymes have three

isoforms ubiquitously expressed in human cells which include IDH1, IDH2, and IDH3. IDH1 and IDH2 enzymes work as a cofactor to nicotinamide adenine phosphate (also known as NADP+) to produce an antioxidant, NADPH, which is a critical component to buffer reactive oxygen species (ROS) and lipid metabolism (Losman & Kaelin, 2013; Park, 2023; Solomou et al., 2023).

IDH1 and IDH2 enzymes catalyze the reaction for oxidative decarboxylation of isocitrate which leads to generation of a-ketoglutarate, a-KG (2-oxoglutarate, 2-OG) either in cytosol (IDH1) or mitochondria (IDH2). As the reactions catalyzed by IDH1 and IDH2 are reversible, IDH3 enzyme mediates a similar but irreversible reaction in Krebs cycle and mainly regulated by the availability of substrates (Losman & Kaelin, 2013; Neumaier et al., 2023; Park, 2023).

2-oxoglutarate (2-OG) functions as a cofactor for various enzymes known as 2-OG dependent dioxygenases. These include histone lysine demethylases (KDM) of the Jumonji-C (JmjC) family and DNA demethylases of the ten-eleven translocation (TET) family. Furthermore, cytosolic dioxygenases such as prolyl hydroxylase domain (PHD) containing enzymes also rely on 2-OG as a cofactor (Kayabolen et al., 2021).

The IDH1 protein is primarily localized in the cytoplasm and peroxisomes of cells, whereas IDH2 and IDH3 are both localized in the matrix of mitochondria. In the cytoplasm, IDH1 plays a crucial role in glucose and lipid metabolism, as well as providing protection against reactive oxygen species (ROS). IDH2 also functions as a regulatory component in the Krebs cycle and ROS prevention, while IDH3 serves as a central enzyme in the citric acid cycle. IDH1 and IDH2 form homodimers, whereas IDH3 is composed of a heterotetrameric structure. The heterotetrameric IDH3 protein consists of two catalytic α subunits, one β subunit, and one γ subunit. The α subunit is responsible for isocitrate binding, the β subunit facilitates the assembly of enzyme subunits, and the γ subunit acts as an allosteric modulator for the binding of citrate and ADP to the enzyme (Solomou et al., 2023).

1.2.1 IDH-mutant glioma

IDH-mutant diffuse gliomas have a more advantageous prognosis and treatment conditions. In comparison with IDH-wildtype gliomas, IDH-mutant gliomas have a better outcome of treatments for the temozolomide, vincristine, and procarbazine (N. Sharma et

al., 2023) IDH1 mutations are prevalent in gliomas which is associated with 2-hydroxyglutarate (2-HG) formation.

Recent studies have revealed recurrent somatic mutations in IDH1 and IDH2 in various cancers, including a high incidence rate of over 70% in low-grade gliomas (LGG) and an incidence ranging from 55% to 88% in grade IV gliomas. However, no mutations associated with tumor formation have been reported for the IDH3 genes, namely IDH3A, IDH3B, and IDH3G (Solomou et al., 2023).

Missense mutations are the predominant type of mutations observed in IDH. These mutations primarily impact specific residues, including R132 and R100 in IDH1, and R172 and R140 in IDH2. It is noteworthy that the altered arginine residues in IDH1 and IDH2 correspond to each other (e.g., R132 in IDH1 corresponds to R172 in IDH2) and are localized within the substrate binding site of the enzyme. Within the substrate binding site, these residues engage in hydrophilic interactions with the α/β-carboxylate of the isocitrate substrate. Specifically, in mutant IDH1, the highly positively charged arginine residue at position 132 is replaced by histidine, cysteine, glycine, or lysine, which possess lower polarity (Reitman et al., 2010; Solomou et al., 2023).The most prevalent mutation in IDH1 found in gliomas is the acquisition of an arginine-to-histidine mutation (R132H) at codon 132, resulting in loss of the wildtype allele. This mutation is present in approximately 90% of IDH-mutant gliomas. Structural changes in the enzyme occur due to this mutation, leading to alterations between open and closed conformations. Consequently, the mutant enzyme exhibits a weakened affinity for isocitrate, while displaying a higher affinity for α-ketoglutarate (α-KG) and NADPH.

Moreover, the mutation impairs citrate formation, leading to the synthesis and accumulation of the oncometabolite 2-hydroxyglutarate (2-HG). This dysregulates cellular metabolism and epigenetics, resulting in inhibition of cellular differentiation and hypermethylation **(Figure 1.2)**. As a result, IDH-mutant gliomas exhibit over 100-fold higher concentrations of 2-HG compared to IDH-wildtype cells. The induction of 2-HG suppresses α-KG-dependent epigenetic regulators, contributing to the pathogenesis of the disease (Alshiekh Nasany & de la Fuente, 2023; Lita et al., 2021; Neumaier et al., 2023; Solomou et al., 2023).

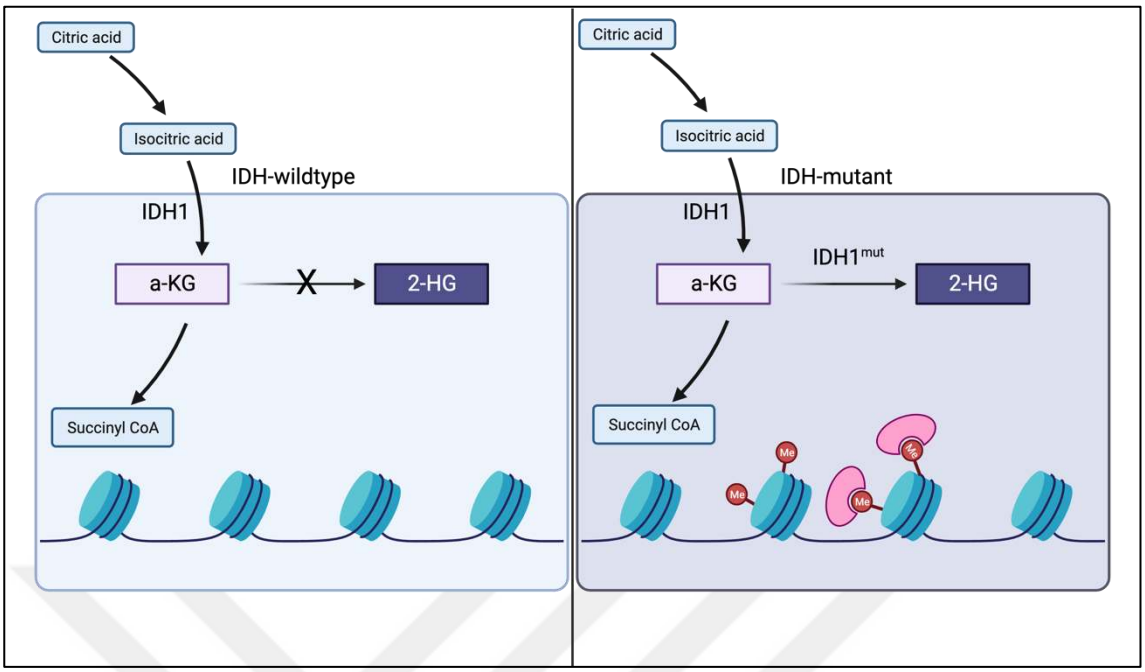

Figure 1.2: IDH mutation leads to 2-HG production and results in DNA and histone hypermethylation

Figure created with Biorender.com

The suppressed α-KG dependent molecules by the 2-HG oncometabolite are ten-eleven translocation (TET) family of 5-methylcytosine hydroxylases and Jumonji C domain containing proteins (JmjC) family of histone lysine demethylases. The suppression occurs competitively and results in the cell de-differentiation and hypermethylation of DNA and histones (Avellaneda Matteo et al., 2017).

IDH-mutant gliomas, specifically, exhibit key alterations, including mutations in the a-thalassemia/mental-retardation-syndrome-X-linked (ATRX) gene and the Tumor protein P53 (TP53) gene. ATRX gene mutations serve as prognostic factors and are more frequently observed in IDH-mutant gliomas compared to IDH-wildtype gliomas. ATRX gene is located on Xq21.1. Also, ATRX is an encoding gene which encodes a protein involved in the chromatin-rearrangement pathway and incorporates histone H3.3 into heterochromatin. ATRX gene mutations often co-occur with IDH1 and TP53 mutations (Grochans et al., 2022).

Another significant mutation is observed in the TP53 gene. TP53 is located on the chromosome 17p13.1 and functions as a tumor suppressor, playing vital roles in regulatory networks and cellular functions such as controlling proliferation and promoting survival. Inactivation of this gene leads to a decrease in cell apoptosis and an

increase in invasiveness. TP53 mutations are also more prevalent in IDH-mutant gliomas (Grochans et al., 2022).

Various therapeutic approaches can be employed to target IDH-mutant gliomas, including IDH-mutant enzyme inhibitors, specific peptide vaccines, strategies aimed at targeting 2-HG induced metabolic bystander effects, and non-IDH-driven therapeutic interventions (J. J. Miller, 2022).

1.2.2 Specific peptide vaccines

With the increased focus on tumor immunotherapy, vaccine therapy for IDH-mutant glioma has been more popular and more promising therapeutic option. After IDH1R132H+ specific peptide vaccine (IDH1-vac) treatment, the T helper cell responses of the mice had induced. The vaccines induce immune response when exposed to the MHC II molecules. However, the clinical trial trials for the IDH1-vac studies are not 100% clear (Y. Huang et al., 2021; N. Sharma et al., 2023). A recent study NOA16 (NCT02454634), a phase I trial with 33 patients from 2015 to 2018 who newly diagnosed $IDH1^{R132H}$ astrocytoma, conducted by Dr. Michael Platten's group showed that the peptide IDH1-vacs are safe and efficient. The study showed that the survival time of the patients have extended, the IDH-vacs were tolerated, and the pseudo-progression (PsPD) has increased. In comparison with the control group, patients received IDH1-vac has a higher PsPD incidence. PsPD is associated with the better prognosis due to IDH1-vac inducing immune responses (Y. Huang et al., 2021; N. Sharma et al., 2023).

1.2.3 Mutant IDH inhibitors

The use of small molecule inhibitors to target IDH-mutant glioma is a rapidly advancing therapeutic approach. Recently, some mutant IDH1 inhibitors have been approved, including ivosidenib (AG120), which is utilized for the treatment of IDH1-mutant Acute Myeloid Leukemia and is classified as a phenyl-glycine compound. Studies have indicated that ivosidenib exhibits a brain penetration rate of 4.1% in rats with an intact blood-brain barrier, suggesting its potential higher penetration in patients. To investigate this further, a clinical study [NCT03343197] is underway for glioma patients (Tian et al., 2022).

In addition to ivosidenib, there are other small molecules targeting IDH1 mutations, such as vorasidenib. Clinical trials (Mellinghoff et al., 2023) [NCT04164901] demonstrated that vorasidenib significantly improved progression-free survival and delayed the need for further interventions in IDH-mutant glioma patients. In this double-blind phase 3 trial, 331 patients were enrolled, with 168 patients receiving vorasidenib and 163 patients receiving a placebo. The vorasidenib group showed a notable improvement in progression-free survival compared to the placebo group. However, it is important to note that the vorasidenib group also experienced adverse effects, which occurred in 22.8% of patients, compared to 13.5% in the placebo group.

Given the single-agent activity of ivosidenib in other cancer types with IDH-mutation, further trials will be necessary to evaluate vorasidenib alone or in combination therapies for IDH-mutant glioma treatment.

1.3 Epigenetics

Epigenetics refers to the investigation of heritable modifications that influence cellular phenotype and gene expression, independent of alterations in the DNA sequence itself. It encompasses DNA-templated processes regulated by chromatin-based events. Epigenetic mechanisms play a vital role in ensuring normal gene expression patterns during the development and maintenance of mammalian organisms (Dawson & Kouzarides, 2012).

Epigenetic mechanisms play a pivotal role in regulating transcriptional processes through a complex network of DNA and histone modifications. These modifications give rise to distinct chromatin states known as heterochromatin and euchromatin. Heterochromatin refers to a condensed chromosomal state that is less accessible and transcriptionally repressed during interphase, whereas euchromatin represents a decondensed and transcriptionally active chromosomal state. By modifying the chromatin structure, epigenetic alterations can either restrict or activate the binding of transcriptional regulators and other regulatory proteins to specific genomic regions, thereby influencing gene expression patterns (Campos & Reinberg, 2009; Hou, 2020; Schübeler, 2015).

However, when these mechanisms become disrupted, it can result in significant changes and modifications in gene expression and function, ultimately leading to cellular transformations. In the context of cancer, global alterations in the epigenetic landscape

are recognized as one of the key hallmarks of the disease. These epigenetic changes contribute to the malignant transformation of cells and can have profound implications for cancer initiation, progression, and therapeutic responses (Dawson & Kouzarides, 2012; Gayon, 2016; S. Sharma et al., 2010).

Epigenetic modifications are classified into three main categories besides DNA and histone modifications as writers, readers, and erasers. The modifications known as "writers" modulate genomic compaction and gene expressions. The second class is known as "readers" which recognize the effector proteins. The modifications known as "erasers" are responsible for removing reversible epigenetic marks and various enzymes (Nicholson et al., 2015a).

The modifiers categorized as writers encompass DNA methyltransferases, histone lysine methyltransferases, protein arginine methyltransferases, and histone acetyltransferases. These chromatin-modifying enzymes add methyl or acetyl marks to chromatin components, leading to diverse effects on transcription, which can vary depending on the cell type. The proteins responsible for mediating methyl and acetyl marks play a crucial role in modulating gene expression through specific mechanisms. The modifiers classified as readers consist of methyl-CpG-binding proteins, histone methylation-binding domains, and histone acetyl-binding domains. Readers are responsible for recognizing the presence of epigenetic modifiers and facilitating their effects on cellular processes. These protein domains bind to the epigenetic marks, serving as crucial mediators in epigenetic regulation. On the other hand, the modifiers classified as erasers include proteins involved in DNA demethylation, histone demethylases, and histone deacetylases. Erasers play a role in modifying the epigenome by removing specific epigenetic marks from chromatin residues. This reversal of epigenetic marks by erasers counteracts the effects of writers, ultimately modulating the transcriptional impact of these marks and influencing gene expression (Nicholson et al., 2015)

DNA Modifications

DNA Methylation

DNA methylation is a well-known epigenetic modification that plays a crucial role in gene regulation. It involves the addition of a methyl group to the cytosine residue at the C-5 position of the cytosine ring in the DNA sequence. This modification is catalyzed by DNA methyltransferases (DNMTs) and is associated with gene silencing. There are

four DNMTs are characterized in human which are DNMT1, DNMT2, DNMT3a, and DNMT3b. De novo DNA methylations are established in DNMT3a and DNMT3b and are maintained by DNMT1. DNA methylation serves as a pivotal mechanism involved in maintaining cellular identity, normal development, genomic imprinting, X-chromosome activation, and suppression of repetitive element transcription. Alterations in DNA methylation patterns have been implicated in various diseases, including cancer. In addition to DNA methylation, there are other DNA modifications that contribute to the epigenetic landscape. These modifications include hydroxymethylation, formylation, and carboxylation (Baylin & Jones, 2011; Egger et al., 2004; Jin et al., 2011; Jones, 2012; Kohli & Zhang, 2013; J. L. Miller & Grant, 2013; Wu & Zhang, 2014).

The DNA methylation mostly occurs on cytosine at CpG islands where CpG dinucleotides are present. Contrary to the expectations, CpG dinucleotides are rare in human genome, around 1%. 70-80% of the CpG dinucleotides are methylated. The unmethylated dinucleotides have the tendency to cluster in islands which are smaller than 200 base pair and contains more than 55% of GC content. About 60% of human gene promoters are associated with CpG islands which are frequently hypermethylated and results in silencing of the promoter of the gene (J. L. Miller & Grant, 2013; Moore et al., 2013).

Hydroxymethylation

Hydroxymethylation, for instance, involves the addition of a methyl group to cytosine at CpG sequences, but with a hydroxyl group replacing the hydrogen at the C-5 position. This modification, known as 5-hydroxymethylcytosine (5-hmC), is generated through oxidation by the TET family of methylcytosine dioxygenases. It has been primarily observed in the brain and other central nervous system tumors in mammals and other organisms. Understanding the various DNA modifications, such as DNA methylation and hydroxymethylation, provides valuable insights into the mechanisms underlying gene expression regulation and developmental processes. These modifications contribute to the complex epigenetic landscape that shapes cellular identity and function. Moreover, dysregulation of DNA modifications can have profound implications for disease development, including cancer. By unraveling the intricate interplay between these DNA modifications and their functional consequences, researchers aim to uncover novel therapeutic strategies and improve our understanding of disease mechanisms (Richa & Sinha, 2014).

Histone Modifications

DNA is packaged in the nucleus with the proteins, called as histones, and forms a DNA-protein complex, called as chromatin. Nucleosome, which is a fundamental unit of chromatin, are consisting of two sets of the four core histones which are H2A, H2B, H3, and H4. Histone H1 ties the nucleosomes together and forms the chromosome. The protruding tail that the histones have might be occurred post-translational modifications (PTMs). Histone modifications represent a category of epigenetic modifications that play a crucial role in regulating gene expression and chromatin structure. The PTMs can be listed as acetylation, phosphorylation, lysine methylation, arginine methylation, deamination, ADP ribosylation, proline isomerization, β-N-acetylglucosamine, ubiquitylation, and sumoylation (Gujral et al., 2020).

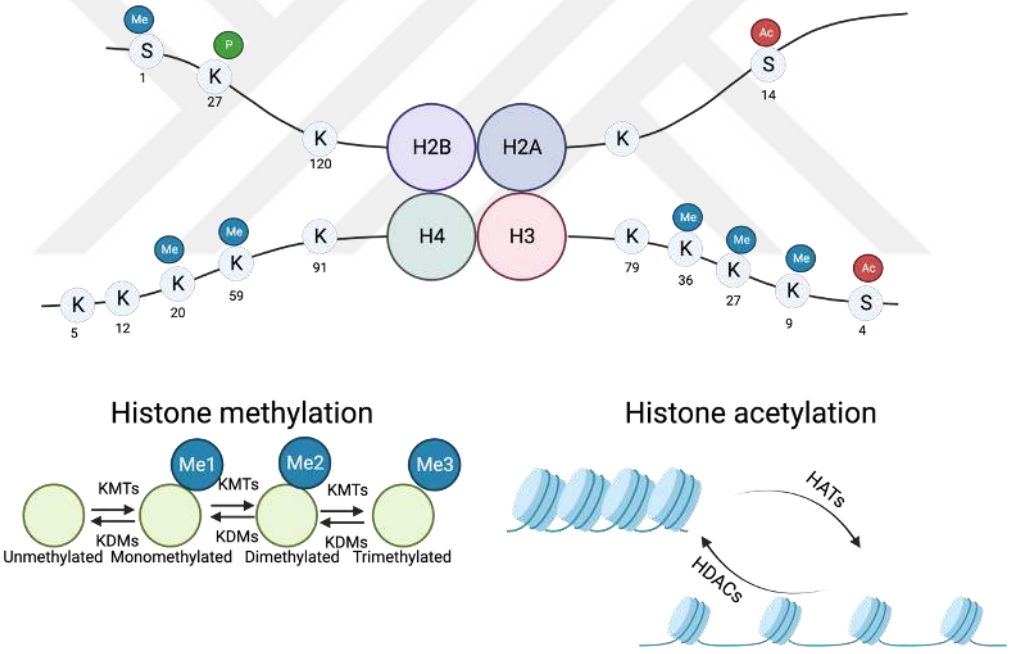

Figure 1.3: Histone modifications.

Figure created with Biorender.com

Histone Acetylation

Histone acetylation plays a crucial role in the regulation of gene expression by impacting the chromatin structure and accessibility of genes. This modification involves the addition of acetyl groups to lysine residues in the histone tails, leading to a more relaxed chromatin conformation and facilitating transcriptional activity. In active and transcriptionally competent regions of the genome, histones are typically highly

acetylated, allowing for increased access of the transcriptional machinery to the underlying DNA. On the other hand, hypoacetylated histones are commonly observed in inactive euchromatic or heterochromatic regions, where gene expression is silenced. The removal of acetyl groups from histones is mediated by histone deacetylases (HDACs), which counterbalance the activity of histone acetyltransferases (HATs) responsible for adding acetyl groups. The dynamic interplay between HATs and HDACs regulates the acetylation status of histones and subsequently influences gene expression patterns (Egger et al., 2004; Gujral et al., 2020).

HATs use CoA as a cofactor and add an acetyl group to the amino group of lysine and they utilize coenzyme A (CoA) as a cofactor to transfer an acetyl group to the amino group of lysine residues on histone proteins. This acetylation neutralizes the positive charge of lysine, thereby weakening the interaction between histones and DNA. Consequently, the loosening of histone-DNA interactions enhances the accessibility of genes, promoting transcriptional activity. HATs can be classified into two main classes: Type A and Type B, based on their subcellular localization and functions. Type A HATs are predominantly found in the nucleus and are involved in histone acetylation related to transcriptional regulation. On the other hand, Type B HATs primarily reside in the cytoplasm and play a role in the acetylation of newly synthesized histones, as well as in modulating nucleosome structure. Dysregulation of HATs has been associated with cancer development, highlighting their significance in cellular processes. HATs function as reversible regulators and are involved in cell cycle progression. Their aberrant activity or expression can contribute to tumorigenesis, making them attractive targets for therapeutic interventions aimed at managing tumor growth (Gujral et al., 2020).

Histone deacetylases (HDACs) are enzymes responsible for the removal of acetyl groups from lysine residues on histone proteins. HDACs can be classified into four groups, namely Class I, Class II, Class III, and Class IV, based on their sequence homology to yeast counterparts. Class I, II, and IV HDACs are Zn2+-dependent enzymes with similar functions, while Class III HDACs are NAD+-dependent. One characteristic of HDACs is their lack of high substrate specificity. A single HDAC can interact with multiple substrates, and multiple HDACs can interact with the same substrate. Furthermore, HDACs often work in complexes with other HDACs and enzymes, making it challenging to discern the individual roles of HDACs within these complexes. In the context of cancer tumorigenesis, HDACs and other epigenetic modifiers exhibit intricate

interactions. HDACs are involved in various cellular mechanisms, including proliferation, cell cycle regulation, and apoptosis. Their dynamic nature as enzymes and protein modifiers contributes to their importance as targets for studying diseases and developing therapeutic interventions (Dokmanovic et al., 2007; Gujral et al., 2020; Haberland et al., 2009).

Histone methylation

Histone methylation is a complex modification that can occur in both active and inactive regions of chromatin. The impact of histone methylation on gene expression is highly context-dependent and varies based on the specific lysine residue being methylated and the extent of methylation (Egger et al., 2004). Histone methyl transferases (HMTs) are responsible for the histone methylation process on the lysine and arginine residues. Histone methylation can take on different forms, including mono-, di-, and trimethylation, at the same residue. Lysine can be mono-, di-, and trimethylated. On the other hand, arginine can be monomethylated or it can be demethylated symmetrically or asymmetrically (Egger et al., 2004; J. L. Miller & Grant, 2013).

Different methylated lysine residues are associated with distinct chromatin states, with some promoting active transcription and others linked to transcriptional repression. For instance, trimethylation of histone H3 at lysine 4 (H3K4me3) is commonly associated with transcriptionally permissive regions, whereas trimethylation of H3 at lysine 27 (H3K27me3) is associated with transcriptional repression. These methylation marks can have permissive or repressive effects depending on the specific residue being modified. For example, H3K4me3 is often associated with transcriptionally active regions, while H3K27me3 is typically associated with transcriptional repression (Egger et al., 2004; Peixoto et al., 2020).

1.3.2 Epigenetic regulation in glioma

The first indications of the connection between cancer and epigenetics appeared with DNA methylation studies. The most crucial point in the analysis of cancer genomes is the driver mutation identification. Mostly, driver mutations are found recurrently in different types of cancers and, they may occur in a high prevalence in a certain tumor type. For example, MLL2, which is a histone methyltransferase, is recurrently found in 90% of

follicular lymphoma. UTX, which is a histone demethylase, is found in 12 different type of cancers (Dawson & Kouzarides, 2012).

In glioma, there are significant changes in cellular metabolism, specifically an increase in the Warburg effect, also referred to as aerobic glycolysis, and impaired phosphorylation. The Warburg effect, which is a prominent characteristic of glioma, is driven by specific glucose transporters (such as GLUT1-4) and glycolytic enzymes (including GAPDH, GLAM, ENO1, and PKM2). The activity of these glycolytic enzymes is tightly regulated by various signaling pathways, including PI3K/Akt, HIF-1/2, p53, tyrosine kinases, and c-Myc. For instance, the activation of the PI3K/AKT pathway in glioma leads to enhanced glucose uptake and glycolysis. Genetic alterations also contribute to the dysregulation of the PI3K/AKT pathway, such as the amplification of epidermal growth factor receptor (EGFR), loss of phosphatase and tensin homolog (PTEN), and amplification of platelet-derived growth factor receptor type A (PDGFRA). Additionally, emerging evidence suggests that epigenetic regulators play critical roles in modulating glioma cell metabolism. These findings underscore the intricate interplay between metabolic reprogramming and epigenetic regulation in glioma cells, shedding light on potential therapeutic targets for intervention (Dong & Cui, 2019; Venneti & Thompson, 2013).

Mutations in IDH1 have been implicated in DNA methylation alterations in gliomas (Noushmehr et al., 2010). IDH1 mutations, such as the common $IDH1^{R132H}$ mutation, result in the production of 2-HG, which structurally resembles α-KG and competitively inhibits α-KG-dependent enzymes (Venneti & Thompson, 2013). One of the affected enzyme families is the TET (Ten-Eleven Translocation) family, which catalyzes the conversion of 5-methylcytosine (5-mC) to 5-hydroxymethylcytosine (5-hmC) and plays a key role in DNA demethylation (Kohli & Zhang, 2013). The presence of $IDH1^{R132H}$ mutation in glioma cells leads to the inhibition of TET2-mediated 5-hmC production (Figueroa et al., 2010). This suggests that IDH1 mutations contribute to DNA methylation patterns and the establishment of the glioma-CpG island methylator phenotype (G-CIMP) (Turcan et al., 2012).

In addition to DNA methylation, $IDH1^{R132H}$-mutated astrocytic cell lines exhibit alterations in histone methylation marks. Specifically, these cell lines show increased levels of H3K27me3, H3K9me3, and H3K36me3 compared to IDH1-wildtype cell lines. The similarity between 2-HG and α-KG allows 2-HG to competitively inhibit α-KG-

dependent enzymes involved in histone lysine demethylation, such as the Jmj-C family of lysine demethylases (KDMs). For example, KDM4C, a member of the Jmj-C family, requires α-KG, Fe(II), and oxygen as cofactors for histone lysine demethylation. However, the presence of 2-HG inhibits the activity of these enzymes, leading to a decrease in histone demethylation and an increase in H3K9 and H3K27 methylation (Chowdhury et al., 2011; Venneti & Thompson, 2013).

Another important regulator in glioma is pyruvate kinase, a key enzyme involved in the glycolytic pathway. Pyruvate kinase catalyzes the conversion of phosphoenolpyruvate (PEP) to pyruvate. There are four isoforms of pyruvate kinase, namely PKM1, PKM2, L, and R. Among these isoforms, PKM2 is upregulated in cancer cells, including glioma, and has been identified as an essential enzyme for the survival of glioma stem-like cells (Lu et al., 2012; Mazurek et al., 2005).

PKM2 has been shown to play a role in the regulation of gene expression through its nuclear translocation and interaction with various transcriptional regulators. Upon activation of the EGFR pathway, PKM2 translocates to the nucleus and phosphorylates histone 3 at threonine 11 (H3T11). This phosphorylation event leads to the removal of histone deacetylase 3 (HDAC3) from the promoter regions of genes such as Cyclin D1 and c-Myc. Subsequently, PKM2 forms a complex with β-catenin, which binds to the promoter regions of Cyclin D1 and c-Myc, resulting in histone acetylation (Luo et al., 2018; Venneti & Thompson, 2013; Yang & Schwartz, 2012).

Notably, mutations in histone 3 (H3) have been associated with altered phosphorylation patterns, which can affect the regulation of gene expression in glioma. The lack of phosphorylation of H3T11 due to H3 mutations may result in the inability to prevent the removal of HDAC3 from the Cyclin D1 and c-Myc promoters, leading to altered transcriptional activation. The phosphorylation of histone 3 at threonine 11 by PKM2 and its correlation with glioma suggest that PKM2 may serve as a key regulator of histone phosphorylation and the EGFR-driven acetylation in glioma (Lewis et al., 2013; Schwartzentruber et al., 2012; Venneti & Thompson, 2013)

1.4 CRISPR-Cas9 mediated knock-out screens

The discovery of the CRISPR-associated endonuclease 9 (Cas9) protein, which is part of the Clustered Regularly Interspaced Short Palindromic Repeats (CRISPR) system,

was made by Charpentier and Doudna in 2012 (Chan et al., 2022). The Cas9 protein, in combination with a guide RNA (gRNA) that matches the target sequence, allows for efficient and specific gene targeting and disruption. This feature has led to the development of widely available CRISPR knockout (KO) libraries (Chan et al., 2022; J. S. L. Yu & Yusa, 2019).

CRISPR-Cas9 mediated knockout screening has emerged as a powerful tool and resource for studying gene functions, identifying potential therapeutic targets, and making biological discoveries. This system enables the introduction of targeted mutations and deletions in genes of interest during screening experiments (Ritchie et al., 2015). Such knockout screens using CRISPR-Cas9 have applications in various fields, including single-cell gene expression analysis, cancer research, studies on specific diseases, and neuroscience research. In cancer research, these screens are used to identify essential genes for cancer cell survival and growth, often leading to the discovery of novel cancer therapies (Ashoti et al., 2020; Bock et al., 2022; Gautron et al., 2020; Ritchie et al., 2015; Straub et al., 2014).

A typical approach in pooled CRISPR screening involves introducing a CRISPR gRNA library to cells in bulk. Each individual cell receives a different gRNA, which perturbs the targeted gene based on the specific gRNA it receives. Lentiviral infection is commonly used for gRNA delivery, integrating the gRNAs into the DNA of the target cells, and inducing perturbations in the genes of interest. Lentiviral delivery is typically performed at a low multiplicity of infection (MOI), such as between 0.1 and 0.6, to ensure that individual cells possess a single gene mutation and to generate a pool of mutant cells. After the cells have treated, the gRNAs usually are counted via high-throughput sequencing. At the end, the representation of the treatment conditions are compared and the depletions or enrichments are identified (Bock et al., 2022; J. S. L. Yu & Yusa, 2019).

1.4.1 EPIKOL

EPIKOL, refers to Epigenetic Knockout Library, is a CRISPR-Cas9 library targeting a wide range of epigenetic modifiers. This library includes 744 epigenetic modifiers, along with 35 essential proteins and provides 10 single guide RNAs (sgRNAs) targeting each gene. Including 80 non-targeting sgRNAs, EPIKOL contains 7870 sgRNAs. Compared with previously published libraries, EPIKOL offers a broader target range and

more sgRNAs per gene with 10 sgRNAs per gene. Moreover, this library can be effectively utilized for both in vitro and in vivo screening approaches. By utilizing the CRISPR-Cas9 system, EPIKOL aims to identify specific vulnerabilities in epigenetic regulation and discover novel target genes, particularly in various biological contexts such as cancer (Yedier-Bayram et al., 2021).

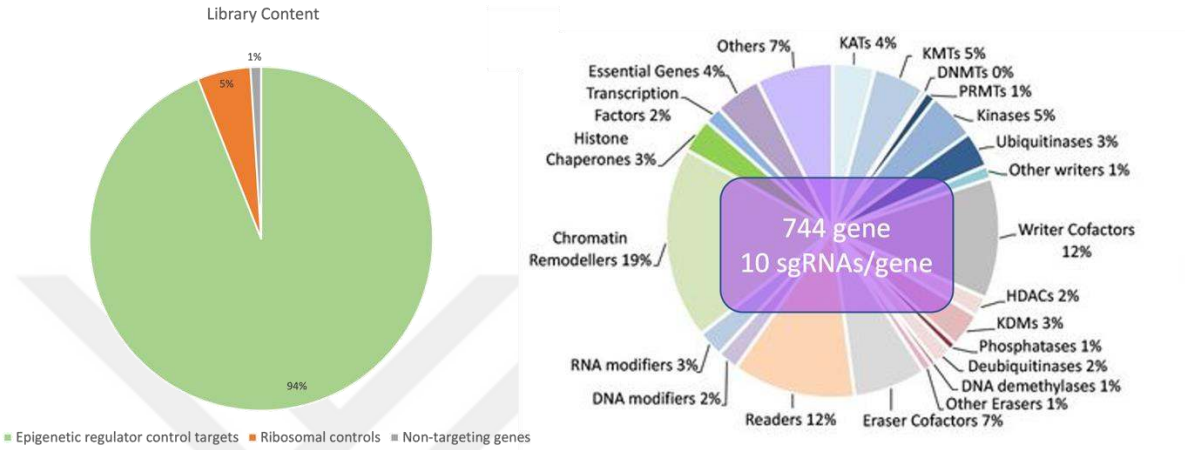

Figure 1.4: Content of EPIKOL Library

(Figure adapted from Yedier-Bayram et al., 2022)

1.5 RBBP7 protein

RBBP7, also referred to as retinoblastoma-binding protein 7 or RBAP46/48 proteins, is a nuclear protein that is widely expressed throughout the body. Its primary function involves regulating gene expression and facilitating chromatin remodeling within various protein complexes, particularly HDAC complexes. RBBP7 participates in several complexes, including the mSin3 co-repressor complex, where it contributes to transcriptional processes by directly interacting with retinoblastoma proteins. Additionally, RBBP7 plays a role in chromatin assembly following DNA replication within the type B histone acetyltransferase complex (Mohajeri et al., 2013; N. Yu et al., 2018).

Furthermore, RBBP7 functions as a promoter of histone deacetylation and transcriptional repression within the core HDAC complex. It also acts as a transcriptional repressor in the nucleosome remodeling and histone deacetylase (NuRD) complex. RBBP7 is involved in the PRC2/EED-EZH2 complex and the nucleosome remodeling factor complex. Notably, RBBP7 interacts with the BRCA1 tumor suppressor protein to

mediate transcriptional regulation, thereby influencing the regulation of cell proliferation and differentiation (Mohajeri et al., 2013; N. Yu et al., 2018).

NuRD complex consists of both enzymatic and non-enzymatic subunits. The non-enzymatic subunits include RBPP7 and its paralog RBPP4, while the enzymatic subunits are CHD3 and CHD4. RBPP7 interacts with HDAC1 and HDAC2, alongside RBPP4, within the NuRD complex, resulting in ATP-dependent chromatin remodeling and histone deacetylation, thereby mediating gene transcription (Mohajeri et al., 2013).

RBPP7 is also a component of the polycomb repressive complex 2 (PRC2) along with RBPP4. While its structural role within the PRC2 complex is not essential for enzymatic activity, RBPP7 interacts with HDAC complexes and is involved in recruiting chromatin modifiers by long noncoding RNAs (lncRNAs) (Davidovich & Cech, 2015; Fischer & Liefke, 2023).

Structurally, RBPP7 is a WD40 domain protein characterized by a seven-bladed β-propeller structure. It interacts with H3 histone through a binding site located on the top of the protein. This interaction occurs through the direct binding of RBPP7 to helix 1 of H4 and H2A, enabling RBPP7 to acquire histone methyltransferase (HMT) activity with specificity for H3K9 and H3K27 (Balboula et al., 2014; H.-J. Li et al., 2016; Millard et al., 2016).

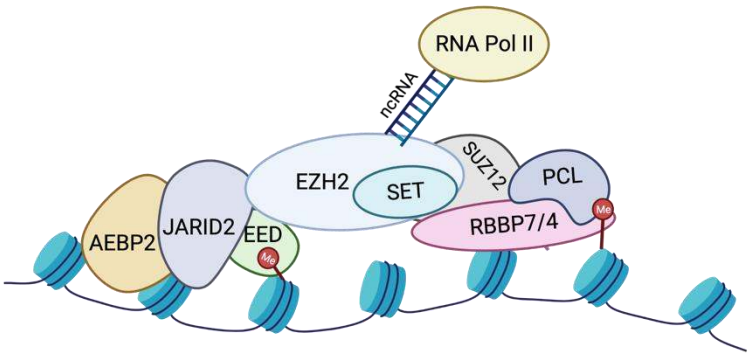

Figure 1.5: PRC2 complex. Figure created with Biorender.com

RBPP7 has been implicated in the regulation of epithelial-mesenchymal transition (EMT), suppression of metastasis, and cancer therapy. Knockdown of RBPP7 affects various biological processes in which it is involved (H.-J. Li et al., 2016).

1.5.1 RBBP7 function in cancers

The involvement of RBBP7 in the development of cancer is intricate. In certain cancer types, like breast cancer and acute leukemias, the expression levels of RBBP7 are elevated. However, an excess of RBBP7 leads to stress-triggered cell death, impeding growth in specific cancer types. Multiple cancer types, including angiocarcinoma, breast cancer, pancreatic cancer, prostate cancer, and gastric cancer, frequently exhibit alterations in the number of RBBP7 copies. Furthermore, mutations in RBBP7 have been identified in colorectal adenocarcinoma, lymphoma, and melanoma. Additionally, RBBP7 has been found to play a role in the advancement of cancer and the spread of cancer cells by inducing EMT (Y. Li et al., 2021; N. Yu et al., 2018).

Mutation or abnormal expression of c-Myc and p53 plays a crucial role in the progression of colorectal cancer. According to Guo (2023)'s findings, a long non-coding RNA called FIT is targeted by c-Myc and is downregulated in colorectal cancer cells. It was also discovered that FIT regulates gene expression by interacting with RBBP7 and p53. This interaction leads to the acetylation of p53 and subsequently reduces the growth of colorectal cancer.

In the context of tumor metastasis, RBBP7 has a dual function depending on its association with different complexes involved in the regulation of EMT-related genes. For instance, in cervical cancer, RBBP7 can activate the E-*cadherin* gene through recruitment by NKX6.1, resulting in the suppression of the *vimentin* gene and inhibition of EMT. In lung cancer, RBBP7 binds to a specific site in the E-*cadherin* promoter, repressing EMT function and acting as a transcriptional activator of the E-*cadherin* gene (Y. Li et al., 2021).

Furthermore, RBBP7 normally interacts with HNF1B, repressing EMT and the SLUG gene. However, in prostate cancer, upregulation of EZH2 suppresses the RBBP7/HNF1B complex. This suppression then leads to the direct inhibition of HNF1B and to promote *SLUG* transcription.

Lastly, in breast cancer, TWIST, which is a transcription factor, recruits the RBBP7/4-MTA1/Mi-2/HDAC1/HDAC2 complex to the proximal regions of the E-cadherin promoter. This recruitment then results in transcriptional repression. This interaction with RBBP7 also contributes to cell invasion and metastasis in breast cancer (Y. Li et al., 2021).

1.6 Aim of the study

The objective of this thesis was to identify the crucial epigenetic modifiers in IDH-mutant glioma cells. To achieve this, we conducted an EPIKOL CRISPR/Cas9 screen on both IDH-wildtype and IDH-mutant glioma cells. This screening allowed us to pinpoint specific essential epigenetic modifiers for each cell type. Subsequently, we selected potential hit genes that could serve as essential candidates for IDH-wildtype and IDH-mutant glioma cells. To validate these modifiers, we performed in vitro assays. After careful consideration, one gene was chosen as the target, and functional assays were conducted to gain a comprehensive understanding of its role and regulation in IDH-mutant glioma.

Chapter 2: **MATERIALS AND METHODS**

2.1 Cell culture

GBM cell line A172, LN229, and human embryonic kidney 293T (HEK293T) cells were purchased from American Type Culture Collection (ATCC, USA). The cell lines were cultured in DMEM (Gibco, USA) supplemented with 10% FBS (Gibco, USA) and 1% Penicillin-Streptomycin (Gibco, USA) in 37^{o}C humidified incubator with 5% CO_2.

2.2 Generation of cell lines

A172 Cas9 stable cells and A172 Cas9 stable IDH1-mutant and IDH-wildtype cells were generated by lentiviral transduction.

2.2.1 Generating Cas9-stable cell lines

A172 Cas9-expressing stable cell lines were generated by lentiviral infection of LentiCas9-blast (AddGene, 52962). The cells were selected with blasticidin for 5 days. Cas9 expression of cells were checked in protein level by western blot, using Cas9 antibody (Table 3).

2.2.2 Generating IDH-wildtype and IDH1-mutant cell lines

IDH1-mutant A172 cells were generated by lentiviral infection of pLenti6.3/TO/V5 containing IDH1 cDNA with R132H mutation. To obtain a paired cell line, the cells were cultured in parallel with A172 IDH-wildtype overexpressed cells. IDH1-mutation expression was checked with western blot by using $IDH1^{R132H}$-mutant specific antibody (DIA-H09, Dianova, Germany).

2.3 CRISPR-Cas9 screening with EPIKOL Library

A172 Cas9 stable IDH1-wildtype and IDH1-mutant cell lines were transduced with EPIKOL (LentiGuide-Puro backbone, Addgene, 52963) at 0.4 MOI with 1000X coverage with 8ug/ml protamine sulphate. The medium of the cells was refreshed after 16 hours. Then, the cells were passaged and selected with 2ug/ml puromycin for 3 days in the next day. After selection ends, $8x10^6$ cells were collected as an initial point sample for sgRNA

distribution to compare with the end point sample. Then, rest of the cells were maintained for 15-16 population doubling. At the end of population doubling time, the end point sample was collected as $8x10^6$ cells. The samples were stored at -80ºC. The screen was conducted by Dr. Fidan Şeker Polat.

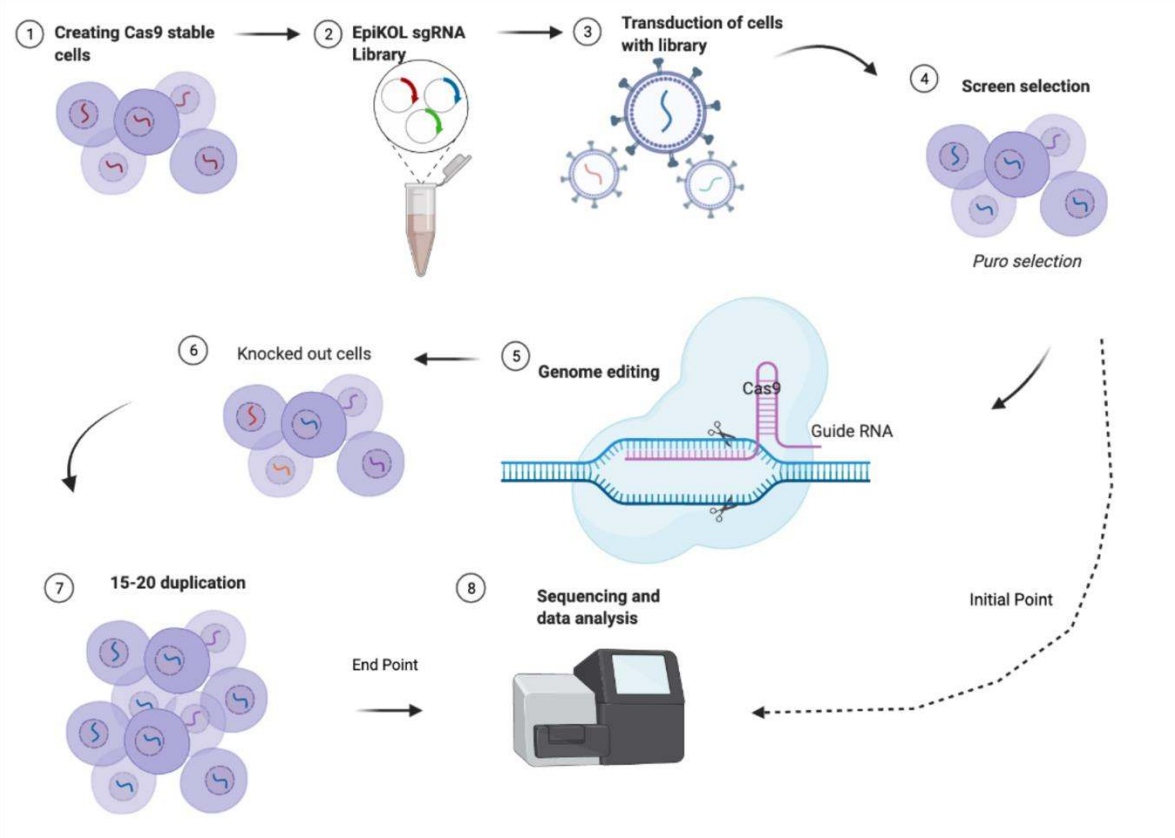

Figure 2.1: CRISPR-Cas9 screening process.

Created with Biorender.com

2.3.1 Genomic DNA isolation and Nested PCR

Using NucleoSpin Tissue Kit (Macherey-Nagel, Germany), genomic DNA (gDNA) was isolated according to the manufacturer's instructions for the tissue lysis protocol. To use as a template for sgRNA amplification, which are integrated into the genome, high quality gDNA is required. For the initial round of nested PCR, also called as external PCR, gDNA amount was calculated as 250x coverage of the library. This coverage equals to the 13.2 µg gDNA per sample. Each sample was divided into four PCR tubes which is corresponding to 3.3 µg of gDNA per 100 µl of reaction. The reaction mixture of nested

PCR includes 3.3 µg of gDNA, 1 µl of Phusion High-Fidelity DNA Polymerase (NEB, USA), 20 µl of 5x GC Buffer (NEB, USA), 2 µl of dNTP mix (10mM) (Thermo Fisher, USA), 5 µl of Forward External Primer (10 µM), 5 µl of Reverse External Primer (10 µM), and Nuclease-free water was added until reaching up to 100 µl of total volume. Next, PCR reaction was performed with an initial denaturation at 95ºC for 3 minutes, then, 17 cycles of denaturation at 95ºC for 25 seconds, annealing at 65ºC for 20 seconds, and extension at 72ºC for 15 seconds. Finally, an extension was performed at 72ºC for 3 minutes. Then, the PCR reactions were combined. In the second round, also known as internal PCR, NGS adapters (Illumina) were added to the end sites of external PCR amplicons together with stagger, index, and index read primer sequences. For the second round PCR, 5 µl of the combined PCR products was used as a template with 5 µl of Forward Stagger Mix (10 µM) and 5 µl of Reverse Index Primer (10 µM) and Nuclease-free water was added up to 100 µl total volume of the reaction. Thermal cycle conditions for the PCR reaction were the same as external PCR, with an only difference in the cycle count was 23 cycles instead of 17. The final amplicons were visualized on agarose gel (2%) and the bands around 350 bp were extracted. NucleoSpin Gel and PCR clean-up kit (Macherey-Nagel, Germany) was used in extraction according to the manufacturer's protocol. The next-generation sequencing (NGS) was performed at Genewiz (USA) with generation of a minimum of 10 million reads/sample.

Table 1: Primer sequences used in nested PCR of EPIKOL screen

External PCR primers for LentiGuide backbone amplification from genomic DNA	
PLG_Ext_Forward	AATGGACTATCATATGCTTACCGTAACTTGAAAGTATTTCG
PLG_Ext_Reverse	CTTTAGTTTGTATGTCTGTTGCTATTATGTCTACTATTCTTTCC
Internal PCR primers	
Forward_stag1	AATGATACGGCGACCACCGAGATCTACACTCTTTCCCTACACGACGCTCTTCCGATCT**A**tcttgtggaaaggacgaaacaccg
Forward_stag2	AATGATACGGCGACCACCGAGATCTACACTCTTTCCCTACACGACGCTCTTCCGATCT**CT**tcttgtggaaaggacgaaacaccg
Forward_stag3	AATGATACGGCGACCACCGAGATCTACACTCTTTCCCTACACGACGCTCTTCCGATCT**GAC**tcttgtggaaaggacgaaacaccg

Forward_stag4	AATGATACGGCGACCACCGAGATCTACACTCTTTCCCTACACGACGCTCTTCCGATCT**TCGA**tcttgtggaaaggacgaaacaccg
Forward_stag5	AATGATACGGCGACCACCGAGATCTACACTCTTTCCCTACACGACGCTCTTCCGATCT**ATCGC**tcttgtggaaaggacgaaacaccg
Forward_stag6	AATGATACGGCGACCACCGAGATCTACACTCTTTCCCTACACGACGCTCTTCCGATCT**GTCAGA**tcttgtggaaaggacgaaacaccg
Forward_stag7	AATGATACGGCGACCACCGAGATCTACACTCTTTCCCTACACGACGCTCTTCCGATCT**TGCATCG**tcttgtggaaaggacgaaacaccg
Forward_stag8	AATGATACGGCGACCACCGAGATCTACACTCTTTCCCTACACGACGCTCTTCCGATCT**CTACGTGA**tcttgtggaaaggacgaaacaccg
Forward_stag9	AATGATACGGCGACCACCGAGATCTACACTCTTTCCCTACACGACGCTCTTCCGATCT**ACTCGTGAT**tcttgtggaaaggacgaaacaccg
lenticrisprV2_rev(index1)	CAAGCAGAAGACGGCATACGAGATCGTGATGTGACTGGAGTTCAGACGTGTGCTCTTCCGATCTctactattctttcccctgcactgt
rev_index2	CAAGCAGAAGACGGCATACGAGAT**ACATCG**GTGACTGGAGTTCAGACGTGTGCTCTTCCGATCTctactattctttcccctgcactgt
rev_index3	CAAGCAGAAGACGGCATACGAGAT**GCCTAA**GTGACTGGAGTTCAGACGTGTGCTCTTCCGATCTctactattctttcccctgcactgt
rev_index4	CAAGCAGAAGACGGCATACGAGAT**TGGTCA**GTGACTGGAGTTCAGACGTGTGCTCTTCCGATCTctactattctttcccctgcactgt
rev_index5	CAAGCAGAAGACGGCATACGAGAT**CACTGT**GTGACTGGAGTTCAGACGTGTGCTCTTCCGATCTctactattctttcccctgcactgt
rev_index6	CAAGCAGAAGACGGCATACGAGAT**ATTGGC**GTGACTGGAGTTCAGACGTGTGCTCTTCCGATCTctactattctttcccctgcactgt
rev_index7	CAAGCAGAAGACGGCATACGAGAT**GATCTG**GTGACTGGAGTTCAGACGTGTGCTCTTCCGATCTctactattctttcccctgcactgt
rev_index8	CAAGCAGAAGACGGCATACGAGAT**TCAAGT**GTGACTGGAGTTCAGACGTGTGCTCTTCCGATCTctactattctttcccctgcactgt
rev_index9	CAAGCAGAAGACGGCATACGAGAT**CTGATC**GTGACTGGAGTTCAGACGTGTGCTCTTCCGATCTctactattctttcccctgcactgt

rev_index10	CAAGCAGAAGACGGCATACGAGAT**AAGCTA**GTGACTGGAG TTCAGACGTGTGCTCTTCCGATCTctactattctttcccctgcactgt
rev_index11	CAAGCAGAAGACGGCATACGAGAT**GTAGCC**GTGACTGGAG TTCAGACGTGTGCTCTTCCGATCTctactattctttcccctgcactgt
rev_index12	CAAGCAGAAGACGGCATACGAGAT**TACAAG**GTGACTGGAG TTCAGACGTGTGCTCTTCCGATCTctactattctttcccctgcactgt
rev_index13	CAAGCAGAAGACGGCATACGAGAT**TTGACT**GTGACTGGAG TTCAGACGTGTGCTCTTCCGATCTctactattctttcccctgcactgt
rev_index14	CAAGCAGAAGACGGCATACGAGAT**GGAACT**GTGACTGGAG TTCAGACGTGTGCTCTTCCGATCTctactattctttcccctgcactgt
rev_index15	CAAGCAGAAGACGGCATACGAGAT**TGACAT**GTGACTGGAG TTCAGACGTGTGCTCTTCCGATCTctactattctttcccctgcactgt
rev_index16	CAAGCAGAAGACGGCATACGAGAT**GGACGG**GTGACTGGA GTTCAGACGTGTGCTCTTCCGATCTctactattctttcccctgcactgt
rev_index17	CAAGCAGAAGACGGCATACGAGAT**CTCTAC**GTGACTGGAG TTCAGACGTGTGCTCTTCCGATCTctactattctttcccctgcactgt
rev_index18	CAAGCAGAAGACGGCATACGAGAT**GCGGAC**GTGACTGGAG TTCAGACGTGTGCTCTTCCGATCTctactattctttcccctgcactgt
rev_index19	CAAGCAGAAGACGGCATACGAGAT**TTTCAC**GTGACTGGAG TTCAGACGTGTGCTCTTCCGATCTctactattctttcccctgcactgt
rev_index20	CAAGCAGAAGACGGCATACGAGAT**GGCCAC**GTGACTGGAG TTCAGACGTGTGCTCTTCCGATCTctactattctttcccctgcactgt
rev_index21	CAAGCAGAAGACGGCATACGAGAT**CGAAAC**GTGACTGGAG TTCAGACGTGTGCTCTTCCGATCTctactattctttcccctgcactgt
rev_index22	CAAGCAGAAGACGGCATACGAGAT**CGTACG**GTGACTGGAG TTCAGACGTGTGCTCTTCCGATCTctactattctttcccctgcactgt
rev_index23	CAAGCAGAAGACGGCATACGAGAT**CCACTC**GTGACTGGAG TTCAGACGTGTGCTCTTCCGATCTctactattctttcccctgcactgt
rev_index24	CAAGCAGAAGACGGCATACGAGAT**GCTACC**GTGACTGGAG TTCAGACGTGTGCTCTTCCGATCTctactattctttcccctgcactgt
rev_index25	CAAGCAGAAGACGGCATACGAGAT**ATCAGT**GTGACTGGAG TTCAGACGTGTGCTCTTCCGATCTctactattctttcccctgcactgt

rev_index26	CAAGCAGAAGACGGCATACGAGAT**GCTCAT**GTGACTGGAG TTCAGACGTGTGCTCTTCCGATCTctactattctttcccctgcactgt
rev_index27	CAAGCAGAAGACGGCATACGAGAT**AGGAAT**GTGACTGGAG TTCAGACGTGTGCTCTTCCGATCTctactattctttcccctgcactgt
rev_index28	CAAGCAGAAGACGGCATACGAGAT**CTTTTG**GTGACTGGAG TTCAGACGTGTGCTCTTCCGATCTctactattctttcccctgcactgt
rev_index29	CAAGCAGAAGACGGCATACGAGAT**TAGTTG**GTGACTGGAG TTCAGACGTGTGCTCTTCCGATCTctactattctttcccctgcactgt
rev_index30	CAAGCAGAAGACGGCATACGAGAT**CCGGTG**GTGACTGGAG TTCAGACGTGTGCTCTTCCGATCTctactattctttcccctgcactgt
rev_index31	CAAGCAGAAGACGGCATACGAGAT**ATCGTG**GTGACTGGAG TTCAGACGTGTGCTCTTCCGATCTctactattctttcccctgcactgt
rev_index32	CAAGCAGAAGACGGCATACGAGAT**TGAGTG**GTGACTGGAG TTCAGACGTGTGCTCTTCCGATCTctactattctttcccctgcactgt
rev_index33	CAAGCAGAAGACGGCATACGAGAT**CGCCTG**GTGACTGGAG TTCAGACGTGTGCTCTTCCGATCTctactattctttcccctgcactgt
rev_index34	CAAGCAGAAGACGGCATACGAGAT**GCCATG**GTGACTGGAG TTCAGACGTGTGCTCTTCCGATCTctactattctttcccctgcactgt
rev_index35	CAAGCAGAAGACGGCATACGAGAT**AAAATG**GTGACTGGAG TTCAGACGTGTGCTCTTCCGATCTctactattctttcccctgcactgt
rev_index36	CAAGCAGAAGACGGCATACGAGAT**TGTTGG**GTGACTGGAG TTCAGACGTGTGCTCTTCCGATCTctactattctttcccctgcactgt
rev_index37	CAAGCAGAAGACGGCATACGAGAT**ATTCCG**GTGACTGGAG TTCAGACGTGTGCTCTTCCGATCTctactattctttcccctgcactgt
rev_index38	CAAGCAGAAGACGGCATACGAGAT**AGCTAG**GTGACTGGAG TTCAGACGTGTGCTCTTCCGATCTctactattctttcccctgcactgt
rev_index39	CAAGCAGAAGACGGCATACGAGAT**GTATAG**GTGACTGGAG TTCAGACGTGTGCTCTTCCGATCTctactattctttcccctgcactgt
rev_index40	CAAGCAGAAGACGGCATACGAGAT**TCTGAG**GTGACTGGAG TTCAGACGTGTGCTCTTCCGATCTctactattctttcccctgcactgt
rev_index41	CAAGCAGAAGACGGCATACGAGAT**GTCGTC**GTGACTGGAG TTCAGACGTGTGCTCTTCCGATCTctactattctttcccctgcactgt

rev_index42	CAAGCAGAAGACGGCATACGAGAT**CGATTA**GTGACTGGAG TTCAGACGTGTGCTCTTCCGATCTctactattctttcccctgcactgt
rev_index43	CAAGCAGAAGACGGCATACGAGAT**GCTGTA**GTGACTGGAG TTCAGACGTGTGCTCTTCCGATCTctactattctttcccctgcactgt
rev_index44	CAAGCAGAAGACGGCATACGAGAT**ATTATA**GTGACTGGAG TTCAGACGTGTGCTCTTCCGATCTctactattctttcccctgcactgt
rev_index45	CAAGCAGAAGACGGCATACGAGAT**GAATGA**GTGACTGGAG TTCAGACGTGTGCTCTTCCGATCTctactattctttcccctgcactgt
rev_index46	CAAGCAGAAGACGGCATACGAGAT**TCGGGA**GTGACTGGAG TTCAGACGTGTGCTCTTCCGATCTctactattctttcccctgcactgt
rev_index47	CAAGCAGAAGACGGCATACGAGAT**CTTCGA**GTGACTGGAG TTCAGACGTGTGCTCTTCCGATCTctactattctttcccctgcactgt
rev_index48	CAAGCAGAAGACGGCATACGAGAT**TGCCGA**GTGACTGGAG TTCAGACGTGTGCTCTTCCGATCTctactattctttcccctgcactgt

The primer sequences were used the same with Yedier-Bayram (2021) are from 5’ to 3’. Genomic DNA isolation and nested PCR was performed by Dr. Fidan Şeker Polat.

2.3.2 CRISPR-Cas9 screen analysis with MAGeCK

To analyze the changes in sgRNA counts at the end of EPIKOL screen, MAGeCK algorithm (version 0.5.8) was used (W. Li et al., 2014). MAGeCK, referred to Model-based Analysis of Genome-wide CRISPR/Cas9 Knockout, is a tool to analyze CRISPR-Cas9 Knockout screens and to determine the essential genes that are required for the survival or the growth of the cells.

Firstly, the raw data was processed, Paired end sgRNA reads of fastq files were counted and normalized to the EPIKOL library size in three biological replicates. During sgRNA counting, the replicates were introduced as individual input files. Then, the replicates were combined in one output file for each sgRNA to determine the levels of log-fold changes. Median normalization was used for the combined counts and the Read Per Million (RPM) normalization of sgRNA counts were used and then converted to Log2 values.

Depleted genes were then performed with p<0.05 cutoff in gene level analysis to identify the significance. Log2 values of the sgRNAs and other plots were then plotted on R, with ggplot2 package. The MAGeCK analysis of the screen and plot generation were performed by Dr. Ali Cenk Aksu.

2.4 Cloning of individual sgRNAs and CRISPR-mediated knock-out

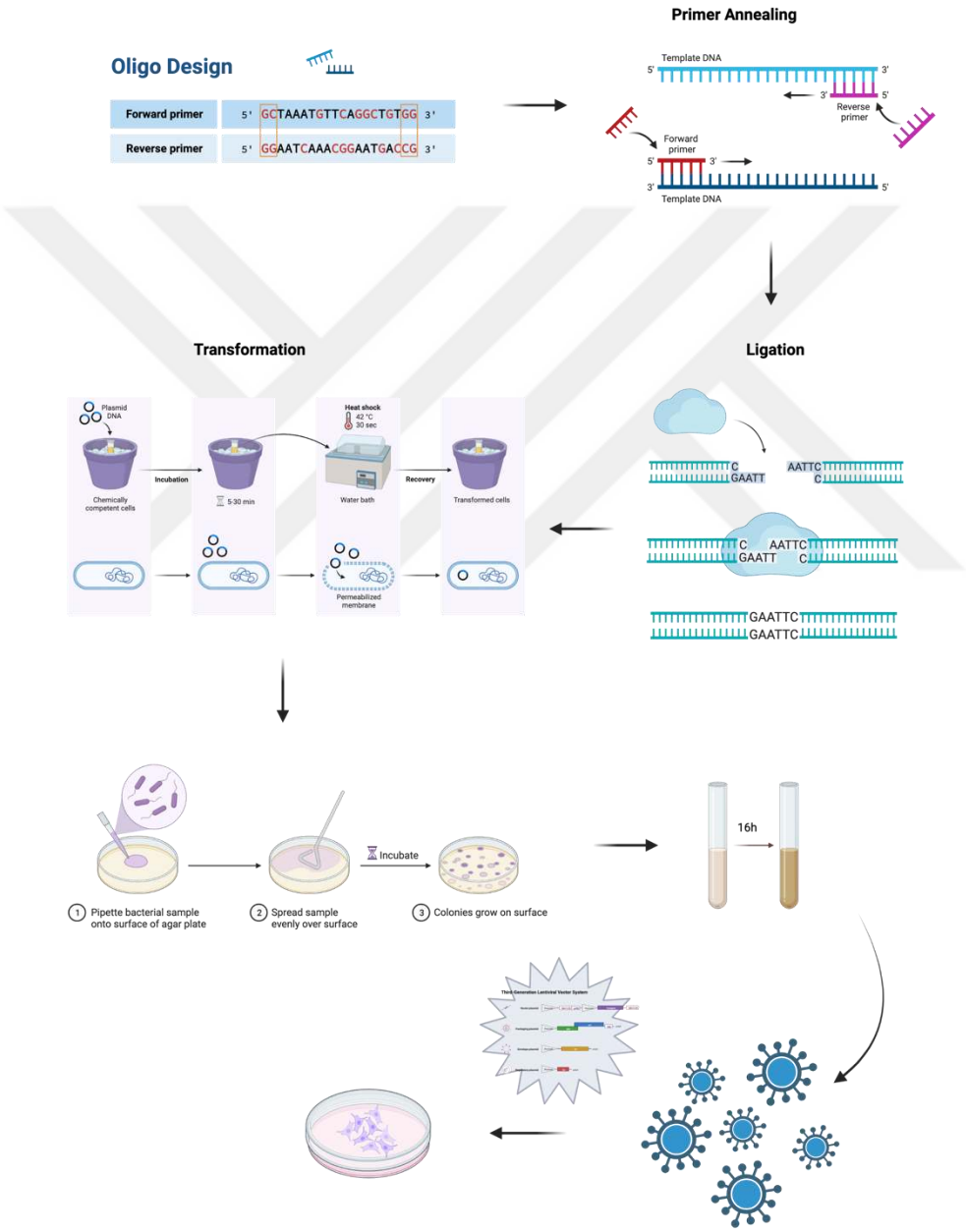

Figure 2.2: Cloning procedure of sgRNAs

sgRNAs were designed and oligos were ordered with overhangs at the 5' end (CACCG) and 3' (CAAA) end which is appropriate for BsmBI v2 (NEB, USA) digestion. The sgRNA list is provided in Table 2.

The oligos were annealed by addition of 1 µl of 100 µM top sgRNA, 1 µl of 100 µM bottom sgRNA, 1 µl of T4 ligase buffer with ATP (NEB) and 0.5 µl of T4 Polynucleotide Kinase enzyme (NEB), and 6.5 µl of ddH_2O to complete the total volume of the reaction to 10 µl. Then, the annealing process was completed on Thermal cycler at 37ºC for 30 minutes, 95ºC for 5 minutes ramping down to 25ºC (5ºC/min). The annealed sgRNA products were diluted in the ratio of 1/200 with nuclease free water and stored at -20ºC.

According to the protocol by Zhang Lab, sgRNAs were cloned into LentiGuide-puro backbone. Before ligation step, backbones were prepared by digesting 5 µg of LentiGuide-puro with 2 µl of BsmBI (NEB, USA) at 55ºC for 4 hours. The digested plasmids were run on 0.8% agarose gel. The upper band on the gel was extracted by using Macherey-Nagel Gel and PCR Clean-up Kit (Macherey-Nagel, Germany) according to the manufacturer's instructions.

The ligation step was then performed by using the mixture of 1 µl of T4 ligase (NEB), 1 µl of 10X T4 Ligase Buffer (NEB), 50 ng of digested plasmid and 1 µl of diluted sgRNAs. Nuclease free water was added up to the total volume is 11 µl and incubated at 16ºC overnight. The ligation products are then transformed into the Stbl3 *Escherichia coli (E. coli)* strain.

For transformation of plasmids, 50 µl of competent bacteria and 5 µl of ligation reaction were mixed and incubated on ice for 30 minutes. Then, the mixture was heat-shocked at 42ºC for 30 seconds in water bath or heat-block. 150 µl of LB broth was added without antibiotics. The bacteria were then growing at 37ºC and 225 rpm for 1 hour. The bacteria were spread on Ampicillin plate and incubated for 16 hours at 37ºC. The colonies were picked and grew in Ampicillin added LB broth for 16 hours at 37ºC by shaking.

The bacteria were centrifuged at 2500 rpm and 4ºC for 25 minutes. The supernatant was removed, and the plasmids were isolated by using either NucleoSpin Plasmid Isolation Kit (Macherey-Nagel, Germany) or NucloSpin Xtra Midi kit (Macherey-Nagel, Germany). All cloned sgRNAs were verified by Sanger sequencing.

2 sgRNA plasmids for each gene, and 1 non-targeting sgRNA was used in the experiments. Cells were infected with lentiviruses of the cloned plasmids. Then, viability

assays, colony forming abilities, and gene expression analysis were performed on the lentivirus infected cells to observe the knock-out effects on the cells.

Table for sgRNA sequences were supplied at Table 2.

2.5 Viral packaging, concentration, and titration

For lentiviral packaging, HEK293T cells were used and $3x10^6$ HEK293T cells were seeded into 10 cm plates one day before transfection. Next day, the confluency reaches approximately 80%. The cells were infected with the mixture of plasmids: 2500 ng target plasmid, 2250 ng psPAX2 (Addgene, 12260), and 225 ng VSV-G (Addgene, 8454) in 200 µl serum-free DMEM. Then, 20 µl of Polyethyleneimine (PEI) (Polyscience, 23966-1) and 180 µl serum-free DMEM. PEI mixture was added to DNA mixture and incubated for 20 minutes. After that, the mixture as 400 µl in total was added onto HEK293T cells drop by drop. 16 hours later, the medium was changed with fresh serum-containing medium. Viral particles containing in the supernatant was collected at the 48 hours and 72 hours after transfection. The total collected medium was filtered with 45um filters.

For concentration, the viruses were mixed with PEG8000 (10% of final volume) (Sigma P2139, dissolved in PBS) for 2 days at 4ºC. Then, supernatants were centrifuged at 2500 rpm for 20 minutes at 4ºC, the supernatant was removed, and the pellets were resuspended in ice-cold PBS to be 50x concentrated. The viruses were aliquoted in 50 µl and stored at -80ºC.

For titer calculation, $2,5x10^5$ cells per well of 6-well plate were seeded. The next day, the cells were transduced with 10, 1, 10^{-1}, and 10^{-2} µl 50x virus together with protamine sulphate (8µg/ml). After 16 hours, the medium was refreshed. The next day, the cells were added puromycin for selection. After selection was completed, the transduced and control cells, were counted to calculate MOI.

2.6 Colony formation assay

To determine the long-term colony forming ability of the cells, cells were seeded into 6-well plates as 2000 cells/well in 3 replicates. Cells were seeded 2^{nd} day after puromycin selection ended. For the irradiation (IR) response experiments, the cells were exposed to the IR (0-8 Gy) after the day of seeding. The cells were grown for 15 days. Then, the medium was discarded, and the wells were washed with PBS. After that, the cells were

fixed with ice-cold 100% methanol for 5-6 minutes. Methanol was removed and the cells were stained with crystal violet for 20 minutes. The crystal violet was removed, and the plates were washed with water. After drying, the plates were scanned, and the colony quantification was done with ImageJ.

2.7 Cell viability with Cell Titer Glo (CTG) assay

To assess the cell viability, Cell Titer Glo (CTG) Luminescent Cell Viability Assay (Promega, Cat# G7570, USA) reagent was used. The cells were seeded into black 96-well plates as 1000 cells per well, with 3 replicates for A172 cell line for each knocked-out genes 5th day after puromycin selection has started. At the timepoints of 0h, 72h, and 120h, the CTG assay was performed. For the day 0 measurement, 10 µl of CTG mix was added onto the wells, for the 72h and 120h timepoints, the medium was discarded, 40 µl of fresh medium was mixed with 4 µl of CTG reagent per well and added onto each well as 44 µl of mixture. After shaking for 2 minutes and incubated at room temperature and in dark for 8 minutes, the measurement was done by reading luminescent by plate reader (Synergy H1 Reader, Bio-Tek, USA). The results were calculated by normalizing each timepoint to the day 0.

2.8 Quantitative Real Time PCR (qRT-PCR)

1000 ng RNA for each sample was used to produce cDNA. RNA samples were melted with 2.5 µl 2mM of dNTP, 100uM random hexamer, and distilled H_2O until the total volume reaches to 16.5 µl. The mixture was incubated for 5 minutes at 65ºC and then transferred to ice. After that, for the reverse transcription reaction, a mixture composed of 5X First Strand Buffer (5 µl per sample), 0.1 M of DTT (2 µl per sample), and RNasin (0.5 µl per sample) was prepared and added 7.5 µl of mixture onto each sample and incubated for 10 minutes at room temperature. After incubation, 1 µl of M-MLV Reverse Transcriptase enzyme (Invitrogen) was added to each sample. Then, the samples were incubated at 37ºC for 1 hour and inactivated at 70ºC for 15 minutes. The complementary DNA (cDNA) samples were diluted by adding 75 µl of dH_2O until the total volume reaches to 100 µl.

After designing qPCR plate, 2 µl of cDNAs were mixed with 18 µl of master mix which contains 10 µl of SYBR-Green Master Mix (Roche), and 1 µl of primer mix, and

7 µl of dH_2O per sample. Samples were measured in Lightcycler 480 Instrument II (Roche). The samples were run for 95ºC for 5 minutes, then 45 cycles of 10 seconds at 95ºC, 30 seconds at 60ºC, and 30 seconds at 72ºC, and resting at 4ºC. By using the normalization to GAPDH, the relative values were calculated with the 2nd absolute derivative method.

Table 2: qPCR primer sequences

Gene	Forward Primer (5' to 3')	Reverse Primer (3' to 5')
GAPDH	AGCCACATCGCTCAGACAC	GCCCAATACGACCAAATCC
RBBP7	TCTGCGGATAAGACCGTAGC	GGCGGTCAGTACCACTTGAA
RPL9	GCACAGTTATCGTGAAGGGC	TTACCCCACCATTTGTCAACC
RPL11	AAAGGTGCGGGAGTATGAGTT	TCCAGGCCGTAGATACCAATG
SIN3A	ACCATTCATGCCTACATTGCCT	CTCCGGTGGCCCCATTATTA
KMT2B	AGTTCTACGATGGGAAGGGCAT	ATGACCCGAGAGAAGCAGTTG
SSRP1	GTCCAAAGAGAAGAAAGAGGAGTGG	ACTTGGATGATGAGCCCCTAGA

2.9 Western blotting

For CRISPR knock-out validation, knocked-out cells were collected, washed with PBS, and the cell pellet was collected. The pellets were stored at -80ºC. During cell lysis, the procedure for whole cell lysates was performed. The pellets were dissolved in RIPA lysis buffer (containing 0.1 mM PMSF and 1X protease inhibitor cocktail (Protease Inhibitor Cocktail Tablets, Roche)) in an appropriate volume for 30 minutes by vortexing in each 10 minutes on ice. Then, the lysates were centrifuged at 1200 rpm and 4ºC for 15 minutes. To check the protein concentrations, Pierce's BCA Protein Assay Kit (Thermo Scientific, 23225, USA) was used according to the manufacturer's instructions.

For each sample, 40 µg of protein was used by mixing 4X Laemmli buffer (Bio-Rad, 1610747, USA) and 10% beta-mercaptoethanol and samples were denatured at 95ºC for 10 minutes. The samples were run on a 4-12% Mini Protean TGX Precast Gel (Bio-Rad, 456-1044, USA). The proteins were then transferred to PVDF membrane using RadTrans-Blot® Turbo™ Transfer System (Bio-Rad, USA). The membrane was blocked for 1 hour at room temperature using 5% non-fat dry milk in TBS-T. The membrane was incubated in primary antibodies at 4ºC overnight. The antibodies listed in … were used in 5% non-fat dry milk prepared in 1X TBST. After the membranes were washed with

1X TBS-T 3 times with 15-minute intervals, the membranes were incubated in appropriate secondary HRP-conjugated antibodies (with 1:10000 dilution) which were prepared in 5% non-fat dry milk. To imaging the membranes, SuperSignal™ West Femto Maximum Sensitivity Substrate (Thermo Scientific, 34095, USA) was used in ChemiDoc XRS+ System (Biorad, USA).

Table 3: Antibody table

Antibody	Brand	Catalog no
IDH1	Dianova	DIA-H09
Cas9	Cell Signaling	14697T
H3 total	Cell Signaling	4499S
a-tubulin	Abcam	ab15246
RBBP7	AB Clonal	A13456
RPL11	AB Clonal	A6407

2.10 Irradiation (IR) response

To determine the IR response of A172 cells, the cells were seeded into 6-well plates as 2000 cells/well. On the next day, the cells were exposed to different dosages of IR (0 Gy, 1 Gy, 2 Gy, 4 Gy, 6Gy, and 8 Gy) in Xstrahl CIX2model irradiator. Then, the cells were incubated at 37°C with 5% CO_2 for 15 days for assessing the long-term colony forming abilities.

2.11 Temozolomide (TMZ) treatment

The A172 cells were seeded into 96-well plates (1000 cells/well) and 12-well plates (1000 cells/well). The cells were treated with Temozolomide (Selleckchem, USA) on the next day. After 72-, 96-, and 120-hours treatments for cell viability assay and 96 hours of treatment for colony formation assay, the medium was removed and for the cell viability assay, 4 µl of Cell Titer Glo (Promega) and 40 µl of serum-free medium was mixed and added per sample and cell viability procedure was performed.

2.12 Statistical analysis

Statistical analyses were performed with student's t test and two-way ANOVA using GraphPad Prism9, version 9.3.1 for Mac (GraphPad Software, San Diego, USA) or Microsoft Excel 365 software. EPIKOL Screen analysis was performed in MAGeCK. Statistical significances were established with asterisks. *P<0.05, **P<0.01, ***P<0.001.

Chapter 3: **RESULTS**

3.1 IDH-wildtype and IDH-mutant cell characterization

In this study, an investigation of epigenetic modifiers on IDH-wildtype and -mutant glioma was undertaken using a custom-made CRISPR-Cas9 library. Glioma cell line A172 was utilized to generate IDH-wildtype and IDH-mutant Cas9 stable cells (**Figure 3.1A**). The cells were initially rendered Cas9 stable to ensure uniform expression levels of Cas9 protein in both IDH-wildtype and IDH-mutant cells. To this end, Cas9 was cloned into the LentiCas9 vector with a blast selection marker, and Cas9 expressing viruses were employed for transduction into A172 cells. Blasticidin antibiotic was utilized to selectively eliminate cells lacking Cas9 protein, ensuring the isolation of A172 cells with integrated Cas9 proteins in their genomes.

Following the successful establishment of Cas9-stable cells, IDH-wildtype and IDH-mutant vectors were post-transduced into cells. To accomplish this, IDH-mutant pLenti6.3/TO/V5 plasmid or IDH-wild type plasmids were utilized to produce lentiviruses. Lentiviral infection and hygromycin selection of A172 cells with the R132H mutation-containing pLenti6.3/TO/V5 resulted in the generation of IDH1-mutant A172 cells.

Finally, the generated cells underwent validation through assessment of protein expression and functional assays. These validation procedures were performed to establish the suitability of the IDH-wildtype and IDH-mutant Cas9 stable cell lines for subsequent investigations of the impact of epigenetic modifiers in glioma pathogenesis.

To examine the stable A172 IDH-wildtype and IDH-mutant cells, firstly, protein levels were assessed using western blotting with IDH1R132H and Cas9 antibodies, along with α-Tubulin antibody as a loading control (**Table 3).** The presence of the IDH1 mutation in the cells was evaluated using the IDH1R132H antibody, which specifically binds to the R132H mutant IDH. As depicted in **Figure 3.1A**, a distinct band at 46 kDa was observed only in IDH-mutant cells, confirming the expression of the mutant IDH1. Additionally, both the IDH-wildtype and IDH-mutant cells exhibited a prominent Cas9 band at 150 kDa, indicating the expression of Cas9 protein in both cell types.

The phenotype of A172 glioma cells exhibits variations between IDH-wildtype and IDH-mutant glioma, particularly concerning cell morphology and growth patterns. IDH-

wildtype cells display an elongated morphology with spindle-shaped characteristics, whereas IDH-mutant cells tend to exhibit a more rounded and polygonal shape. **Figure 3.1B** illustrates these morphological distinctions between A172 Cas9 stable IDH-wildtype and IDH-mutant cells.

IDH-mutant glioma exhibits increased vulnerability and responsiveness to adjuvant therapies, such as radiation therapy and temozolomide, and is associated with prolonged survival. In this study, the response disparities between IDH-wildtype and IDH-mutant cells to varying doses of radiation were evaluated using a long-term colony formation assay (**Figure 3.1 C**). The results revealed that IDH-mutant cells demonstrated higher vulnerability to radiation. Specifically, a significant difference was observed in IDH-wildtype cells exposed to 2 Gy of ionizing radiation (IR), while a significant change in effect was evident at 4 Gy of IR exposure. Subsequently, at 6 Gy and 8 Gy of radiation exposure, all IDH-wildtype cells were eradicated, with no colonies formed.

On the other hand, IDH-mutant cells exhibited a notable difference in colony formation ability starting from the 2 Gy IR exposure. Cell eradication commenced at 4 Gy of IR exposure, and no colonies were formed after 6 Gy and 8 Gy of IR exposure. These findings indicate the differential sensitivity of IDH-wildtype and IDH-mutant cells to varying doses of radiation, with IDH-mutant cells being more susceptible to the deleterious effects of radiation in comparison to their IDH-wildtype counterparts.

In addition, response differences between IDH-wildtype and IDH-mutant cells to another adjuvant therapy, temozolomide therapy, were assessed using cell viability and long-term colony formation assays (**Figure 3.2**). Ascending doses of temozolomide were administered to A172 IDH-wildtype and IDH-mutant cells.

In the colony formation assay (**Figure 3.2A**), both IDH-wildtype and IDH-mutant A172 glioma cells were exposed to different doses of temozolomide, including 25 μM, 50 μM, and 100 μM, along with DMSO control. In the case of IDH-wildtype glioma, the cells displayed a gradual decrease in colony density starting from 12.5 μM, reaching about 30% of the initial density. Subsequently, the colony density continued to decrease with increasing doses. On the other hand, IDH-mutant cells exhibited a more pronounced response to temozolomide, showing a dramatic reduction in colony density of approximately 10% at 12.5 μM. As the temozolomide doses increased, the colonies were significantly diminished, indicating that IDH-mutant cells were more susceptible to temozolomide treatment compared to IDH-wildtype cells. These results suggest that IDH-

mutant glioma cells displayed a heightened vulnerability to temozolomide, similar to their response to previous adjuvant therapies.

In the cell viability assay of TMZ (**Figure 3.2**), cells were exposed to 25 μM, 50 μM, and 100 μM of temozolomide for 96 hours, with DMSO (100 μM) as a control. From the 25 μM temozolomide exposure onwards, discernible differences in cell response were observed. At 25 μM of TMZ, IDH-wildtype cells exhibited approximately 80% survival, while IDH-mutant cells demonstrated around 65% survival. When exposed to 50 μM of TMZ, IDH-wildtype cells displayed a decrease to 75% survival, and IDH-mutant cells experienced a decrease to approximately 60% survival. Upon exposure to 100 μM of TMZ, IDH-mutant cells were significantly impacted, with survival falling below 50%, whereas IDH-wildtype cells experienced a decline to around 65% survival. Overall, the TMZ response was more profound in the IDH-mutant cells compared to IDH-wildtype cells.

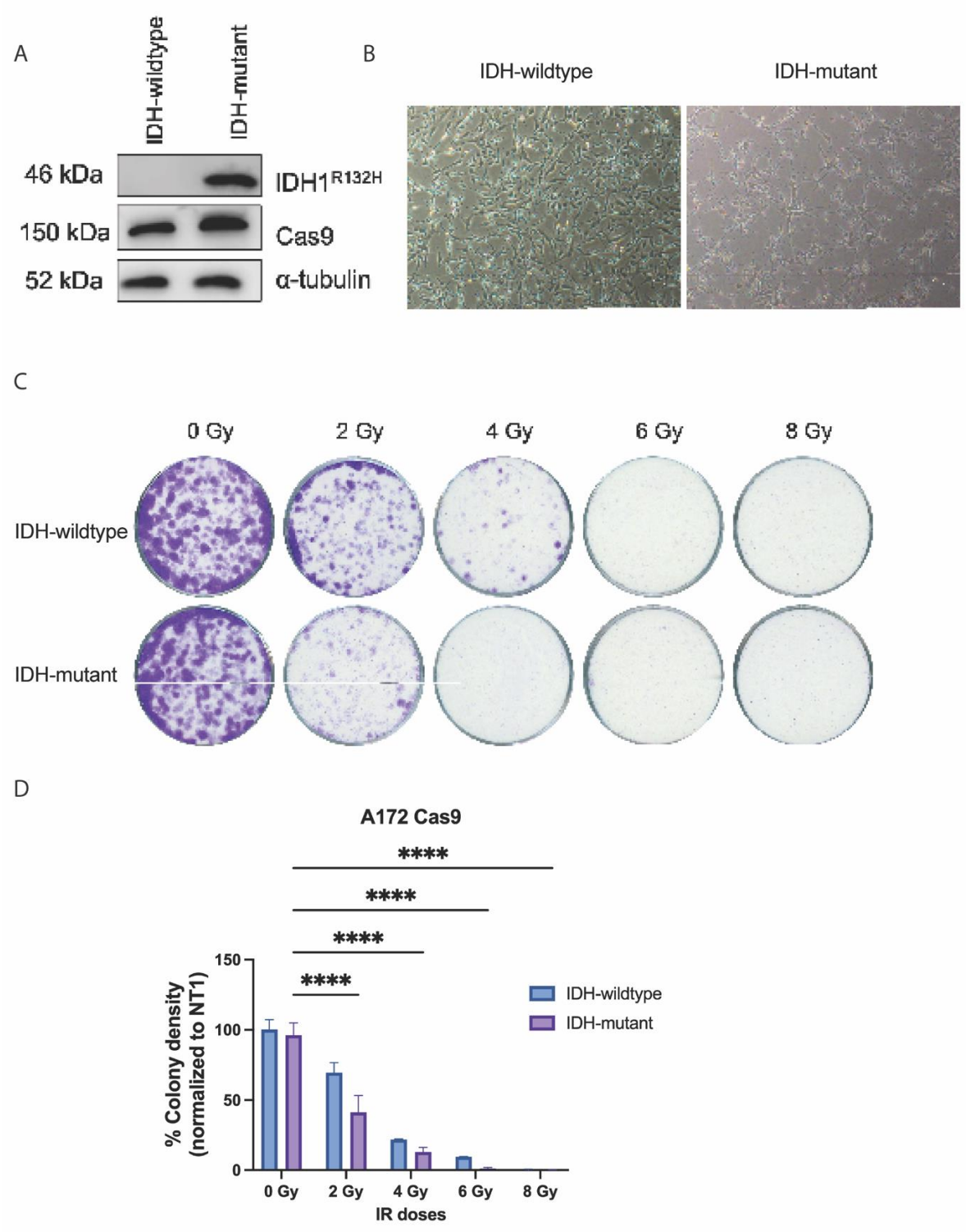

Figure 3.1: Characterization of A172 IDH-wildtype and IDH-mutant cells.

A. Western blot image for assessing protein levels of IDHR132H mutation and Cas9 proteins in IDH-wildtype and IDH1^{R132H} -mutant cells. IDH-mutant cells show expression to IDH1^{R132H} antibody. Both cells show Cas9 expression. **B.** Brightfield microscope images of morphologies of IDH-wildtype and IDH-mutant cells. After IDH-wildtype and

IDH-mutant overexpression, cell phenotype and growth rates differ. IDH-mutant cells grow slower compared to IDH-wildtype cells. **C, D.** Colony formation abilities of IDH-wildtype and IDH-mutant cells after IR exposure and quantification of colony formation assay. IDH-mutant cells show more response in IR exposure starting at 2 Gy compared to IDH-wildtype cells.

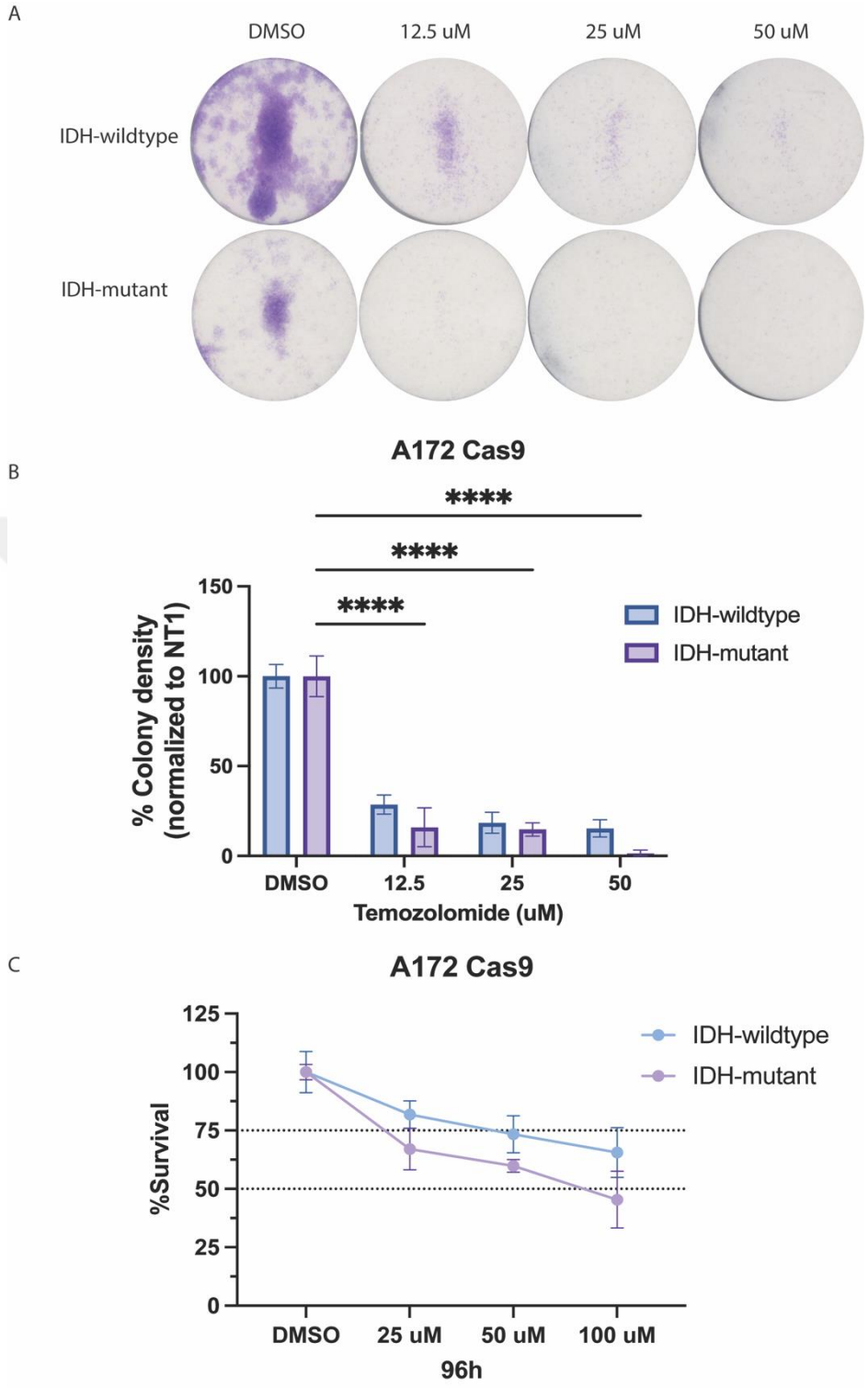

Figure 3.2: Temozolomide response of A172 IDH-wildtype and IDH-mutant cells.

A, B. Colony formation assay for Temozolomide response of IDH-wildtype and IDH-mutant glioma cells in different dosages (DMSO, 12.5 µM, 25 µM, and 50 µM) and quantification of colony formation assay. IDH-mutant cells are more responsive to TMZ treatment. As IDH-mutant colony density decreased around 15%, IDH-wildtype

colony density decreased about 25%. **C.** Cell viability response to different dosages of Temozolomide (DMSO, 25 μM, 50 μM, 100 μM). In the highest dose (100 μM) of TMZ, IDH-mutant cell viability decreased below 50% in 96 hours.

3.2 EPIKOL Screen in IDH1-wildtype and IDH1-mutant glioma cells

Epigenetic vulnerabilities of IDH-wildtype and IDH-mutant glioma were assessed through the utilization of a CRISPR-Cas9 screen employing the custom-made epigenome wide library, EPIKOL. The EPIKOL screen was executed on A172 IDH-wildtype and IDH-mutant cell lines. In order to evaluate the screen's quality and dependability, several analyses were conducted, as detailed below:

3.2.1 EPIKOL sgRNA read counts and distributions

The EPIKOL screen was conducted on Cas9 stable A172 IDH-wildtype and IDH-mutant cells, performed by Dr. Fidan Şeker-Polat. The distribution of the single guide RNAs (sgRNAs) from the library was examined in the screen using the MAGeCK analysis method. MAGeCK is a bioinformatics tool widely utilized to analyze CRISPR-Cas9 screens and infer sgRNA distributions (W. Li et al., 2014).

The read-count distribution of sgRNAs in both the IDH-wildtype and IDH-mutant cells, specifically focusing on the after puromycin (AP) and endpoint (EP) samples, were assessed via MAGeCK. AP samples represent the initial point samples collected after the puromycin selection phase, while EP samples represent the final samples collected at the end of the experiment.

As shown in the **Figure 3.3,** the results obtained from the MAGeCK analysis, the sgRNA distribution in the IDH-wildtype cells exhibit a balanced distribution across both AP and EP samples. This suggests a consistent representation of the sgRNAs in the IDH-wildtype cells throughout the course of the experiment.

In contrast, the sgRNA distribution in the IDH-mutant cells showed variability between the repeats of AP and EP samples. This observation implies a non-uniform representation of sgRNAs in the IDH-mutant cells, suggesting potential differences in the epigenetic vulnerabilities and gene regulation pathways between the two cell types.

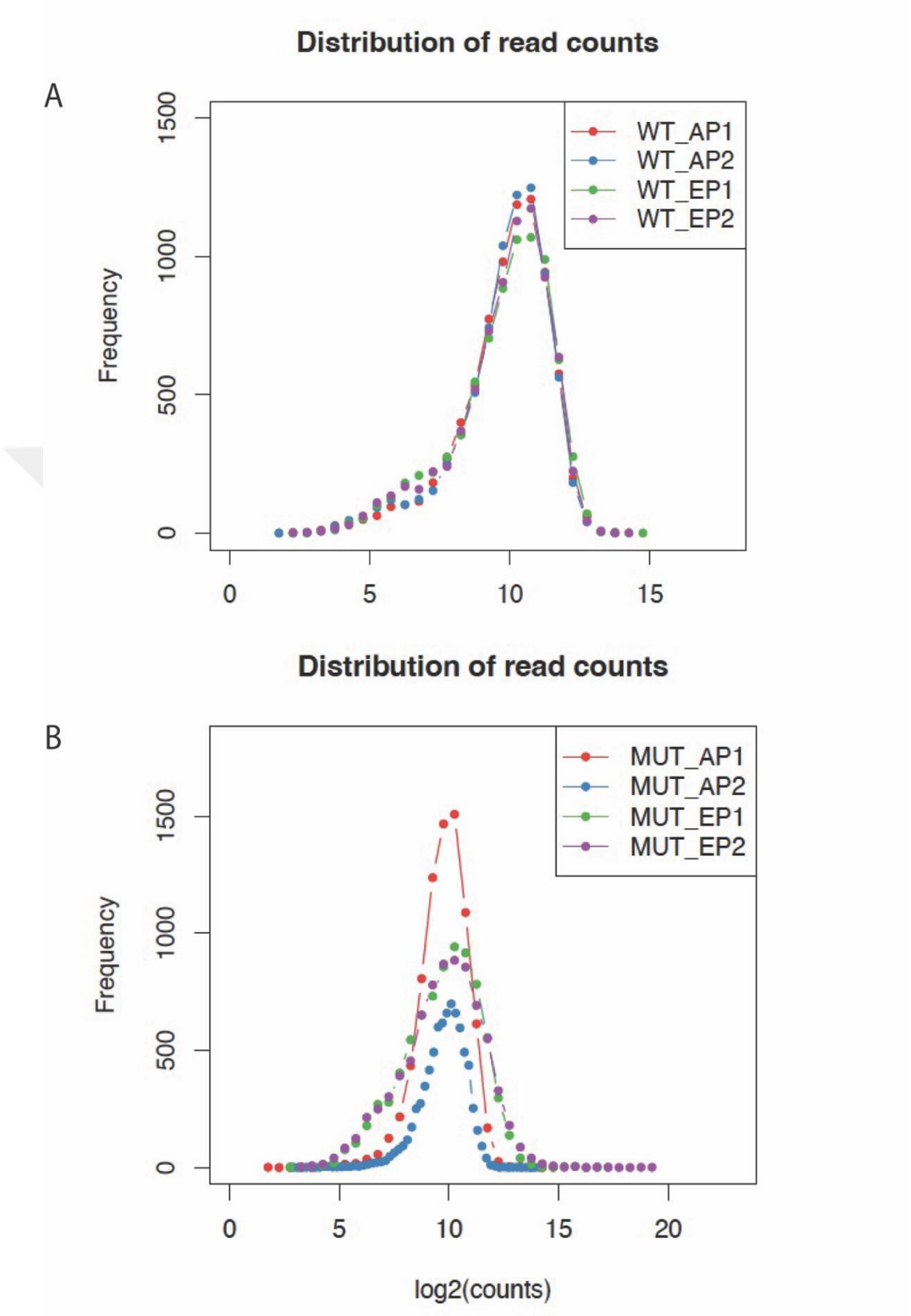

Figure 3.3: Distribution of sgRNA counts on A172 cells transduced with LentiGuide EPIKOL and the data was analyzed with MAGeCK algorithm.

A, B. sgRNA distribution of Cas9-stable A172 IDH-wildtype cells (A) and the sgRNA distribution of Cas9 stable A172 IDH-mutant cells (B). Both IDH-wildtype and IDH-mutant sgRNA read-counts show normal distribution.

After the AP and EP sample distributions of IDH-wildtype and IDH-mutant cells, single guide RNAs (sgRNA) of different genes were identified using the normalized count data of sgRNAs. By using the sgRNA representation of each gene, the most optimal working sgRNA pair was chosen for the following experiments. The optimum sgRNAs were chosen according to their representation at the initial point (AP) and endpoint (EP) for both IDH-wildtype and IDH-mutant cells.

Following the analysis of the AP and EP sample distributions in IDH-wildtype and IDH-mutant cells, the identification of sgRNAs targeting various genes was accomplished by employing the normalized count data of sgRNAs (**Figure 3.4 and 3.5).** This process involved assessing the representation of each gene through its corresponding sgRNAs. To infer the normalized counts of sgRNAs, the normalized counts were then calculated to account for variations in sequencing depth and efficiency, enabling a more accurate comparison between samples.

With the normalized counts of sgRNAs at hand, the most optimal working sgRNA pair for subsequent experiments was selected. This crucial step involved carefully examining the representation of sgRNAs at the AP and EP in both IDH-wildtype and IDH-mutant cells. The objective was to identify sgRNA pairs that consistently exhibited balanced representation across the AP and EP samples, indicative of their reliability and effectiveness in targeting specific genes.

By choosing the most appropriate sgRNA pairs, researchers ensure robust and reproducible results in their investigations. These optimal sgRNA pairs serve as reliable tools for functional assays, enabling the perturbation of specific genes in IDH-wildtype and IDH-mutant cells.

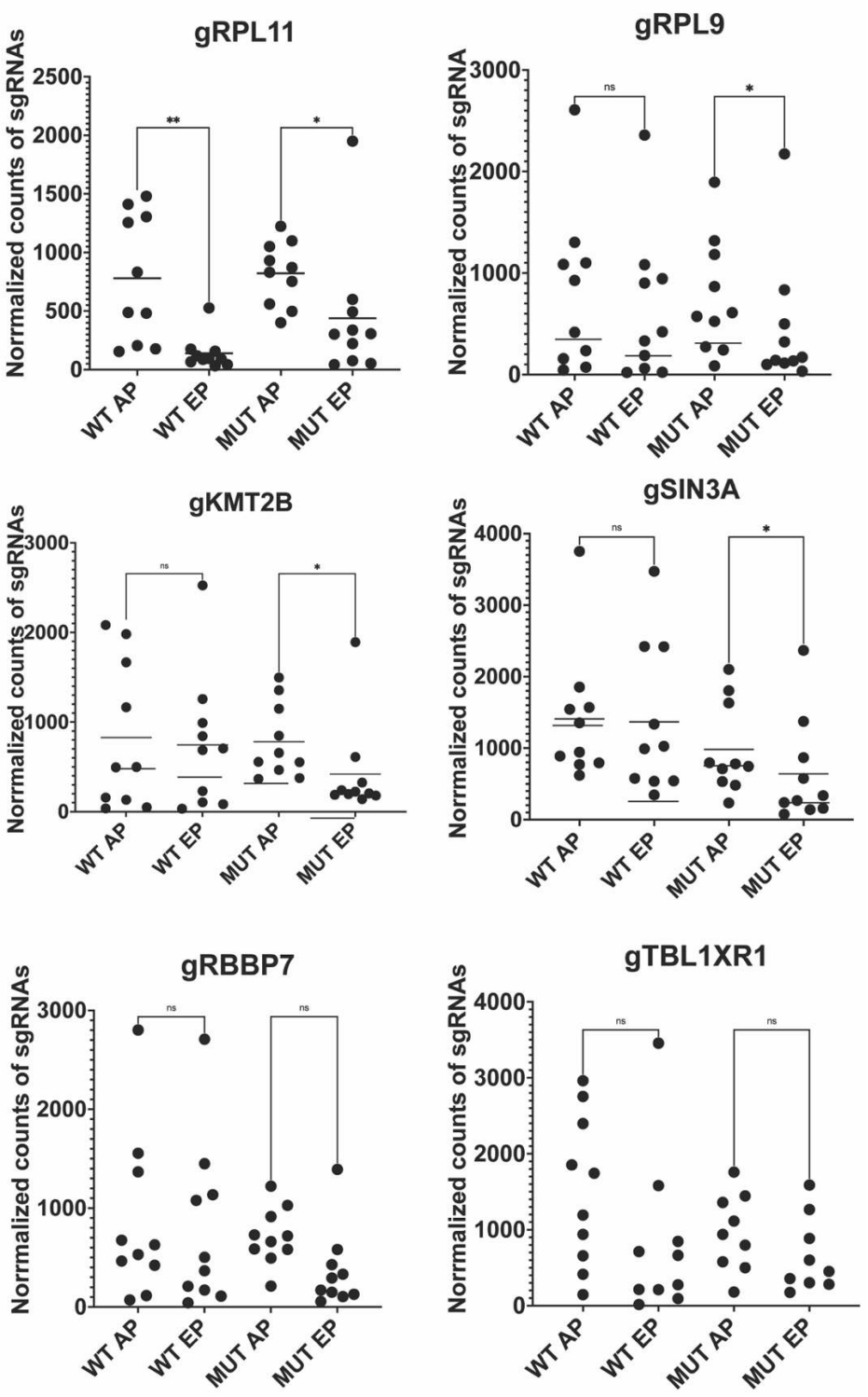

Figure 3.4: Normalized counts of sgRNAs at AP and EP for IDH-wildtype and IDH-mutant cells for individual genes.

Normalized sgRNA counts for RPL9, RPL11, KMT2B, SIN3A, RBBP7, and TBL1XR1 were demonstrated at the initial (AP) and end (EP) points for the Cas9 stable A172 IDH-wildtype and IDH-mutant cells.

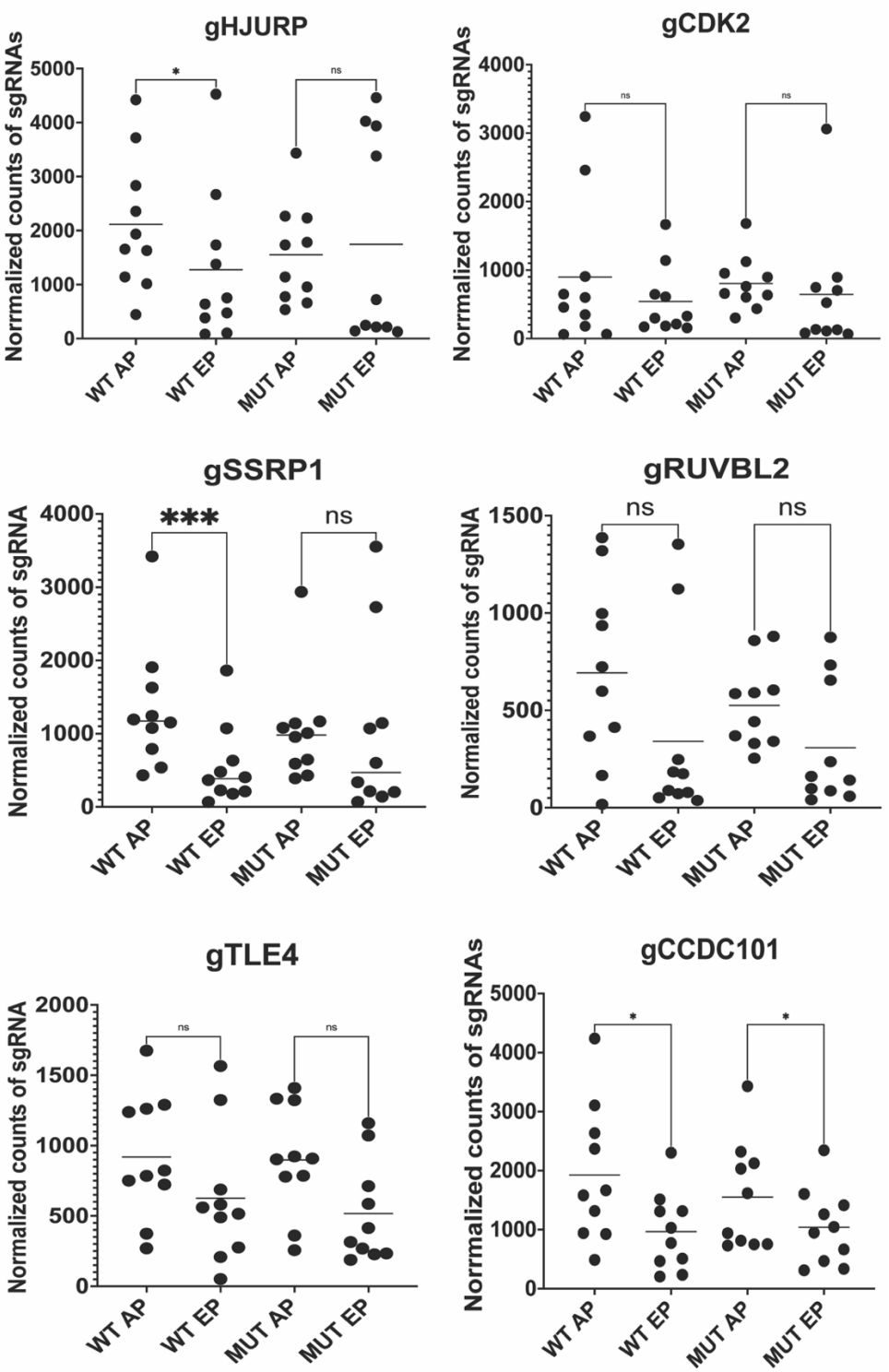

Figure 3.5: Normalized counts of sgRNAs at AP and EP for IDH-wildtype and IDH-mutant cells for individual genes.

Normalized sgRNA counts for HJURP, CDK2, SSRP1, RUVBL2, TLE4, and CCDC101 were demonstrated at the initial (AP) and end (EP) points for the Cas9 stable A172 IDH-wildtype and IDH-mutant cells.

3.2.2 Quality Assessment of the EPIKOL Screen

The assessment of EPIKOL screen quality and its characteristics was conducted through the examination of sgRNA distributions in A172 IDH-wildtype and IDH-mutant glioma cells (**Figure 3.5**) and by employing principal component analysis (PCA) (**Figure 3.7).**

For the evaluation of screen quality, the distribution of non-targeting sgRNAs and positive control sgRNA (for genes encoding ribosomal proteins) counts was translated to Log2 values, as depicted in **Figure 3.6**. As anticipated, non-targeting sgRNAs clustered around the diagonal, as they do not exert any effect on either IDH-wildtype or IDH-mutant cells. Conversely, ribosomal sgRNAs, which target essential genes for both cell types, were positioned below the diagonal. This observation was due to the loss of cells harboring sgRNAs against cellular fitness genes during the experiment, resulting in a reduced number of sgRNAs.

Furthermore, the application of principal component analysis demonstrated the separation between the initial and endpoint samples in both IDH-wildtype (**Figure 3.7A**) and IDH-mutant (**Figure 3.7B**) cells. The distinct clustering of samples along the principal components suggests dynamic changes in the cellular landscape between the initial and endpoint time points.

Together, the assessment of sgRNA distributions and principal component analysis provided valuable insights into the quality and performance of the EPIKOL screen. These analyses confirmed the reliability of the screen results for both IDH-wildtype and IDH-mutant cells. The observed separation of samples in PCA highlights potential differences in gene regulation and cellular responses between the two glioma cell types, hinting on their distinct functional characteristics.

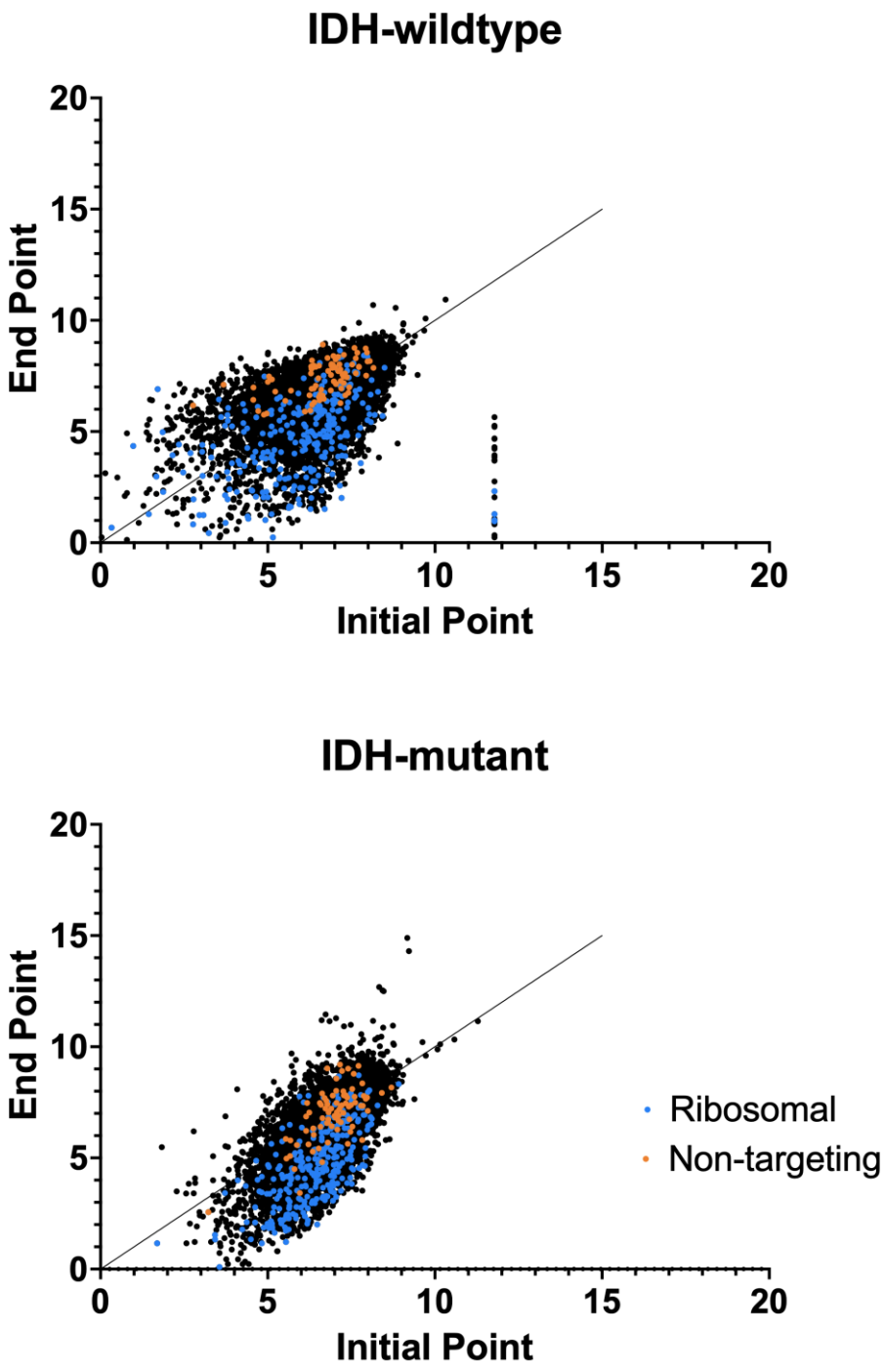

Figure 3.6: sgRNA distributions of EPIKOL screen on A172 IDH-wildtype and IDH-mutant cells.

Read counts of initial point (AP) and endpoint (EP) were normalized as read per million and transformed to Log2 values. Non-targeting sgRNAs are localized on diagonal and the representations do not show decrease. Ribosomal controls (positive controls) are located below the diagonal which shows a decrease in endpoint samples compared to initial point.

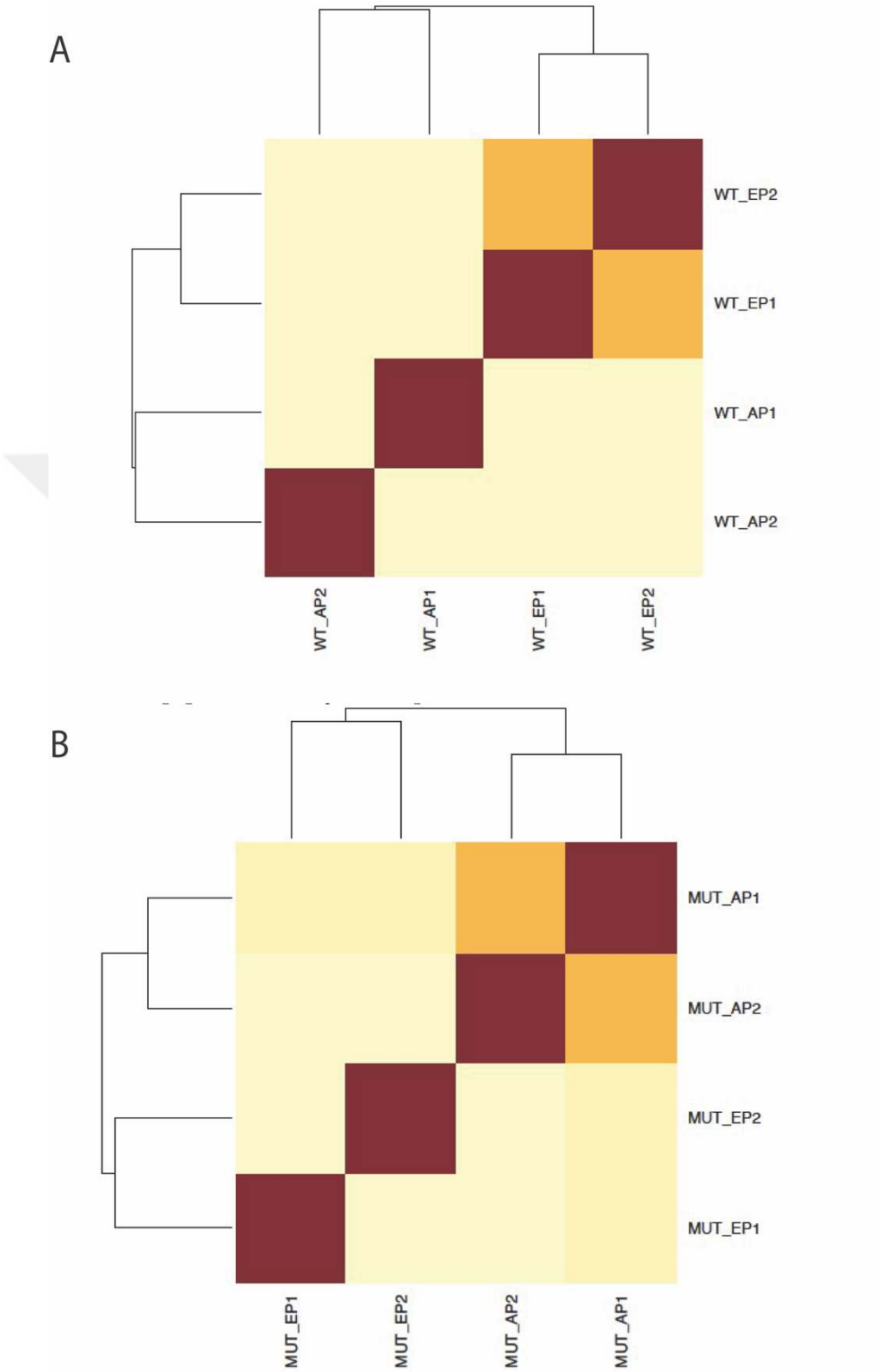

Figure 3.7: Principal component analysis of A172 IDH-wildtype (A) and IDH-mutant glioma cells (B)

3.2.3 EPIKOL sgRNA depletions

Following the completion of the quality check of the EPIKOL screen, MAGeCK analysis was performed on A172 IDH-wildtype and IDH-mutant cells. The MAGeCK analysis is an algorithm utilized for assessing gene-level depletions, employing median normalization of the three biological replicates (**Figure 3.8).**

In this analysis, essential genes were identified as those exhibiting depletion at the end of the screen, while non-targeting sgRNAs showed minimal or negligible changes. The results of the MAGeCK analysis unveiled several epigenetic modifiers deemed essential for Cas9 stable A172 IDH-wildtype and IDH-mutant cells on a waterfall graph. The waterfall graph visually portrays the gene-level depletions, indicating the extent of essential gene targeting in both IDH-wildtype and IDH-mutant cells. This graph aids in identifying the most significant gene depletions to offer valuable insights into the epigenetic vulnerabilities specific to each cell type.

To assess essentiality in IDH-mutant cells, we focused on genes with an overall higher log2 fold change compared to IDH-wildtype cells. Consequently, the representation of sgRNAs targeting essential genes was observed to be lower in terms of sgRNA count within the pool of IDH-mutant cells at the endpoint sample.

For instance, the essential genes for IDH-mutant cells, such as KMT2B, SIN3A, and RBBP7, were identified, while IDH-wildtype cells had their own set of essential genes, including CCDC101, SSRP1, and TBL1XR1. These essential genes were also identified through scaling based on both log10 p-value and Log2 fold change values, as depicted in **Figure 3.9.**

The genes identified through MAGeCK analysis were represented on the Venn scheme to identify common gene depletions in both IDH-wildtype and IDH-mutant cells, as depicted in figure 3.10. The Venn scheme revealed 44 genes that were solely depleted in IDH-wildtype cells, 35 genes exclusively depleted in IDH-mutant cells, and 33 genes that showed depletion in both cell types. This analysis highlights the distinct gene regulation patterns between IDH-wildtype and IDH-mutant cells and provides valuable insights into the unique epigenetic vulnerabilities specific to each glioma cell type.

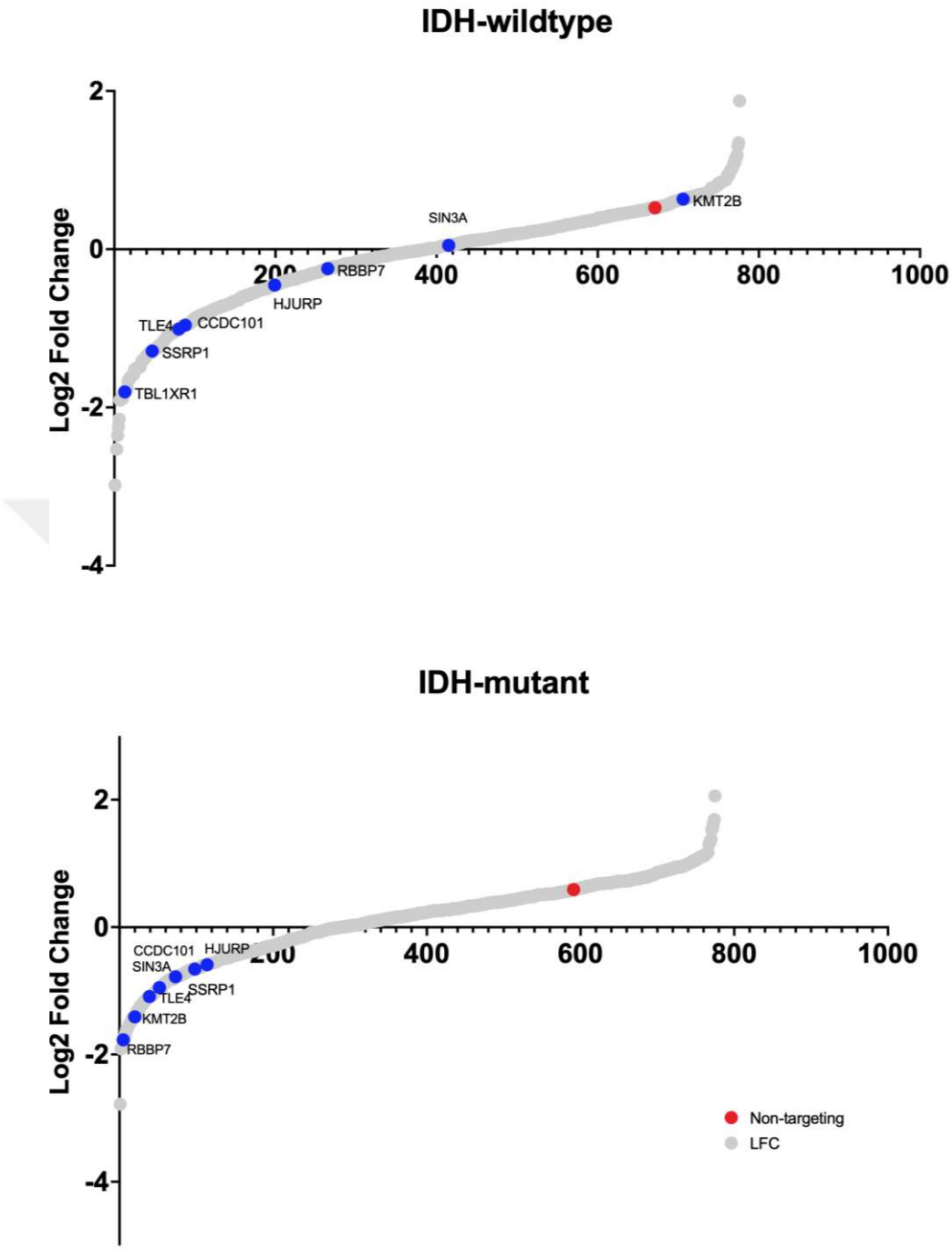

Figure 3.8: Waterfall plots for gene level depletions in EPIKOL screen on A172 IDH-wildtype and IDH-mutant glioma cells.

sgRNA counts were used as input for the MAGeCK to reveal depleted genes. RBBP7, KMT2B, and SIN3A show depletion in IDH-mutant cells compared to IDH-wildtype cells. CCDC101, SSRP1, and TBL1XR1 show depletion in IDH-wildtype cells in comparison to IDH-mutant cells. Those genes are inferred as target essential genes in the depleted cell group.

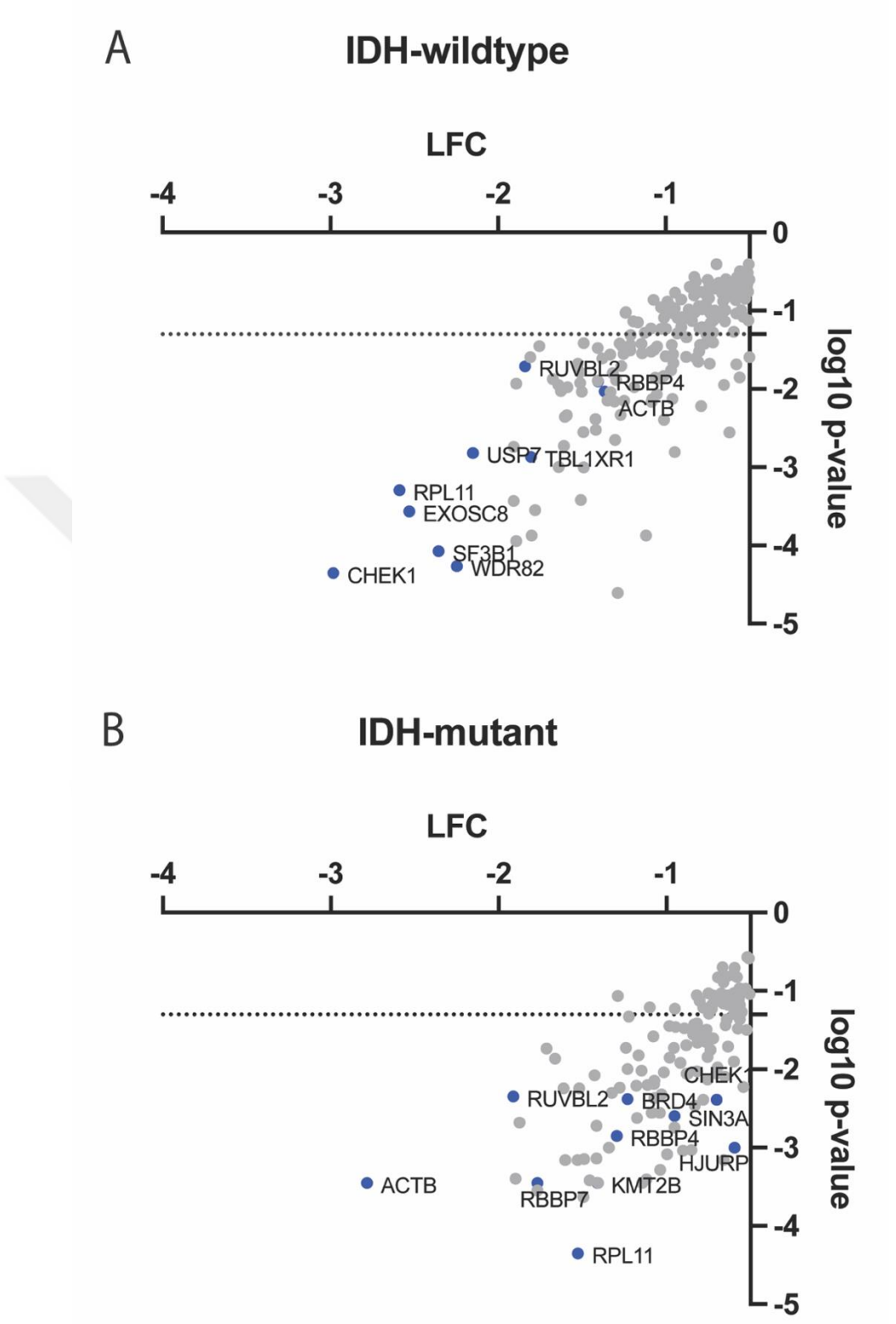

Figure 3.9: The essential genes scaled on Log2 fold change and log10 p-value graph.

sgRNA counts were used as input for the MAGeCK to reveal depleted genes. After MAGeCK analysis for EPIKOL screen on Cas9 stable A172 IDH-wildtype **(A)** and IDH-mutant **(B)** cells, the target genes were identified on LFC vs log p-value graph.

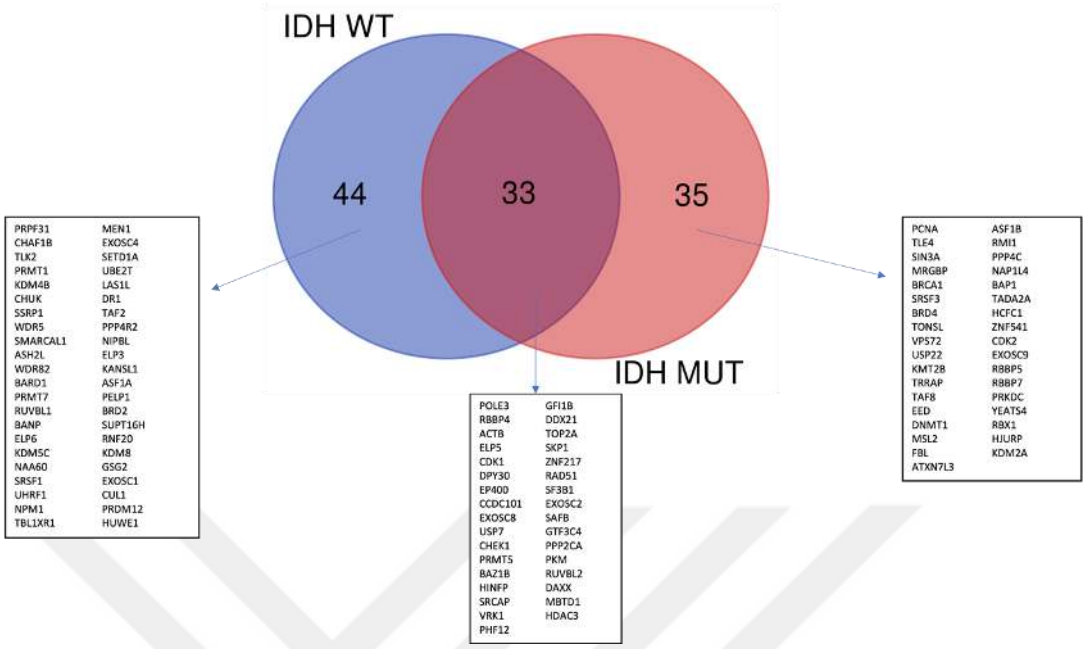

Figure 3.10: Depleted genes in A172 IDH-wildtype and IDH-mutant glioma cells.

Venn diagram shows significantly depleted genes ($p<0.05$) in Cas9 stable A172 IDH-wildtype, IDH-mutant, and common depleted genes in both cells. 44 genes were only show essentiality in IDH-wildtype cells, 35 genes show essentiality in IDH-mutant cells, and 33 genes were identified as essential in both cells.

3.3 EPIKOL screen in vitro validation

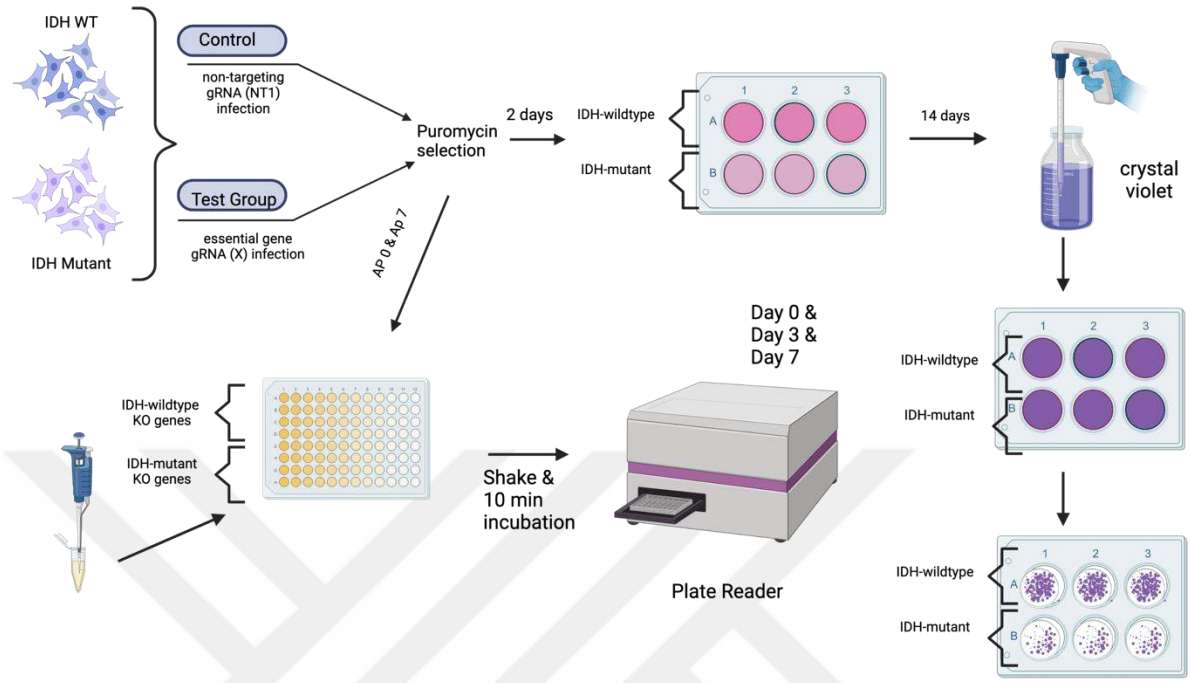

Figure 3.11: Experimental design of in vitro validation

Experimental design is schematized as 2 days after puromycin selection, control and test groups were seeded for colony formation assay and cell viability assays. Cells for colony formation assay (2000 cells/well) was grown for 14 days. Cell viability assay was read on day 0 (to normalize), day 3, and day7.

After identifying genes with significant p-values and log fold changes, the selected genes were subjected to *in vitro* validation in Cas9 stable A172 IDH-wildtype and IDH-mutant cells. The validation process continued with the knockout of KMT2B and RBBP7 genes through viral transduction in both cell types (**Figure 3.11).** Following puromycin selection, the cells were seeded for long-term colony formation assays to evaluate their colony-forming abilities and subjected to cell viability assays (**Figure 3.12A)**. As controls, non-targeting guide RNA and the ribosomal gene RPL9 were

utilized. As expected, the ribosomal control yielded low colony numbers and reduced cell viability in both cell types (**Figure 3.12C**).

Regarding the knockout of KMT2B, it was anticipated that IDH-mutant cells would exhibit lower colony formation due to its identification in IDH-mutant glioma. However, the quantification indicated only a slight decrease with no significant change observed between IDH-wildtype and IDH-mutant cells, as well as in the cell viability assay. Conversely the knockout of RBBP7 resulted in a notable decrease in the number of colonies in IDH-mutant cells compared to IDH-wildtype cells. Supporting the colony formation assay, the RBBP7 knockout demonstrated a similar impact on cell viability.

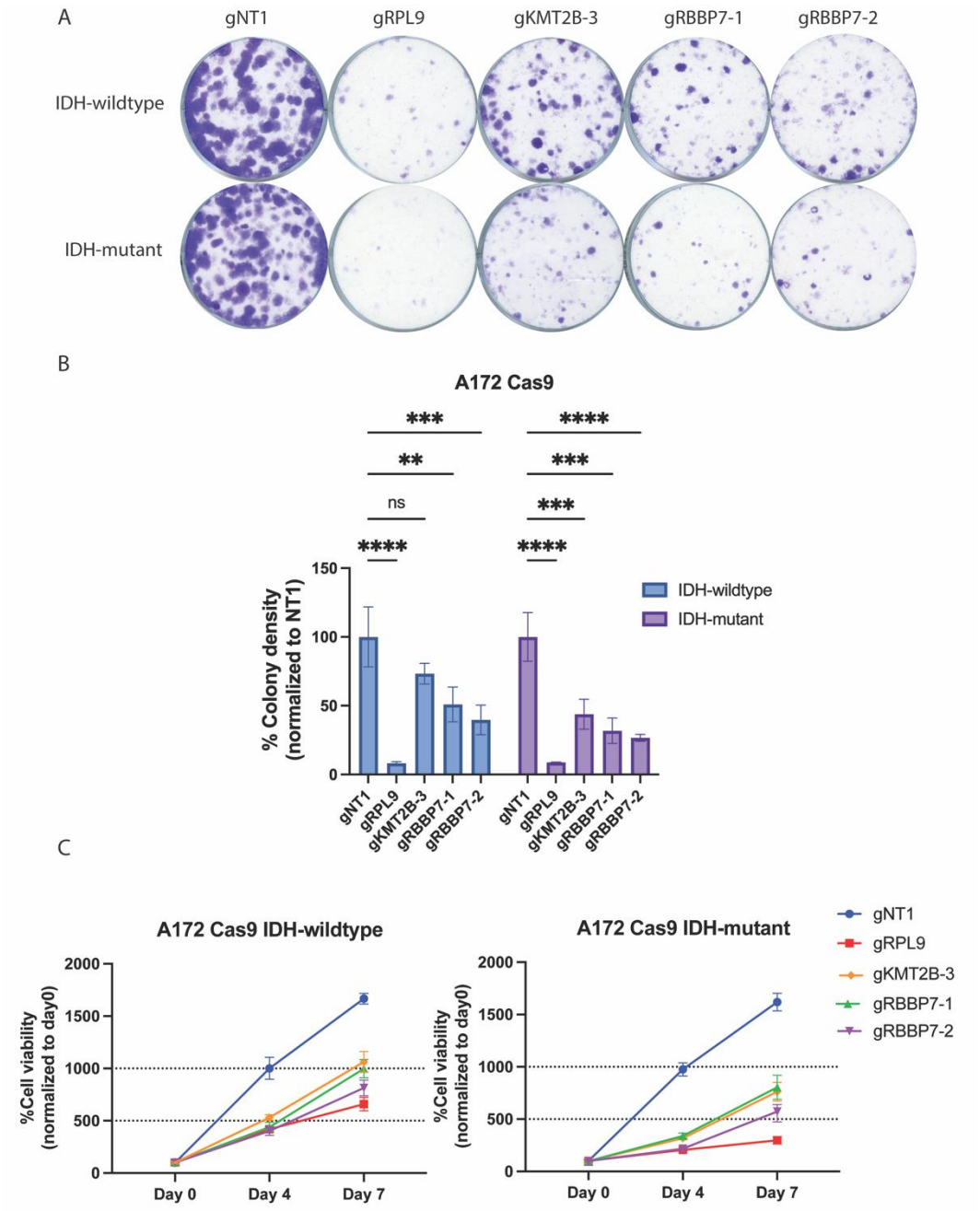

Figure 3.12: Effects of RPL9, KMT2B, RBBP7 knockouts on A172 IDH-wildtype and IDH-mutant cells

A, B. Long term colony formation assay upon knock out of the genes in IDH-wildtype and IDH-mutant cells and quantification of colony formation assay. Colony density of gKMT2B and gRBBP7 knockout was assessed. In both genes, colony density was decreased in IDH-mutant cells in comparison to IDH-wildtype cells. **C.** Cell viability response of gKMT2B and gRBBP7 knockout in comparison with gNT1 was assessed. Compared to IDH-wildtype cells, cell survival of IDH-mutant cells was more affected.

Figure 3.13 presents the results of the knockout experiments conducted on essential genes for IDH-wildtype and IDH-mutant cells. Three genes essential for IDH-wildtype cells, namely TBL1XR1, CCDC101, and SSRP1, were knocked out, along with one essential gene for IDH-mutant cells, TLE4, to assess their effects on the cells. The positive (gRPL11) and negative (gNT1) controls exhibited the expected outcomes. As non-targeting gRNA were not showed any change in both cells, ribosomal gene knockout, RPL11, wiped out the colonies on IDH-wildtype and IDH-mutant cells.

However, interestingly, the knockout of TLE4 and CCDC101 genes did not yield any significant effects on either IDH-wildtype or IDH-mutant cells in the colony formation assay (**Figure 3.13A).** In contrast, the SSRP1 gene knockout showed a significant effect on both IDH-wildtype and IDH-mutant cells, contrary to the expectation that it would have a significant effect on IDH-wildtype cells and little to no effect on IDH-mutant cells. The cell viability data supported the findings from the colony formation assay, providing further evidence for the observed effects of SSRP1 gene knockout on both cell types **(Figure 3.13A).**

A decrease in colony density was observed in IDH-wildtype cells following the knockout of the TBL1XR1 gene, in comparison to IDH-mutant cells **(Figure 3.13B).** Furthermore, the cell viability results corroborated the findings from the colony formation assay at both 72 hours and 96 hours of measurement (**Figure 3.13C**).

Upon examining the effects of gene knockout on both IDH-wildtype and IDH-mutant cells, it was found that only TBL1XR1 could be validated as an essential gene for IDH-wildtype cells. However, for IDH-mutant cells, particularly the RBBP7 gene, was identified as an essential gene. **Figure 3.14** and **Figure 3.15** depict the effects of RBBP7 gene knockout on IDH-wildtype and IDH-mutant cells in two distinct glioma cell lines, A172 and LN229, respectively.

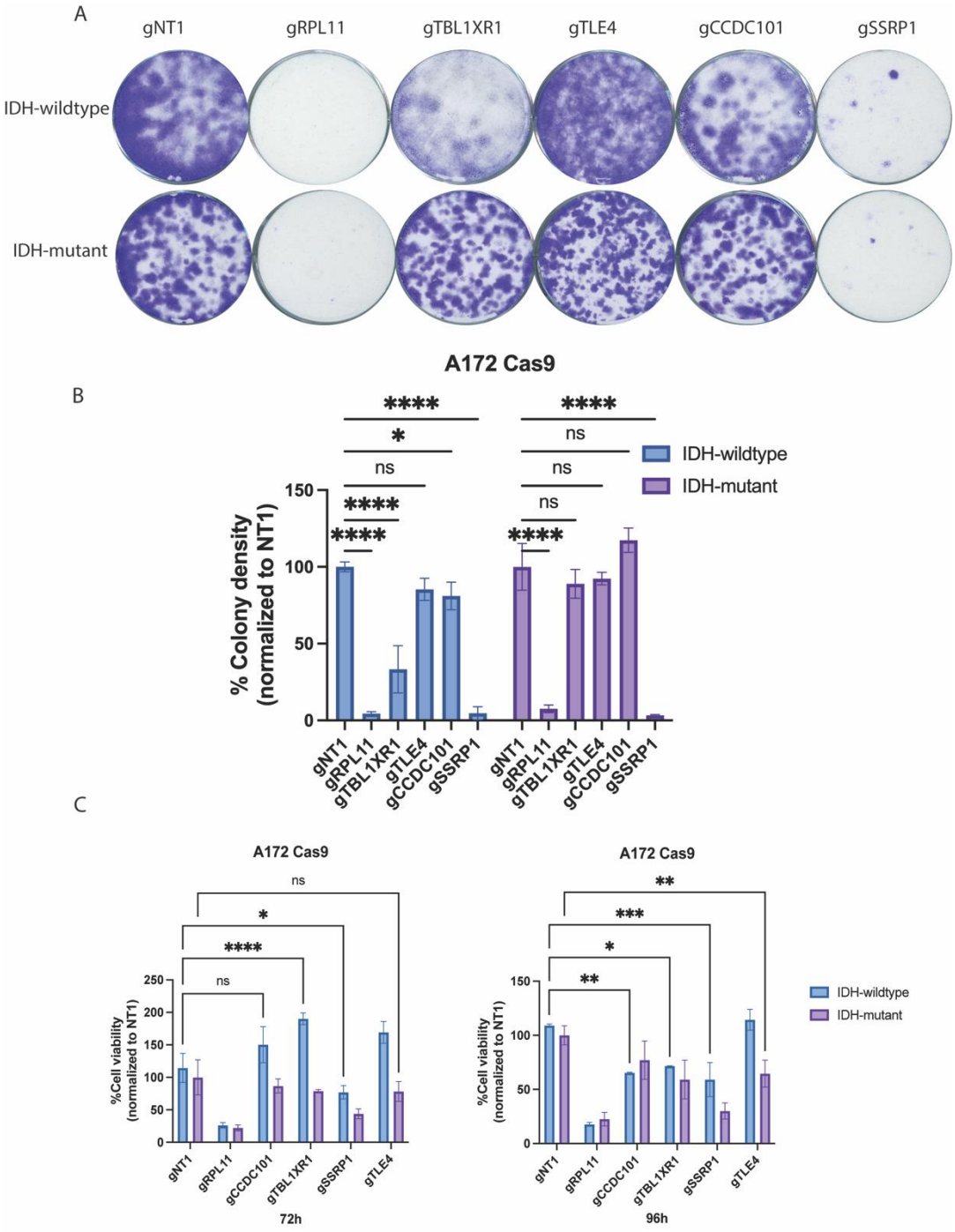

Figure 3.13: Effects of RPL11, TBL1XR1, TLE4, CCDC101, SSRP1 knockouts on A172 IDH-wildtype and IDH-mutant cells

A. Long term colony formation assay upon knock out of gCCDC101, gTBL1XR1, gSSRP1, and gTLE4 in IDH-wildtype and IDH-mutant cells **B.** Quantification of colony formation assay C. Cell viability response of gCCDC101, gTBL1XR1, gSSRP1, and gTLE4 in comparison with gNT1.

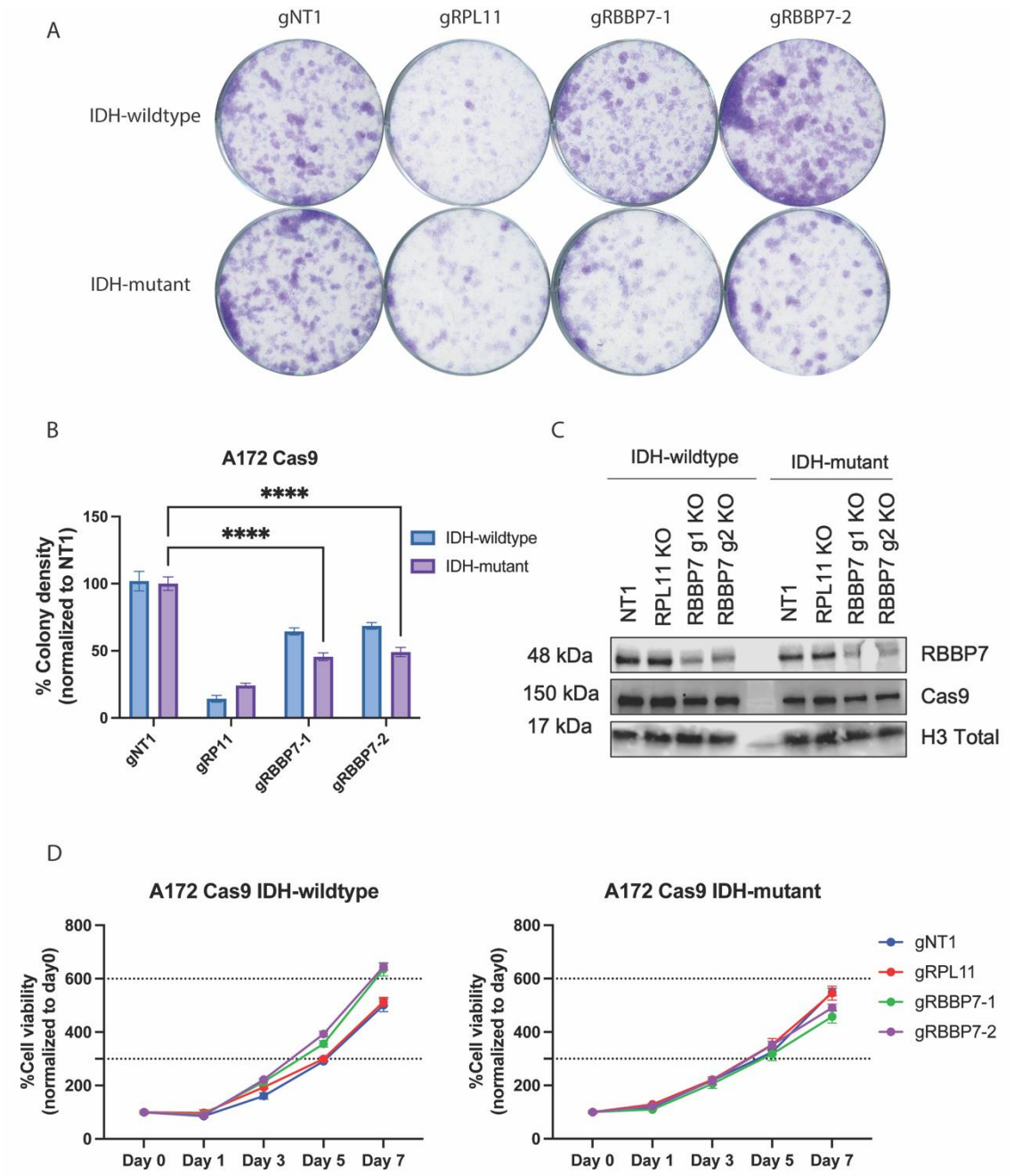

Figure 3.14: Effects of RPL11, RBBP7 knockouts on A172 IDH-wildtype and IDH-mutant cells

A, B. Long term colony formation assay upon knock out of gRBBP7-1 and gRBBP7-2 in IDH-wildtype and IDH-mutant cells and quantification of colony formation assay on A172 cell line. **C**. RBBP7, Cas9, and H3 total protein expression levels of RPL11 and RBBP7 knockout cells in comparison with gNT1 on A172 cell line. **D**. Cell viability response of genes in comparison with gNT1 on A172 cell line.

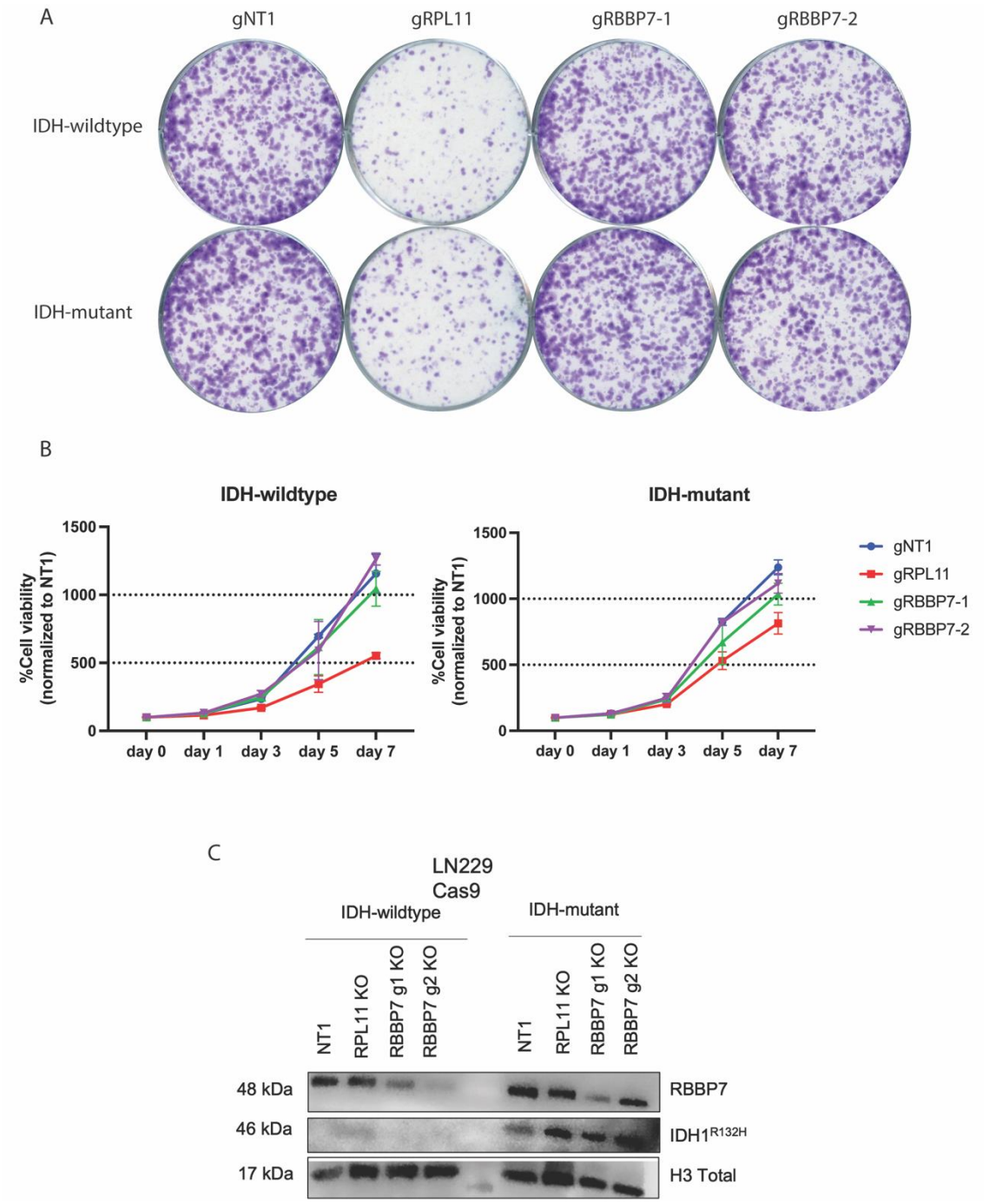

Figure 3.15: Effects of RPL11, RBBP7 knockouts on LN229 IDH-wildtype and IDH-mutant cells

A. Long term colony formation assay upon knock out of the gRBBP7-1 and gRBBP7-2 in Cas9 stable LN229 IDH-wildtype and IDH-mutant cells **B**. Quantification of colony formation assay **C.** RBBP7, IDH1^{R132H}, and H3 total protein expression levels of gRPL11 and gRBBP7 knockout cells in comparison with gNT1 on LN229 cell line. **D.** Cell viability response of genes in comparison with gNT1 on LN229 cell line.

The RBBP7 gene was subjected to knockout in A172 cells (**Figure 3.14**), and the successful knockout was confirmed by assessing the protein expression levels via western blot. The protein level analysis revealed a decrease in RBBP7 expression in both IDH-wildtype and IDH-mutant cells upon RBBP7 knockout. Additionally, Cas9 protein expression was detected in the cells, and the levels of Cas9 protein were found to be similar in both cell types (**Figure 3.14C**).

The colony formation assay demonstrated a decrease in colony density in RBBP7 knockout IDH-mutant cells compared to RBBP7 knockout IDH-wildtype cells and the non-targeting controls for both cell types (**Figure 3.14A**). When the colonies were quantified, it was observed that RBBP7 knockout in IDH-mutant cells led to a significant reduction in the colony-forming ability compared to IDH-wildtype cells (**Figure 3.14B**). The cell viability data aligned with the colony formation results, providing further support for the observed effects. However, it was also noticed that there was no substantial decrease between non-targeting gRNA and RBBP7 knockout in IDH-mutant cells, despite the evident difference between IDH-wildtype and IDH-mutant cells **(Figure 3.14D).**

Figure 3.15 presents a replicated experiment using another glioma cell line pair, LN229, to explore potential cell line-specific effects. As controls, non-targeting gRNA and RPL11 knockout were utilized. The successful knockout of RBBP7 in LN229 cells was confirmed through western blot analysis, revealing a decrease in RBBP7 protein levels in IDH-wildtype cells and in guide 1 of RBBP7 knockout in IDH-mutant cells, whereas guide 2 levels remained unchanged in IDH-mutant cells (**Figure 3.15C**).

Contrary to the findings in A172 cells, in this case, there were no noticeable differences in colony densities between IDH-wildtype and IDH-mutant cells (**Figure 3.15A).** Moreover, the assessment of cell viability demonstrated no significant changes between non-targeting sgRNA and RBBP7 knockouts in both IDH-wildtype and IDH-mutant cells (**Figure 3.15B**). These results indicate that the impact of RBBP7 knockout might be cell line-specific, as evidenced by the differing outcomes between A172 and LN229 cells.

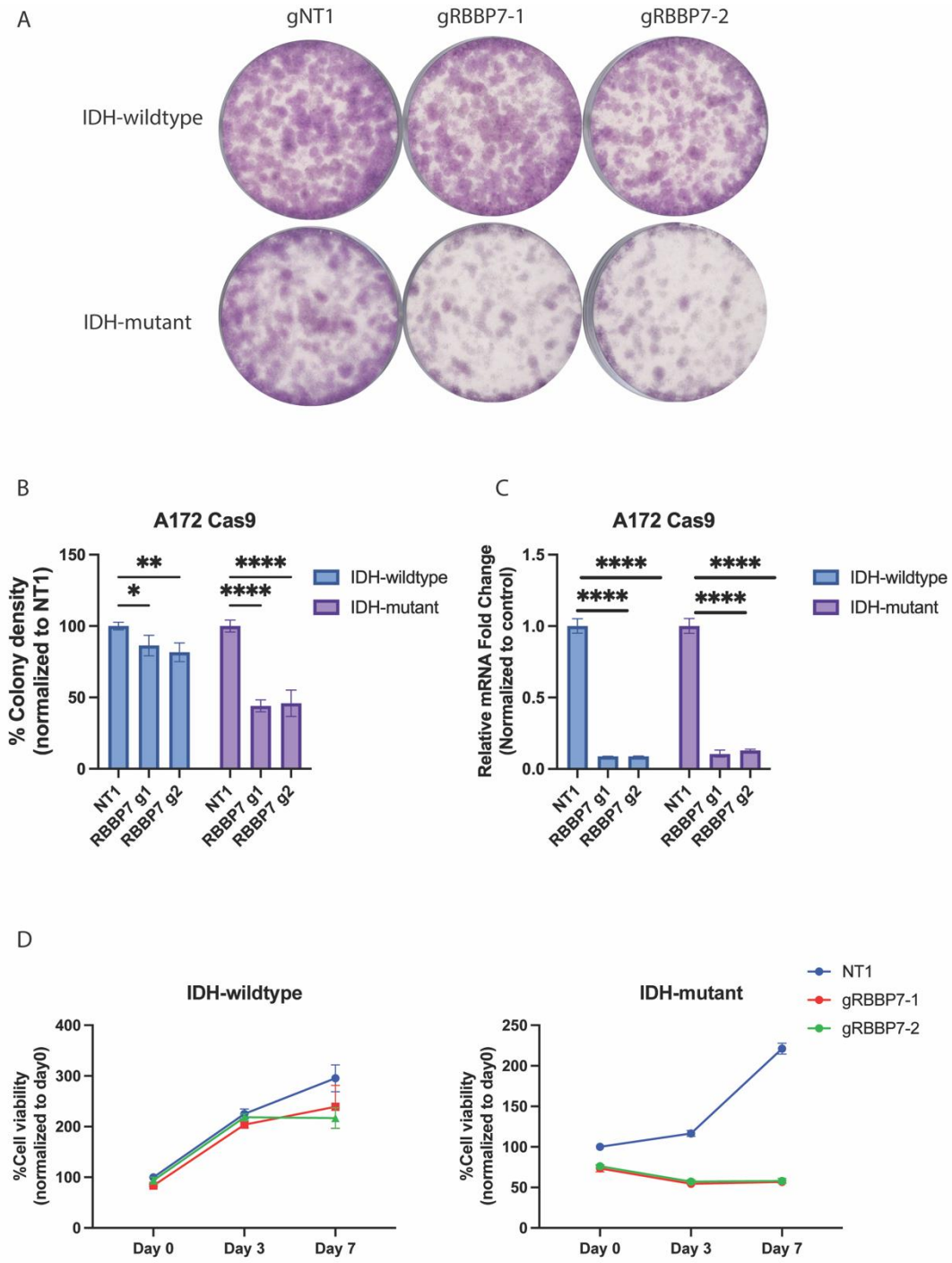

Figure 3.16: Effects of RBBP7 knockouts on A172 IDH-wildtype and IDH-mutant cells

A. Long term colony formation assay upon knock out of the gRBBP7-1 and gRBBP7-2 in Cas9 stable A172 IDH-wildtype and IDH-mutant cells **B**. Quantification of colony formation assay **C**. Relative RBBP7 mRNA expression levels of gRBBP7-1 and gRBBP7-2 knockout cells in comparison with gNT1. **D**. Cell viability response of genes in comparison with gNT1 on A172 cell line.

After confirming the impact of RBBP7 on the IDH-mutant A172 cell line in comparison to IDH-wildtype cells, the experiment was repeated to prepare samples for further RNA-sequencing (RNA-seq) analysis. RNA-seq will be employed to discern the transcriptomic changes resulting from the gene knockout in both cell types, therefore the samples used for RNA-seq were first validated for their phenotype (**Figure 3.16**). The successful knockout of the RBBP7 gene was confirmed through qPCR, showing a decrease in mRNA levels (**Figure 3.16C**).

In the A172 cell line, the colony density of IDH-mutant cells exhibited a decrease compared to IDH-wildtype cells (**Figure 3.16A**), and this difference was further quantified through colony formation assay results (**Figure 3.16B**). Additionally, RBBP7 knockout had a notable effect on cell viability in IDH-mutant cells, reducing their viability to below 50%, while IDH-wildtype RBBP7 knockout cells reached around 200% of cell viability (**Figure 3.16D**).

The differences in the transcriptome, caused by RBBP7 KO is currently under investigation and will be reported after completion of this thesis.

Chapter 4: **DISCUSSION**

Gliomas, which are central nervous system tumors derived from glial cells, have an incidence rate of 6 per 100,000 people in the US. They are diffusely infiltrative tumors that impact the surrounding brain tissues and are classified into grades ranging from I to IV, with grade IV being known as glioblastoma, the most common and aggressive type of brain tumor. With the updated WHO classification in 2021, IDH-mutant gliomas are characterized as grade IV IDH-mutant astrocytoma with GBM histology. It is noteworthy that IDH-mutant gliomas show a more favorable response to chemical drug treatments (Neumaier et al., 2023; Schaff & Mellinghoff, 2023; N. Sharma et al., 2023).

IDH-wildtype gliomas have normal IDH enzyme isoforms and regulate the cellular metabolism. Generally, IDH-wildtype gliomas are common in adult patients, while IDH-mutant glioma is commonly observed in younger patients. The genetic alterations and expressions differ between IDH-wildtype and IDH-mutant gliomas. $IDH1^{R132H}$ mutation in gliomas was reported to induce the upregulation of CD24 which is normally expressed in the early development of CNS (Haddock et al., 2022). Additionally, homologous CDKN2A/B loss in IDH-mutant glioma is very commonly occur in patient. The loss leads toa poorer survival for the patients (Verheul et al., 2021).

Even though the IDH-mutant glioma cells show vulnerability to the conventional treatments and chemical drugs, there is no currently used inhibitor for IDH-mutant glioma patients in clinics. On the other hand, ivosidenib is an FDA-approved and clinically utilized drug to target the mutant IDH1 enzyme in IDH-mutant acute myeloid leukemia patients. Recently, vorasidenib is reported as it successfully completed phase III clinical trials and is significantly promising dual inhibitor for IDH1 and IDH2 mutation in glioma patients (Mellinghoff et al., 2023; Tian et al., 2022).

The primary focus of this thesis was to explore essential epigenetic modifiers that may confer vulnerabilities in both IDH-wildtype and IDH-mutant glioma cells. To achieve this, we employed a CRISPR-Cas9 mediated screen using the EPIKOL library on the A172 glioma cell line. CRISPR-Cas9 mediated screens are designed with low MOI rate such as 0.4, the reason for that is to make each cell receive only 1 sgRNA to integrate its genome. In our project, this method leads to only one gene knock out in each cell.

For this purpose, we established Cas9 stable IDH-wildtype and IDH-mutant glioma cell lines derived from A172 cells. To ensure consistent Cas9 expression in both cell types, we initially generated parental cells expressing Cas9 protein and optimized the blasticidin antibiotic dose for the selection process. Subsequently, the Cas9 stable A172 cells were divided into two groups: one group overexpressing wildtype IDH1 and the other expressing $IDH1^{R132H}$ mutation. The successful integration of overexpression plasmids was confirmed using hygromycin antibiotic selection, along with validation of $IDH1^{R132H}$ and Cas9 expression through western blot analysis (**Figure 3.1A**).

Observations on the morphology and growth patterns of the IDH-mutant overexpressed cells revealed distinct differences compared to IDH-wildtype cells. While IDH-wildtype cells exhibited aggressive and rapid growth with a spindle-like shape, IDH-mutant cells divided at a slower rate and displayed a more rounded and polygonal shape (**Figure 3.1B**). Additionally, the cells exhibited varying responses to ionizing radiation (IR). IDH-mutant cells demonstrated increased vulnerability to IR, with their colony-forming ability decreasing by approximately 40% following exposure to 2 Gy of radiation. In contrast, IDH-wildtype cells displayed a colony density of over 60% after the same radiation exposure. Furthermore, IDH-mutant cells were significantly affected by 4 Gy of IR exposure, resulting in a considerable reduction in colony density, whereas IDH-wildtype cells still retained around 30% of colony density compared to the control (0 Gy).

Furthermore, we conducted a comprehensive assessment of the response of both cell types to Temozolomide drug (**Figure 3.2**) at various doses. Additionally, for a more extended observation, we performed a colony formation assay on the cells using lower doses. The results of the colony formation assay revealed that IDH-wildtype cells were capable of forming colonies even at the highest dose tested (**Figure 3.2A**). However, the density of IDH-mutant cells decreased dramatically starting from the lowest dose, indicating that IDH-mutant cells are considerably more vulnerable to adjuvant therapies. These findings not only confirm the heightened vulnerability of IDH-mutant cells to the drug but also align with previous literature reports, providing further support for the increased susceptibility of IDH-mutant cells to various therapeutic approaches (Alshiekh Nasany & de la Fuente, 2023; N. Sharma et al., 2023). Overall, in the colony formation assay **(Figure 3.2A)**, the control group for IDH-mutant cells were not comparable with IDH-wildtype cells. That might be caused by several reasons such as the cell count might

be miscalculated, or the DMSO, which is used as a control for the test group might have affected IDH-mutant cells more than IDH-wildtype cells and led to a slower growth of colonies.

In general, **Figure 3.1** and **Figure 3.2** illustrate that the cells with IDH mutations are more susceptible to standard treatments, namely IR and TMZ treatments. The cells exhibit varying reactions at different dosage levels. Notably, IDH-mutant cells display responsiveness even at minimal doses, whereas IDH-wildtype cells demonstrate greater durability in contrast.

The EPIKOL library comprises 744 epigenetic regulatory genes and 35 essential genes, with each gene having 10 sgRNAs. For the EPIKOL screen, an MOI of 0.4 with 1000X coverage was used, and the screening cells were cultured for 15-16 population doubling times. The MAGeCK analysis was employed to analyze the results of the screen, and the distribution of sgRNA read counts was examined based on their frequencies **(Figure 3.3)** to assess the screen's quality and repeatability. Accordingly, the IDH-wildtype sgRNAs' initial point samples (AP1 and AP2) and endpoint samples (EP1 and EP2) exhibit similar frequencies and distributions, indicating a proper distribution. In Figure 3.3B, the same trend is observed in the IDH-mutant sgRNAs' samples, with the exception of AP1, which shows a lower frequency compared to the IDH-wildtype samples. Both cells showed a normal distribution.

To further analyze the data, normalized counts of sgRNAs for each gene of interest were used and schematized and the most suitable and effective sgRNA pair was selected for use in subsequent validations. Following that, we examined the adequacy and accuracy of the screen by analyzing the sgRNA distribution in the initial and end-point samples (**Figure 3.6**). The diagram illustrates that both cell types display non-targeting genes along the diagonal, indicating the absence of depletion in the non-targeting sgRNAs. In contrast, a considerable proportion of ribosomal sgRNAs are situated below the diagonal, implying their depletion within the cells.

Subsequently, we proceeded to select target genes with potential essentiality for IDH-wildtype and IDH-mutant glioma cells, using specific p-value ($p<0.05$) and log fold change ($LFC<-1$) cutoffs to assess their statistical significance and relevance in the context of our study. A p-value smaller than 0.05 indicates that the observed differences are not likely due to chance and are considered statistically significant. Additionally, the log fold change represents the magnitude of expression differences between two

conditions, specifically the sgRNA representation change between endpoint and initial point samples. An LFC less than -1 indicates downregulated genes, which may be indicative of potential essential genes for IDH-wildtype and IDH-mutant cells.

After excluding ribosomal genes, we identified candidate genes that might be essential, comprising 44 genes for IDH-wildtype cells, 35 genes for IDH-mutant cells, and 33 genes that might be essential for both cell types.

Next, we visually represented the depleted genes on a log fold change graph to compare the depletion rates between IDH-wildtype and IDH-mutant cells, with a focus on genes significantly depleted in one cell type but not in the other. The goal was to identify genes showing differential essentiality between the two cell types. For instance, if a gene was found essential for IDH-mutant glioma cells but not for IDH-wildtype cells, we anticipated that IDH-mutant glioma cells with the knockout of that specific gene would be unable to grow or form colonies. This analysis aimed to provide insights into the potential differences in essential genes between IDH-wildtype and IDH-mutant glioma, contributing to a deeper understanding of their unique biology and therapeutic vulnerabilities.

Following the log fold change graphs, we proceeded with Principal Component Analysis (PCA) to represent the gene depletion distribution in a reduced-dimensional space, enabling us to visualize the gene essentiality patterns and detect potential dissimilarities between IDH-wildtype and IDH-mutant glioma cells **(Figure 3.7).** Notably, the initial point samples of IDH-mutant cells and endpoint samples of IDH-wildtype cells exhibited a remarkably similar pattern.

Next, we represented the genes meeting the p-value and LFC cutoff criteria on a Log2 Fold Change depletion graph, as shown in **Figure 3.8**. Our focus was on genes exhibiting a significant LFC in one group while having a non-significant LFC in the other group. RBBP7 emerged as a target gene for validation, as it displayed a significant LFC (-2) in IDH-mutant cells but did not show a substantial depletion rate in IDH-wildtype cells. This suggests that the depletion of RBBP7 may not significantly impact IDH-wildtype cells but is expected to have a substantial effect on IDH-mutant glioma cells. Similarly, KMT2B and SIN3A are potential candidate targets worthy of consideration.

On the other hand, in prior research conducted within our laboratory, the inhibition of H3K27me3 demethylases, which are KDM6A and KDM6B, and the HDAC inhibitor, GSK-J4, were identified as potential therapies, both individually and in combination, with

a selective focus on targeting IDH-mutant glioma cells (Kayabolen et al., 2020). However, in the results of the screening analysis, a significant LFC for either KDM6A or KDM6B in isolation was not detected. This observation could likely be attributed to the limitations inherent in CRISPR screens.

Namely, CRISPR/Cas9-mediated screens involve the delivery of a single sgRNA targeting a specific gene into each cell. Regrettably, this approach lacks the capacity to simultaneously target two genes within the same cell during the screening process. Thus, the individual deletion of KDM6A or KDM6B might not yield a significant LFC alteration in IDH-mutant cells, as the impact of one gene's deletion might be masked by the presence of the other. If both KDM6A and KDM6B were simultaneously knocked out within a single cell, it is plausible that we could observe effects similar to those reported by Kayabolen (2020) when using inhibitors.

To confirm the significance of these genes, we conducted in vitro assays, specifically colony formation and cell viability assays, to assess the cells' ability to proliferate, survive, and form colonies under the influence of gene manipulation. These assays help determine whether a gene is essential for IDH-mutant cells by comparing the number or density of colonies with those resulting from a non-essential gene ablation. The in vitro assays provide crucial functional evidence that complements the statistical significance observed in the thesis.

First, we have knocked RPL9, KMT2B, and RBBP7 genes out on IDH-wildtype and IDH-mutant cells and revealed the successfully working negative and positive controls. There was a significant difference in RBBP7 knockout IDH-wildtype and IDH-mutant cells. On the other hand, IDH-wildtype was also markedly affected by the RBBP7 knockout in contrast to our first expectations that it should not have an influence on IDH-wildtype cells. Also, KMT2B knockout affected the colony density. Supporting the colony formation assay, cell viability assay is also correlated with the colony formation assay.

KMT2B, also known as MLL4, is a lysine methyltransferase that plays a crucial role in histone methylation processes. Specifically, it adds methyl groups to lysine 4 on histone 3 (H3K4), which is an important modification involved in regulating gene expression (Zhao et al., 2023).

On the other hand, RBBP7, also known as RbAp48, is a highly conserved protein that has multiple functions in cellular processes. It is known to be involved in chromatin

remodeling, cell cycle regulation, gene transcription, and recruitment of histone deacetylases (HDACs). RBBP7 is a part of the nucleosome remodeling and histone deacetylase (NuRD) and polycomb repressive complex 2 (PRC2) complexes, which are involved in modifying histones and regulating gene expression (Davidovich & Cech, 2015; Fischer & Liefke, 2023; Mohajeri et al., 2013). Structurally, RBBP7 interacts with histone H3 through a binding site located on top of the protein. This interaction enables RBBP7 to acquire histone methyltransferase (HMT) activity with a specificity for modifying H3K9 and H3K27 residues (Balboula et al., 2014; Millard et al., 2016).

In the context of IDH-mutant glioma, the IDH mutation leads to the accumulation of 2-HG. This oncometabolite can alter the activity of histone demethylases and histone methyltransferases, resulting in changes in histone modification patterns, including hypermethylation of histones and DNA (Avellaneda Matteo et al., 2017; Neumaier et al., 2023; Solomou et al., 2023). Moreover, in other cancer types, RBBP7 has been found to interact with tumor suppressor proteins such as BRCA1 and p53 in breast and colorectal cancers, suggesting its involvement in regulating cell growth and survival in these cancers (Guo et al., 2023; N. Yu et al., 2018). Thus, RBBP7 influence on IDH-mutant glioma might be through the histone H3 methylation or acetylation, prompting further studies.

Following that, we conducted similar assays for TBL1XR1, TLE4, CCDC101, and SSRP1. TBL1XR1, a member of the HDAC-containing NCOR/SMRT complexes, has been linked to developmental diseases (Mastrototaro et al., 2021). On the Log2 Fold Change graph, we observed a depletion of TBL1XR1 in IDH-wildtype cells compared to IDH-mutant cells. Figure 3.13A illustrates a decrease in colony density, which is further supported by the quantification. However, interestingly, the cell viability assay showed a reverse effect, with IDH-mutant cells being more affected by the gene knockout than IDH-wildtype cells.

As for CCDC101, also known as SGF29 (SAGA complex associated factor 29), it is a subunit of the SAGA acetyl-transferase complex that recognizes and interacts with H3K4me3 (L.-Y. Huang et al., 2021). Similar to TBL1XR1, we observed a depletion of CCDC101 in IDH-wildtype glioma cells on the LFC graphs. However, in this case, we did not observe a significant difference between the two groups, although there was a slight decrease in cell viability for IDH-mutant cells after 96 hours. This suggests that the knockout of CCDC101 had a similar impact on both IDH-wildtype and IDH-mutant cells.

Regarding SSRP1 (Structure Specific Recognition Protein 1), which also showed depletion in IDH-wildtype cells on the LFC graph, it plays a role in promoting the removal of histone H1 from chromatin and forms the major chromatin remodeler, FACT complex, in conjunction with SPT16 (Falbo et al., 2020). In **Figure 3.13**, the knockout of SSRP1 affected both IDH-wildtype and IDH-mutant cells at a similar rate. The initial expectation was that the knockout of SSRP1 would not significantly impact IDH-mutant glioma cells but would affect IDH-wildtype cells. However, the results indicated that the depletion of SSRP1 had a comparable effect on both cell types.

Lastly, we examined the effects of the TLE4 gene (Transducin-like enhancer protein 4), which showed depletion in IDH-mutant cells, on both cell types in **Figure 3.14**. The initial expectation was that the gene ablation of TLE4 would have a greater impact on IDH-mutant cells compared to IDH-wildtype cells. TLE4 gene encodes the TLE4 tumor suppressor protein, and its expression is higher in colorectal cancer tissues (Wang et al., 2016). Contrary to our expectations, TLE4 had an influence on both cell types, and as a result, the colony density and cell viability decreased in both IDH-wildtype and IDH-mutant cells.

Following the RBBP7 knockout on A172 cells, we validated the gene knockout and Cas9 levels, as depicted in Figure 3.14. The results consistently showed an effect of the RBBP7 knockout. To determine if this effect is specific to the A172 cell line, we performed the same procedure on another glioma cell line, LN229, as shown **in Figure 3.15.** Surprisingly, we did not observe any difference between the Cas9 stable IDH-wildtype and IDH-mutant LN229 cells, even after successfully knocking out RBBP7 (**Figure 3.15C**). In IDH-mutant cells, RBBP7 guide 2 was not successfully knocked out, even though guide 1 decreased the protein expression. However, in both conditions, we did not observe any significant effect on the cells. These results suggest that the essentiality of the RBBP7 gene may be specific to the A172 cell line and not applicable to LN229 cells.

After careful evaluation of the validation results and considering the novelty of findings, we focused on a specific target gene, RBBP7, and proceeded with functional assays to gain insights into its role and regulatory mechanisms in IDH-mutant glioma.

To target RBBP7, if we consider the scenario where RBBP7 operates via the PRC2 complex in gliomas, a plausible strategy involves directing attention towards EZH2. This is because RBBP7 assumes a structural role, not an enzymatic one, within the PRC2

complex. Notably, there is currently no inhibitor designed specifically for targeting RBBP7 or its related protein RBBP4. By employing inhibitors that target PRC2 and EZH2, an investigation into the potential susceptibility of IDH-wildtype and IDH-mutant glioma cells to these inhibitors can be conducted to identify any selective vulnerabilities. Alternatively, inhibitors designed to directly disrupt the functionality of PRC2 could be considered. An example of an inhibitor aimed at EZH2 is tazemetostat, an inhibitory drug with approval from the FDA. Tazemetostat effectively inhibits EZH2, including its gain-of-function mutations like Y646X. Approval of tazemetostat follows successful completion of Phase I and Phase II trials focused on follicular lymphoma (Julia & Salles, 2021; Straining, & Eighmy, 2022). Another instance of an EZH2 inhibitor is GSK126, which competes with S-adenosylmethionine (SAM). Furthermore, GSK126 demonstrated heightened apoptosis in multiple myeloma when used alongside bortezomib, attributed to its inhibitory impact on the Wnt/β-catenin pathway. Successful Phase I and Phase II trials of GSK126 have also been carried out for follicular lymphoma. (Wei et al., 2021; Zeng et al., 2017).

An alternate strategy for targeting RBBP7 involves impeding the PRC2 complex via EED, a constituent of the PRC2 complex that facilitates PRC2's association with H3K27me3. EED also spurs the activity of EZH2's H3K27me3 HMTase. While the presence of RBBP7 proteins isn't an absolute requirement for EZH2's HMTase activity, they play a significant role in PRC2's functioning. In 2017, Novartis unveiled EED226 as one of the inhibitors of EED. Notably, EED226 prompts structural alterations in residues F97, Y148, W364, and Y365 upon competitively binding to H3K27me3 sites. Similar to other EED inhibitors, A-395 also competes for H3K27me3 binding sites, leading to a reduction in H3K27me3 levels. Although this inhibitor's effectiveness has been established in xenograft models, no clinical investigations have been conducted to date (He et al., 2017; Liu et al., 2022; Shi et al., 2017).

Our hypothesis suggests that RBBP7 could induce a distinct susceptibility in IDH-mutant glioma cells due to the hypermethylation pattern observed on histones, a consequence of the overproduction and aggregation of 2-HG oncometabolite catalyzed by the $IDH1^{R132H}$ mutation. 2-HG inhibits several enzymes including histone demethylases. Due to the histone demethylases inhibition, methyl groups on histones cannot be removed but accumulate. The hypermethylation phenotype is the distinctive characteristic of IDH-mutant glioma cells (Solomou et al., 2023).

Furthermore, our proposal extends to the notion that the hypermethylation process, particularly involving H3K27me3, facilitated by RBBP7, is orchestrated through its integration within the PRC2 complex. Given its integral role, RBBP7's participation in the PRC2 complex, which governs histone methylation, is of paramount importance (Shi et al., 2017), particularly within the context of IDH-mutant gliomas, where the hypermethylation pattern is already established. In the context of the PRC2 complex, RBBP7 serves to direct the complex to specific genomic loci, thereby augmenting its methyltransferase activity and ultimately leading to hypermethylation.

In IDH-mutant cells, where there is an existing elevation in these epigenetic modifications, targeting RBBP7 could potentially disrupt this heightened state. Consequently, this disruption could impede cell growth and survival. The rationale behind this strategy is rooted in exploiting the tumor's dependency on these particular epigenetic changes for sustained proliferation.

To find out the transcriptional regulation led by RBBP7 in IDH-mutant and IDH-wildtype glioma cells, we continued with RNA-sequencing. In the subsequent steps, we wish to delve into the transcription regulatory effects of RBBP7 through RNA-sequencing and carefully prepared the samples for sequencing, ensuring the reliability and reproducibility of our findings. Notably, we consistently observed a decrease in mRNA levels, corroborating the results obtained from previous RBBP7 knockout trials. The RNA-seq analysis will play a crucial role in unraveling the intricate transcriptomic interactions involving RBBP7 and shedding light on the gene expression changes resulting from its knockout. By comparing the transcriptomic profiles of IDH-wildtype and IDH-mutant glioma cells, we aim to pinpoint the specific genes and pathways that are affected by the absence of RBBP7. This comprehensive analysis will provide valuable insights into the regulatory mechanisms governing gene expressions and the overall impact of RBBP7 on IDH-mutant glioma cells.

As part of the future research directions, the first step would be to conduct RNA-seq analysis to investigate the changes in gene expression resulting from RBBP7 knockout. To validate the differential expression patterns observed in the RNA-seq data, qRT-PCR can be performed to quantify mRNA levels and confirm the findings.

Next, the impact of RBBP7 knockout on protein expression levels can be assessed using western blot assays. This will allow for the examination and comparison of RBBP7

and other relevant genes' protein expression levels, providing insights into the downstream effects of RBBP7 ablation.

To gain a deeper understanding of the role of RBBP7 in chromatin remodeling and histone modifications, it would be crucial to investigate changes in histone marks and other epigenetic modifications resulting from RBBP7 knockout. This can be accomplished through techniques such as ChIP-seq or ATAC-seq, which will assess alterations in chromatin accessibility and histone modifications.

Furthermore, pathway analysis can be employed to identify the molecular pathways that are affected by RBBP7 knockout and uncover the biological processes influenced by RBBP7. This analysis will help elucidate the broader implications of RBBP7 in the context of IDH-mutant glioma.

Lastly, in vivo studies using animal models will be of utmost importance to assess the effects of RBBP7 knockout on tumor growth, invasion, and overall glioma progression. These in vivo experiments will provide valuable insights into the potential therapeutic implications of targeting RBBP7.

By combining these further experiments, the influence and role of RBBP7 in IDH-mutant glioma can be comprehensively characterized. The findings from these investigations may lead to the identification of novel potential therapeutic targets for the treatment of IDH-mutant glioma.

BIBLIOGRAPHY

Aasland, D., Götzinger, L., Hauck, L., Berte, N., Meyer, J., Effenberger, M., Schneider, S., Reuber, E. E., Roos, W. P., Tomicic, M. T., Kaina, B., & Christmann, M. (2019). Temozolomide Induces Senescence and Repression of DNA Repair Pathways in Glioblastoma Cells via Activation of ATR–CHK1, p21, and NF-κB. *Cancer Research*, *79*(1), 99–113. https://doi.org/10.1158/0008-5472.CAN-18-1733

Alshiekh Nasany, R., & de la Fuente, M. I. (2023). Therapies for IDH-Mutant Gliomas. *Current Neurology and Neuroscience Reports*, *23*(5), 225–233. https://doi.org/10.1007/s11910-023-01265-3

Ashoti, A., Limone, F., Van Kranenburg, M., Alemany, A., Baak, M., Vivié, J., Piccioni, F., Creyghton, M., Eggan, K., & Geijsen, N. (2020). *A genome-wide CRISPR/Cas phenotypic screen for modulators of DUX4 cytotoxicity reveals screen complications* [Preprint]. Molecular Biology. https://doi.org/10.1101/2020.07.27.223420

Avellaneda Matteo, D., Grunseth, A. J., Gonzalez, E. R., Anselmo, S. L., Kennedy, M. A., Moman, P., Scott, D. A., Hoang, A., & Sohl, C. D. (2017). Molecular mechanisms of isocitrate dehydrogenase 1 (IDH1) mutations identified in tumors: The role of size and hydrophobicity at residue 132 on catalytic efficiency. *The Journal of Biological Chemistry*, *292*(19), 7971–7983. https://doi.org/10.1074/jbc.M117.776179

Balboula, A. Z., Stein, P., Schultz, R. M., & Schindler, K. (2014). Knockdown of RBBP7 unveils a requirement of histone deacetylation for CPC function in mouse oocytes. *Cell Cycle*, *13*(4), 600–611. https://doi.org/10.4161/cc.27410

Baylin, S. B., & Jones, P. A. (2011). A decade of exploring the cancer epigenome—Biological and translational implications. *Nature Reviews Cancer*, *11*(10), 726–734. https://doi.org/10.1038/nrc3130

Bock, C., Datlinger, P., Chardon, F., Coelho, M. A., Dong, M. B., Lawson, K. A., Lu, T., Maroc, L., Norman, T. M., Song, B., Stanley, G., Chen, S., Garnett, M., Li, W., Moffat, J., Qi, L. S., Shapiro, R. S., Shendure, J., Weissman, J. S., & Zhuang, X. (2022). High-content CRISPR screening. *Nature Reviews Methods Primers*, *2*(1), 8. https://doi.org/10.1038/s43586-021-00093-4

Campos, E. I., & Reinberg, D. (2009). Histones: Annotating Chromatin. *Annual Review of Genetics*, *43*(1), 559–599. https://doi.org/10.1146/annurev.genet.032608.103928

Chan, Y.-T., Lu, Y., Wu, J., Zhang, C., Tan, H.-Y., Bian, Z., Wang, N., & Feng, Y. (2022). CRISPR-Cas9 library screening approach for anti-cancer drug discovery: Overview and perspectives. *Theranostics*, *12*(7), 3329–3344. https://doi.org/10.7150/thno.71144

Chowdhury, R., Yeoh, K. K., Tian, Y., Hillringhaus, L., Bagg, E. A., Rose, N. R., Leung, I. K. H., Li, X. S., Woon, E. C. Y., Yang, M., McDonough, M. A., King, O. N., Clifton, I. J., Klose, R. J., Claridge, T. D. W., Ratcliffe, P. J., Schofield, C. J., & Kawamura, A. (2011). The oncometabolite 2-hydroxyglutarate inhibits histone lysine demethylases. *EMBO Reports*, *12*(5), 463–469. https://doi.org/10.1038/embor.2011.43

Davidovich, C., & Cech, T. R. (2015). The recruitment of chromatin modifiers by long noncoding RNAs: Lessons from PRC2. *RNA*, *21*(12), 2007–2022. https://doi.org/10.1261/rna.053918.115

Dawson, M. A., & Kouzarides, T. (2012). Cancer Epigenetics: From Mechanism to Therapy. *Cell*, *150*(1), 12–27. https://doi.org/10.1016/j.cell.2012.06.013

Dokmanovic, M., Clarke, C., & Marks, P. A. (2007). Histone Deacetylase Inhibitors: Overview and Perspectives. *Molecular Cancer Research*, *5*(10), 981–989. https://doi.org/10.1158/1541-7786.MCR-07-0324

Dong, Z., & Cui, H. (2019). Epigenetic modulation of metabolism in glioblastoma. *Seminars in Cancer Biology*, *57*, 45–51. https://doi.org/10.1016/j.semcancer.2018.09.002

Egger, G., Liang, G., Aparicio, A., & Jones, P. A. (2004). Epigenetics in human disease and prospects for epigenetic therapy. *Nature*, *429*(6990), 457–463. https://doi.org/10.1038/nature02625

Falbo, L., Raspelli, E., Romeo, F., Fiorani, S., Pezzimenti, F., Casagrande, F., Costa, I., Parazzoli, D., & Costanzo, V. (2020). SSRP1-mediated histone H1 eviction promotes replication origin assembly and accelerated development. *Nature Communications*, *11*(1), 1345. https://doi.org/10.1038/s41467-020-15180-5

Figueroa, M. E., Abdel-Wahab, O., Lu, C., Ward, P. S., Patel, J., Shih, A., Li, Y., Bhagwat, N., Vasanthakumar, A., Fernandez, H. F., Tallman, M. S., Sun, Z., Wolniak, K., Peeters, J. K., Liu, W., Choe, S. E., Fantin, V. R., Paietta, E., Löwenberg, B., … Melnick, A. (2010). Leukemic IDH1 and IDH2 Mutations Result in a Hypermethylation Phenotype, Disrupt TET2 Function, and Impair Hematopoietic Differentiation. *Cancer Cell*, *18*(6), 553–567. https://doi.org/10.1016/j.ccr.2010.11.015

Fischer, S., & Liefke, R. (2023). Polycomb-like Proteins in Gene Regulation and Cancer. *Genes*, *14*(4), 938. https://doi.org/10.3390/genes14040938

Gautron, A., Bachelot, L., Quéméner, A. M., Corre, S., Aubry, M., Rambow, F., Paris, A., Tardif, N., Leclair, H. M., Coulouarn, C., Marine, J.-C., Galibert, M.-D., & Gilot, D. (2020). *Gain-of-function CRISPR screens identify tumor-promoting genes conferring melanoma cell plasticity and therapy-resistance* [Preprint]. Cancer Biology. https://doi.org/10.1101/2020.07.08.193102

Gayon, J. (2016). From Mendel to epigenetics: History of genetics. *Comptes Rendus Biologies*, *339*(7), 225–230. https://doi.org/10.1016/j.crvi.2016.05.009

Grochans, S., Cybulska, A. M., Simińska, D., Korbecki, J., Kojder, K., Chlubek, D., & Baranowska-Bosiacka, I. (2022). Epidemiology of Glioblastoma Multiforme–Literature Review. *Cancers*, *14*(10), Article 10. https://doi.org/10.3390/cancers14102412

Gujral, P., Mahajan, V., Lissaman, A. C., & Ponnampalam, A. P. (2020). Histone acetylation and the role of histone deacetylases in normal cyclic endometrium. *Reproductive Biology and Endocrinology*, *18*(1), 84. https://doi.org/10.1186/s12958-020-00637-5

Guo, L., Xia, Y., Li, H., Wang, Z., Xu, H., Dai, X., Zhang, Y., Zhang, H., Fan, W., Wei, F., Li, Q., Zhang, L., Cao, L., Zhang, S., Hu, W., & Gu, H. (2023). FIT links c-Myc and P53 acetylation by recruiting RBBP7 during colorectal carcinogenesis. *Cancer Gene Therapy*. https://doi.org/10.1038/s41417-023-00624-z

Haberland, M., Montgomery, R. L., & Olson, E. N. (2009). The many roles of histone deacetylases in development and physiology: Implications for disease and therapy. *Nature Reviews Genetics*, *10*(1), Article 1. https://doi.org/10.1038/nrg2485

Haddock, S., Alban, T. J., Turcan, Ş., Husic, H., Rosiek, E., Ma, X., Wang, Y., Bale, T., Desrichard, A., Makarov, V., Monette, S., Wu, W., Gardner, R., Manova, K.,

Boire, A., & Chan, T. A. (2022). Phenotypic and molecular states of IDH1 mutation-induced CD24-positive glioma stem-like cells. *Neoplasia*, *28*, 100790. https://doi.org/10.1016/j.neo.2022.100790

He, Y., Selvaraju, S., Curtin, M. L., Jakob, C. G., Zhu, H., Comess, K. M., Shaw, B., The, J., Lima-Fernandes, E., Szewczyk, M. M., Cheng, D., Klinge, K. L., Li, H.-Q., Pliushchev, M., Algire, M. A., Maag, D., Guo, J., Dietrich, J., Panchal, S. C., … Pappano, W. N. (2017). The EED protein–protein interaction inhibitor A-395 inactivates the PRC2 complex. *Nature Chemical Biology*, *13*(4), Article 4. https://doi.org/10.1038/nchembio.2306

Hou, J. (2020). Mouse models of tight junction physiology. In *A Laboratory Guide to the Tight Junction* (pp. 303–340). Elsevier. https://doi.org/10.1016/B978-0-12-818647-3.00008-8

Huang, L.-Y., Hsu, D.-W., & Pears, C. J. (2021). Methylation-directed acetylation of histone H3 regulates developmental sensitivity to histone deacetylase inhibition. *Nucleic Acids Research*, *49*(7), 3781–3795. https://doi.org/10.1093/nar/gkab154

Huang, Y., Wang, Y., & Huang, Z. (2021). A Specific Peptide Vaccine Against IDH1(R132H) Glioma. *Neuroscience Bulletin*, *38*(2), 223–225. https://doi.org/10.1007/s12264-021-00791-9

Jin, B., Li, Y., & Robertson, K. D. (2011). DNA Methylation. *Genes & Cancer*, *2*(6), 607–617. https://doi.org/10.1177/1947601910393957

Jones, P. A. (2012). Functions of DNA methylation: Islands, start sites, gene bodies and beyond. *Nature Reviews Genetics*, *13*(7), 484–492. https://doi.org/10.1038/nrg3230

Julia, E., & Salles, G. (2021). EZH2 inhibition by tazemetostat: Mechanisms of action, safety and efficacy in relapsed/refractory follicular lymphoma. *Future Oncology*, *17*(17), 2127–2140. https://doi.org/10.2217/fon-2020-1244

Kayabolen, A., Yilmaz, E., & Bagci-Onder, T. (2021). IDH Mutations in Glioma: Double-Edged Sword in Clinical Applications? *Biomedicines*, *9*(7), 799. https://doi.org/10.3390/biomedicines9070799

Kayabolen, A., Yilmaz, E., Sahin, G. N., Seker-Polat, F., Cingoz, A., Isik, B., Acar, S., Wakimoto, H., Cahill, D. P., Solaroglu, I., Cribbs, A. P., Oppermann, U., & Bagci-Onder, T. (2020). *Orthogonal targeting of KDM6A/B and HDACs mediates potent therapeutic effects in* IDH1 *-mutant glioma* [Preprint]. Cancer Biology. https://doi.org/10.1101/2020.11.26.400234

Kohli, R. M., & Zhang, Y. (2013). TET enzymes, TDG and the dynamics of DNA demethylation. *Nature*, *502*(7472), 472–479. https://doi.org/10.1038/nature12750

Lewis, P. W., Müller, M. M., Koletsky, M. S., Cordero, F., Lin, S., Banaszynski, L. A., Garcia, B. A., Muir, T. W., Becher, O. J., & Allis, C. D. (2013). Inhibition of PRC2 Activity by a Gain-of-Function H3 Mutation Found in Pediatric Glioblastoma. *Science*, *340*(6134), 857–861. https://doi.org/10.1126/science.1232245

Li, H.-J., Yu, P.-N., Huang, K.-Y., Su, H.-Y., Hsiao, T.-H., Chang, C.-P., Yu, M.-H., & Lin, Y.-W. (2016). NKX6.1 functions as a metastatic suppressor through epigenetic regulation of the epithelial–mesenchymal transition. *Oncogene*, *35*(17), 2266–2278. https://doi.org/10.1038/onc.2015.289

Li, W., Xu, H., Xiao, T., Cong, L., Love, M. I., Zhang, F., Irizarry, R. A., Liu, J. S., Brown, M., & Liu, X. S. (2014). MAGeCK enables robust identification of

essential genes from genome-scale CRISPR/Cas9 knockout screens. *Genome Biology*, *15*(12), 554. https://doi.org/10.1186/s13059-014-0554-4

Li, Y., Gong, H., Wang, P., Zhu, Y., Peng, H., Cui, Y., Li, H., Liu, J., & Wang, Z. (2021). The emerging role of ISWI chromatin remodeling complexes in cancer. *Journal of Experimental & Clinical Cancer Research*, *40*(1), 346. https://doi.org/10.1186/s13046-021-02151-x

Lita, A., Pliss, A., Kuzmin, A., Yamasaki, T., Zhang, L., Dowdy, T., Burks, C., de Val, N., Celiku, O., Ruiz-Rodado, V., Nicoli, E.-R., Kruhlak, M., Andresson, T., Das, S., Yang, C., Schmitt, R., Herold-Mende, C., Gilbert, M. R., Prasad, P. N., & Larion, M. (2021). IDH1 mutations induce organelle defects via dysregulated phospholipids. *Nature Communications*, *12*(1), Article 1. https://doi.org/10.1038/s41467-020-20752-6

Liu, K.-L., Zhu, K., & Zhang, H. (2022). An overview of the development of EED inhibitors to disable the PRC2 function. *RSC Medicinal Chemistry*, *13*(1), 39–53. https://doi.org/10.1039/D1MD00274K

Losman, J.-A., & Kaelin, W. G. (2013). What a difference a hydroxyl makes: Mutant IDH, (R)-2-hydroxyglutarate, and cancer. *Genes & Development*, *27*(8), 836–852. https://doi.org/10.1101/gad.217406.113

Luo, S., Valencia, C. A., Zhang, J., Lee, N.-C., Slone, J., Gui, B., Wang, X., Li, Z., Dell, S., Brown, J., Chen, S. M., Chien, Y.-H., Hwu, W.-L., Fan, P.-C., Wong, L.-J., Atwal, P. S., & Huang, T. (2018). Biparental Inheritance of Mitochondrial DNA in Humans. *Proceedings of the National Academy of Sciences*, *115*(51), 13039–13044. https://doi.org/10.1073/pnas.1810946115

Mastrototaro, G., Zaghi, M., Massimino, L., Moneta, M., Mohammadi, N., Banfi, F., Bellini, E., Indrigo, M., Fagnocchi, G., Bagliani, A., Taverna, S., Rohm, M.,

Herzig, S., & Sessa, A. (2021). TBL1XR1 Ensures Balanced Neural Development Through NCOR Complex-Mediated Regulation of the MAPK Pathway. *Frontiers in Cell and Developmental Biology*, *9*, 641410. https://doi.org/10.3389/fcell.2021.641410

Mellinghoff, I. K., Van Den Bent, M. J., Blumenthal, D. T., Touat, M., Peters, K. B., Clarke, J., Mendez, J., Yust-Katz, S., Welsh, L., Mason, W. P., Ducray, F., Umemura, Y., Nabors, B., Holdhoff, M., Hottinger, A. F., Arakawa, Y., Sepulveda, J. M., Wick, W., Soffietti, R., … Cloughesy, T. F. (2023). Vorasidenib in IDH1- or IDH2-Mutant Low-Grade Glioma. *New England Journal of Medicine*, NEJMoa2304194. https://doi.org/10.1056/NEJMoa2304194

Mesfin, F. B., & Al-Dhahir, M. A. (2023). Gliomas. In *StatPearls*. StatPearls Publishing. http://www.ncbi.nlm.nih.gov/books/NBK441874/

Millard, C. J., Varma, N., Saleh, A., Morris, K., Watson, P. J., Bottrill, A. R., Fairall, L., Smith, C. J., & Schwabe, J. W. (2016). The structure of the core NuRD repression complex provides insights into its interaction with chromatin. *ELife*, *5*, e13941. https://doi.org/10.7554/eLife.13941

Miller, J. J. (2022). Targeting IDH-Mutant Glioma. *Neurotherapeutics*, *19*(6), 1724–1732. https://doi.org/10.1007/s13311-022-01238-3

Miller, J. L., & Grant, P. A. (2013). The Role of DNA Methylation and Histone Modifications in Transcriptional Regulation in Humans. In T. K. Kundu (Ed.), *Epigenetics: Development and Disease* (Vol. 61, pp. 289–317). Springer Netherlands. https://doi.org/10.1007/978-94-007-4525-4_13

Mohajeri, A., Tayebwa, J., Collin, A., Nilsson, J., Magnusson, L., Von Steyern, F. V., Brosjö, O., Domanski, H. A., Larsson, O., Sciot, R., Debiec-Rychter, M.,

Hornick, J. L., Mandahl, N., Nord, K. H., & Mertens, F. (2013). Comprehensive genetic analysis identifies a pathognomonic *NAB2/STAT6* fusion gene, nonrandom secondary genomic imbalances, and a characteristic gene expression profile in solitary fibrous tumor: *NAB2/STAT6* Fusion Gene in Solitary Fibrous Tumor. *Genes, Chromosomes and Cancer*, *52*(10), 873–886. https://doi.org/10.1002/gcc.22083

Moore, L. D., Le, T., & Fan, G. (2013). DNA Methylation and Its Basic Function. *Neuropsychopharmacology*, *38*(1), 23–38. https://doi.org/10.1038/npp.2012.112

Neumaier, F., Zlatopolskiy, B. D., & Neumaier, B. (2023). Mutated Isocitrate Dehydrogenase (mIDH) as Target for PET Imaging in Gliomas. *Molecules*, *28*(7), Article 7. https://doi.org/10.3390/molecules28072890

Nicholson, T. B., Veland, N., & Chen, T. (2015a). Chapter 3—Writers, Readers, and Erasers of Epigenetic Marks. In S. G. Gray (Ed.), *Epigenetic Cancer Therapy* (pp. 31–66). Academic Press. https://doi.org/10.1016/B978-0-12-800206-3.00003-3

Nicholson, T. B., Veland, N., & Chen, T. (2015b). Writers, Readers, and Erasers of Epigenetic Marks. In *Epigenetic Cancer Therapy* (pp. 31–66). Elsevier. https://doi.org/10.1016/B978-0-12-800206-3.00003-3

Noushmehr, H., Weisenberger, D. J., Diefes, K., Phillips, H. S., Pujara, K., Berman, B. P., Pan, F., Pelloski, C. E., Sulman, E. P., Bhat, K. P., Verhaak, R. G. W., Hoadley, K. A., Hayes, D. N., Perou, C. M., Schmidt, H. K., Ding, L., Wilson, R. K., Van Den Berg, D., Shen, H., … Aldape, K. (2010). Identification of a CpG Island Methylator Phenotype that Defines a Distinct Subgroup of Glioma. *Cancer Cell*, *17*(5), 510–522. https://doi.org/10.1016/j.ccr.2010.03.017

Park, J.-W. (2023). Metabolic Rewiring in Adult-Type Diffuse Gliomas. *International Journal of Molecular Sciences*, *24*(8), Article 8. https://doi.org/10.3390/ijms24087348

Peixoto, P., Cartron, P.-F., Serandour, A. A., & Hervouet, E. (2020). From 1957 to Nowadays: A Brief History of Epigenetics. *International Journal of Molecular Sciences*, *21*(20), Article 20. https://doi.org/10.3390/ijms21207571

Reitman, Z. J., Parsons, D. W., & Yan, H. (2010). IDH1 and IDH2: Not Your Typical Oncogenes. *Cancer Cell*, *17*(3), 215–216. https://doi.org/10.1016/j.ccr.2010.02.024

Richa, R., & Sinha, R. P. (2014). Hydroxymethylation of DNA: An epigenetic marker. *EXCLI Journal*, *13*, 592–610. https://www.ncbi.nlm.nih.gov/pmc/articles/PMC4464262/

Ritchie, M. E., Phipson, B., Wu, D., Hu, Y., Law, C. W., Shi, W., & Smyth, G. K. (2015). Limma powers differential expression analyses for RNA-sequencing and microarray studies. *Nucleic Acids Research*, *43*(7), e47–e47. https://doi.org/10.1093/nar/gkv007

Rong, L., Li, N., & Zhang, Z. (2022). Emerging therapies for glioblastoma: Current state and future directions. *Journal of Experimental & Clinical Cancer Research*, *41*(1), 142. https://doi.org/10.1186/s13046-022-02349-7

Schaff, L. R., & Mellinghoff, I. K. (2023). Glioblastoma and Other Primary Brain Malignancies in Adults: A Review. *JAMA*, *329*(7), 574–587. https://doi.org/10.1001/jama.2023.0023

Schübeler, D. (2015). Function and information content of DNA methylation. *Nature*, *517*(7534), 321–326. https://doi.org/10.1038/nature14192

Schwartzentruber, J., Korshunov, A., Liu, X.-Y., Jones, D. T. W., Pfaff, E., Jacob, K., Sturm, D., Fontebasso, A. M., Quang, D.-A. K., Tönjes, M., Hovestadt, V., Albrecht, S., Kool, M., Nantel, A., Konermann, C., Lindroth, A., Jäger, N., Rausch, T., Ryzhova, M., … Jabado, N. (2012). Driver mutations in histone H3.3 and chromatin remodelling genes in paediatric glioblastoma. *Nature*, *482*(7384), 226–231. https://doi.org/10.1038/nature10833

Sharma, N., Mallela, A. N., Shi, D. D., Tang, L. W., Abou-Al-Shaar, H., Gersey, Z. C., Zhang, X., McBrayer, S. K., & Abdullah, K. G. (2023). Isocitrate dehydrogenase mutations in gliomas: A review of current understanding and trials. *Neuro-Oncology Advances*, *5*(1), vdad053. https://doi.org/10.1093/noajnl/vdad053

Sharma, S., Kelly, T. K., & Jones, P. A. (2010). Epigenetics in cancer. *Carcinogenesis*, *31*(1), 27–36. https://doi.org/10.1093/carcin/bgp220

Shi, Y., Wang, X., Zhuang, Y., Jiang, Y., Melcher, K., & Xu, H. E. (2017). Structure of the PRC2 complex and application to drug discovery. *Acta Pharmacologica Sinica*, *38*(7), Article 7. https://doi.org/10.1038/aps.2017.7

Solomou, G., Finch, A., Asghar, A., & Bardella, C. (2023). Mutant IDH in Gliomas: Role in Cancer and Treatment Options. *Cancers*, *15*(11), Article 11. https://doi.org/10.3390/cancers15112883

Straining, R., & Eighmy, W. (2022). Tazemetostat: EZH2 Inhibitor. *Journal of the Advanced Practitioner in Oncology*, *13*(2), 158–163. https://doi.org/10.6004/jadpro.2022.13.2.7

Straub, C., Granger, A. J., Saulnier, J. L., & Sabatini, B. L. (2014). CRISPR/Cas9-Mediated Gene Knock-Down in Post-Mitotic Neurons. *PLoS ONE*, *9*(8), e105584. https://doi.org/10.1371/journal.pone.0105584

Tian, W., Zhang, W., Wang, Y., Jin, R., Wang, Y., Guo, H., Tang, Y., & Yao, X. (2022). Recent advances of IDH1 mutant inhibitor in cancer therapy. *Frontiers in Pharmacology*, *13*. https://www.frontiersin.org/articles/10.3389/fphar.2022.982424

Turcan, S., Rohle, D., Goenka, A., Walsh, L. A., Fang, F., Yilmaz, E., Campos, C., Fabius, A. W. M., Lu, C., Ward, P. S., Thompson, C. B., Kaufman, A., Guryanova, O., Levine, R., Heguy, A., Viale, A., Morris, L. G. T., Huse, J. T., Mellinghoff, I. K., & Chan, T. A. (2012). IDH1 mutation is sufficient to establish the glioma hypermethylator phenotype. *Nature*, *483*(7390), 479–483. https://doi.org/10.1038/nature10866

Venneti, S., & Thompson, C. B. (2013). Metabolic Modulation of Epigenetics in Gliomas: Metabolic Modulation of Epigenetics in Gliomas. *Brain Pathology*, *23*(2), 217–221. https://doi.org/10.1111/bpa.12022

Verheul, C., Ntafoulis, I., Kers, T. V., Hoogstrate, Y., Mastroberardino, P. G., Barnhoorn, S., Payán-Gómez, C., Tching Chi Yen, R., Struys, E. A., Koolen, S. L. W., Dirven, C. M. F., Leenstra, S., French, P. J., & Lamfers, M. L. M. (2021). Generation, characterization, and drug sensitivities of 12 patient-derived IDH1-mutant glioma cell cultures. *Neuro-Oncology Advances*, *3*(1), vdab103. https://doi.org/10.1093/noajnl/vdab103

Wang, S.-Y., Gao, K., Deng, D.-L., Cai, J.-J., Xiao, Z.-Y., He, L.-Q., Jiao, H.-L., Ye, Y.-P., Yang, R.-W., Li, T.-T., Liang, L., Liao, W.-T., & Ding, Y.-Q. (2016). TLE4 promotes colorectal cancer progression through activation of JNK/c-Jun signaling pathway. *Oncotarget*, *7*(3), 2878–2888. https://doi.org/10.18632/oncotarget.6694

Wei, X., Zhang, Y., Xie, L., Wang, K., & Wang, X. (2021). Pharmacological inhibition of EZH2 by GSK126 decreases atherosclerosis by modulating foam cell formation and monocyte adhesion in apolipoprotein E-deficient mice. *Experimental and Therapeutic Medicine*, *22*(2), 841. https://doi.org/10.3892/etm.2021.10273

Wu, H., & Zhang, Y. (2014). Reversing DNA Methylation: Mechanisms, Genomics, and Biological Functions. *Cell*, *156*(1–2), 45–68. https://doi.org/10.1016/j.cell.2013.12.019

Yang, I. V., & Schwartz, D. A. (2012). Epigenetic mechanisms and the development of asthma. *Journal of Allergy and Clinical Immunology*, *130*(6), 1243–1255. https://doi.org/10.1016/j.jaci.2012.07.052

Yedier-Bayram, O., Gokbayrak, B., Aksu, A. C., Cavga, A. D., Kayabolen, A., Kala, E. Y., Karabiyik, G., Günsay, R., Morova, T., Uyulur, F., Lack, N. A., Önder, T. T., & Bagci-Onder, T. (2021). EPIKOL, a chromatin-focused CRISPR/Cas9-based screening platform, to identify cancer-specific epigenetic vulnerabilities. *BioRxiv*, 2021.05.14.444239. https://doi.org/10.1101/2021.05.14.444239

Yu, J. S. L., & Yusa, K. (2019). Genome-wide CRISPR-Cas9 screening in mammalian cells. *Methods*, *164–165*, 29–35. https://doi.org/10.1016/j.ymeth.2019.04.015

Yu, N., Zhang, P., Wang, L., He, X., Yang, S., & Lu, H. (2018). RBBP7 is a prognostic biomarker in patients with esophageal squamous cell carcinoma. *Oncology Letters*. https://doi.org/10.3892/ol.2018.9543

Zeng, D., Liu, M., & Pan, J. (2017). Blocking EZH2 methylation transferase activity by GSK126 decreases stem cell-like myeloma cells. *Oncotarget*, *8*(2), 3396–3411. https://doi.org/10.18632/oncotarget.13773

Zhao, D., Yuan, H., Fang, Y., Gao, J., Li, H., Li, M., Cong, H., Zhang, C., Liang, Y., Li, J., Yang, H., Yao, M., Du, M., Tu, H., & Gan, Y. (2023). Histone Methyltransferase KMT2B Promotes Metastasis and Angiogenesis of Cervical Cancer by Upregulating EGF Expression. *International Journal of Biological Sciences*, *19*(1), 34–49. https://doi.org/10.7150/ijbs.72381